UNIVERSIDAD DE GUANAJUATO

Campus Irapuato–Salamanca

División de Ingenierías

"Motor Imagery Brain-Computer Interface Powered by Artificial Neural Networks"

Dissertation to Obtain the Degree of:

Doctor in Electrical Engineering

Author:

M.Eng. Tat'y Mwata Velu

Advisors:

Dr. Juan Gabriel Aviña Cervantes

Dr. José Ruiz Pinales

Salamanca, Gto., México.

March 10, 2022

Salamanca, Gto., a 1 de marzo del 2022.

M. en I. HERIBERTO GUTIÉRREZ MARTIN
COORDINADOR DE ASUNTOS ESCOLARES
P R E S E N T E.-

Por medio de la presente, se otorga autorización para proceder a los trámites de impresión, empastado de tesis y titulación al alumno(a) _ Mwata Velu Tat'y _____ del ***Programa de Doctorado en_*** _____ Ingeniería Eléctrica _____ y cuyo número de ***NUA*** es: 145790 __ del cual soy director. El título de la tesis es: ____ "Motor Imagery Brain-Computer Interface Powered by Artificial Neural Networks".

Hago constar que he revisado dicho trabajo y he tenido comunicación con los sinodales asignados para la revisión de la tesis, por lo que no hay impedimento alguno para fijar la fecha de examen de titulación.

A T E N T A M E N T E

Dr. Juan Gabriel Avina Cervantes
NOMBRE Y FIRMA
DIRECTOR DE TESIS
SECRETARIO

Dr. José Ruiz Pinales
NOMBRE Y FIRMA
DIRECTOR DE TESIS

Dr. Arturo García Pérez
NOMBRE Y FIRMA
PRESIDENTE

Dr. Juan Manuel Sierra Hernández
NOMBRE Y FIRMA
VOCAL

Dr. Alejandro Israel Barranco Gutiérrez
NOMBRE Y FIRMA
VOCAL

González José Barbosa Joel

Dr. José Joel González Barbosa
NOMBRE Y FIRMA
VOCAL

Epigraph

Due to all mine who have left us, I presume the graveyard and the sky are filled with unconditional love.

Tat'y Mwata Velu

Preface

This thesis of which I savor the prestigious honor of writing marks the successful culmination of my doctoral cycle in electrical engineering at the Universidad de Guanajuato, División de Ingeniería Campus Irapuato-Salamanca (DICIS). Therefore, I defend it to obtain the official Doctor in Electrical Engineering degree. This doctoral thesis entitled ”Motor Imagery Brain-Computer Interface Powered by Convolutional Neural Networks” is the result of the extensive knowledge acquired during my academic training and all combined efforts in the search for effective and profitable outcomes. From September 2018 to December 2021, I focused on research and laboratory experiments, which led to thesis writing.

The motivation for this doctoral thesis arose from my enthusiasm to tentatively propose practical solutions to social problems based on innovative technology. Specifically, to lay the foundations in a brain-computer system implementation based on electroencephalogram signals to assist people who have lost their mobility to communicate autonomously with their environment.

I would like to thank here my thesis advisers, Doctor Juan Gabriel Aviña-Cervantes and Doctor José Ruiz-Pinales, who, during long and intense work moments, helped answer with a thorough and adequate approach to the hypothesis raised by this thesis.

Ultimately, I gratefully thank the shadow heroes, all of whom, by your conscious efforts, privations and evident intentions, subscribed to the challenge of winning this crown. Therefore, this doctoral thesis is the result of everyone’s commitment.

Tat’y Mwata Velu

Personal Acknowledgments

Let me introduce these brief words of thanks to my mom, who imparted life to me:
Ginami Josée, ngatshiginyine egi ukhala unu nu henyaha... Guanubalega go ndaga imwe, nga hugo ditshi, ame gugutangiza ndo. Wanotagenesa masugu ekima gutendelela gwaye ha gulomba gudi Nzambi mukunda na eswe. Mangino nu masugu agaswe, mbatutumbwisa jina diaye mu mitshima yetu. Hambadiahana Ginami (Pende language - Dem. Rep. of Congo) [1]

This is an extremely special acknowledgment to my father Narcisse Velu A Gulenga from whom I learned that the conscious effort is not thankless. From Kitondolo, through Totshi, Kalumbu, Gungu, Kikwit, Bukavu, and even Bordeaux (France), you wanted to reveal the way to a job well done, an academic honor to deserve despite all twists and life turns. These triumph moments are dedicated to you, triumph against discouragement, triumph against adverse weather everywhere, triumph against the race abandonment. For all that you have done for me, may life be generous to you.

To my wife Lucienne Magazini Baniaya, much appreciated for these long moments of noble sacrifice, deprivation, concession, and solid accompaniment, unconditional and admirable patience. You represent the co-author of this success. You set me on this doctoral program and honored it. Therefore, I am profoundly obliged to you.

May Lucrece, Scotty, Tatito, and Quetzalli find the greatest reward of so many times spent away from them in this thesis. I left you a pathway to follow, an honor to fight for.

I am sincerely grateful to Doctors Juan Gabriel Aviña Cervantes and José Ruiz Pinales for their remarkable dedication and commitment to boost this thesis completion. Esteemed Doctors, coherent words are not enough to adequately express your adequate support in this doctoral thesis issue. Enormously productive seminars, laborious and endless practices, interminable nights of academic work, debriefing forums and so many other memorable moments will undoubtedly remain for me a rich training experience. I am privileged to have been their student.

To all my teachers of the División de Ingenierías Campus Irapuato-Salamanca (DICIS), I heartily thank you for the teaching quality and your lofty sense of responsibility in the student academic training.

[1] Translation: Dear Josée,
How I would have ardently wanted you to live these moments physically!. No significant second passes without my thinking to you. You accomplish your promise everyday, interceding with God for our family. Today and forever, we will celebrate your presence among us. Thank you, Mom.

Particularly to Doctor Pablo Ramírez Paredes, Doctor Raúl Enrique Sánchez Yáñez, Doctor Roberto Rojas Laguna, Doctor Juan Manuel Sierra Hernández, and to Doctor Horacio Rostro González.

I express my deep gratitude to the jury members of my doctoral thesis examination for their precious time and their commendable comments on the earlier versions of this thesis.

I thank the Teresian Institution in Mexico for the valuable support during these research years. May each and every one of you receive with these sincere words the expression of my profound gratitude.

To my close friends Adán Antonio Alonso Ramírez and Jairo Javier Martínez Juárez, for all the best moments shared together, I am deeply thankful.

I am profoundly obliged to Mr. Gaspard Bomo Masebe and to Mrs. Lucie Mukwa Nkubindi (rest in peace) whose memory we honor, for all their support in the success of this thesis.

Ultimately, I dedicate this thesis to all my family, they may find the fruits of long-term work and countless sacrifices here. Thank you very much, Ange Mushigo, Dory, Rachel, and Joél Velu.

Tat'y Mwata Velu

Salamanca, Guanajuato
March, 2022.

Institutional Acknowledgments

To the Universidad de Guanajuato: allowing me to achieve this dream and believe in myself. This truth that I learned sets me free.

UNIVERSIDAD DE GUANAJUATO

To the Mexican National Council of Science and Technology (CONACYT from Spanish): for the financial support provided for the Doctorate program in Electrical Engineering under the scholarship number 63527/600853.

CONACYT
Consejo Nacional de Ciencia y Tecnología

Abstract

This doctoral thesis focuses on developing a Brain-Computer Interface based on motor imagery Electroencephalogram (EEG) signals using EMOTIV EPOC+ equipment, a SoCKit FPGA development card, and a walking robot.

Brain-Computer Interfaces (BCIs) meaningfully improve what was already known as assistive devices for people with disabilities, especially in the lack of global or partial motor skills, employing technological advancements. These brain-computer interfaces enable effective communication between the brain and a given machine using specific cerebrum signals, highlighting challenges such as instant and efficient signal processing, accurate signal decoding and classification, and the conception of universal BCIs using adaptive processing algorithms for all brain signal types.

Therefore, EMOTIV EPOC+ headset detects the neuronal activity generated by the defined task and wirelessly sends the corresponding signals to the SoCKit FPGA board for parallel processing using neural networks. Movement imagery signals of right and left fists are processed and converted into operational commands to move the hexapod robot forward or backward.

Motor imagery (MI)-EEG signals from the F3, F4, FC5, and FC6 channels are processed using a hybrid architecture of Convolutional Neural Networks (CNNs) and Long Short-Term Memory (LSTM) networks. This method uses the deep learning recognition model to develop a real-time embedded BCI system, where signal processing must be seamless and precise. In addition, to deal with the noisy and the non-stationary EEG signal processing problems, two approaches based on the Empirical Mode Decomposition (EMD) method are analyzed.

The validation of the results found using the k-fold cross-validation method and two public databases showed the successful functioning of the developed BCI. The bases established in this thesis serve to develop more complex and precise BCIs.

Keywords

Brain-Computer Interface (BCI), Motor Imagery (MI), Electroencephalogram (EEG), Convolutional Neural Networks (CNN), Long Short-Term Memory (LSTM)

Contents

List of Figures

List of Tables

List of Algorithms

Chapter 1

Introduction

"I believe that the future of humanity is in the progress of reason through science. I believe that the pursuit of truth, through science, is the divine ideal which man should propose to himself."

Emile Zola

This chapter presents the issue in the doctoral thesis, the hypotheses put forward, and the principal motivations leading to the subject choice. The objectives pursued, along with the thesis organization, round off this chapter.

1.1 Preliminaries

Science undoubtedly possesses, in its essence, the function of improving the vital conditions of populations by solving, if not proposing, solutions to the various problems faced by humanity. Promoting social justice means, among other initiatives, looking into the life situations of people who are severely disadvantaged by their health conditions, enabling them to benefit from advantages as everyone else.

The recent United Nations World Report 2011 reveals that over a billion people (15% of the world population) live with at least one disability[1]. According to the same report, between 785 and 975 million people aged 15 and over live with a handicap, of which 3.8% have severe functional disabilities such as quadriplegia, depression, or blindness.

The Convention on the Rights of Persons with Disabilities and Optional Protocol [7] defines in the preamble (a) this: "Recognizing that disability is an evolving concept and that disability results from the

[1] https://www.who.int/disabilities/world_report/2011/summary_es.pdf

interaction between persons with impairments and attitudinal and environmental barriers that hinders their full and effective participation in society on an equal basis with others...".

Therefore, people living with disabilities cannot participate fully and effectively in society on an equal footing with others, considering their long-term physical, intellectual, mental or sensory impairments.

To date, disability is already a matter of deep concern due to the increasing population aging, since the handicap risks are higher in older adults than in childlike people [8]. In addition, the statistics indicate the increase in cardiovascular diseases [9], cancer [10], mental health disorders [11], and accidents of all kinds that, in various situations, cause disability [12].

In general, like other disability types, motor impairment undoubtedly constitutes a factor of social discrimination and dependence in various situations [13]. Concretely, orthopedic, neuromuscular, cardiovascular, and pulmonary disorders are considered physical disabilities [14].

A fact, motor disability maintains a close relationship with extreme poverty [15], and lack of access to essential education [16], to name but a few.

In parallel, the sustainable development goals and the United Nations commitment to leave no one behind by 2030 aim to "empower and to promote the social, economic, and political inclusion of all, irrespective of age, sex, disability, race, ethnicity, origin, religion, or other status" [17].

Therefore, a battery of all-around strategies is put in place to improve the vital conditions of people with disabilities. Since the inclusion of policies developed at the international level [18] and by the respective governments [19], passing across more effective laws and monitoring mechanisms [20], until searching for appropriate medical and technological solutions, the problem of people with disabilities is seen as a weak node for societies development.

From very early on (500 B. J.), devices' assistance for people with disabilities was implemented [21]. Firstly, prosthetic limbs and later wheelchairs; whose complexity has been improved thanks to technological progress. Among assistance devices for people with motor disabilities, are improving prostheses [22], assisting robots, wheelchairs, feeding devices [23], actuators manipulated by the body, and others.

The assistive device use depends on the user's specific needs, by extension, on the degree of his handicap. Its specifications are based on the user's physiological, kinematic, geometric, dynamic, and economic information.

The concept of the brain-computer interface (BCI) was born [24], taking advantage of Hans Berger's first works on the electromagnetic functioning of the human brain [25]. It empowered people with motor disabilities by providing them with the cognitive ability to control an assistive device instead of automating it. In these systems, the user uses the "electromagnetic potential" of the brain to communicate with the environment through an interface.

BCIs are typically built based on biological signals such as an electroencephalogram (EEG) [26], Electrooculogram (EOG) [27], Electromyogram (EMG) [28], resulting from cerebral activity, eye

movements, and muscle contraction, respectively. The Functional magnetic resonance imaging (fMRI) technology, for its part, measures changes in blood flow caused by brain activity, and is reserved for clinical uses [29].

EEG signals turn out to be the most used for BCIs dedicated to people with severe disabilities, compared to the Electrooculogram and Electromyogram. The specific case of people who lost their muscular activity (locked-in syndrome) but have their brain and sensory functions lively illustrates the considerable advantage of EEG over other techniques in BCI systems design.

BCIs based on EEG use different paradigms, methods, and applications. The literature is flooded with BCI paradigms based on EEG signals. Among the main ones are BCIs based on State-State Visual Evoked Potentials (SSVEP) [30], stimulated by a flickering visual; BCIs-based on auditory evoked potentials (ERPs) [31] and BCIs-based on stimulated sensorimotor rhythms (SMR)(*Beta* and *mu* rhythms), by the imagination of body limb movements [32] or by the real execution of these movements [33].

From a summarized approach, EEG signals processing methods for BCI applications cover the following steps:

1. **Signal preprocessing**, to increase the signal-to-noise ratio.
2. **Feature extraction**, to constitute the features vector.
3. **Feature selection and dimensionality reduction**, to ease computer processing.
4. **Classification**, to generate labels.
5. **Application**: to convert labels into logical control signals.

Among EEG signal preprocessing techniques for BCI systems, one finds: filtering algorithms based on Common Average Referencing (CAR) [34], Common Spatial Patterns (CSP) [35], Independent Component Analysis (ICA) [36], Principal Component Analysis (PCA) [37], Singular Value Decomposition (SVD) [38], Maximum Noise Fraction (MNF) [39], and other relevant approaches [40].

The feature extraction and selection steps merge for some complex algorithms. The extraction step is explicit for EEG signals linked to sensorimotor activity where spectral parameters are assumed to constitute features [41].

Numerous works have developed specific techniques for features selection and dimensionality reduction, among which are the Genetic Algorithm (GA) [42], the Sequential Forward Feature Selection (SFFS) [43], the Linear Discriminant Analysis (LDA) [44], Empirical Mode Decomposition (EMD) [45], and the Fisher Discriminant Analysis (FDA) [46].

For classification, efficient linear classifiers such as Support Vector Machine (SVM) [47] and Linear Discriminant Analysis (LDA) are used in various works [48]. Bayesian classifiers, Hidden Markov Model

classifiers (HMM) [49], and k-Nearest Neighbour (k-NN) classifiers [50] likewise offer noticeable results for EEG classification.

Recently, Artificial Neural Networks (ANN) [51], Convolutional Neural Network (CNN) [52], and Recurrent Neural Network (RNN) [53] have been implemented to learn features deeply and give best classification results.

Several BCI applications are flooding life sciences, from scientific research to ordinary living. BCIs are used both in deepening the study of brain function [54] and in the diagnosis [55] and neurorehabilitation of certain diseases [56]. The NESSI (NEural Signal Surfing Interface) internet browser [57], the control of prosthesis [58], autonomous cars [59], aerospace systems, and wheelchairs [60] serve as typical illustrations of successful BCI applications.

The invasive and non-invasive nomenclatures for BCI systems typically refer to the electrode placement technique: electrodes are placed in the skull using surgery in invasive BCI. It is principally for medical purposes. Whereas, non-invasive BCIs use electrodes placed on the scalp and do not require skull surgery for manipulation.

Embedded systems are a significant alternative for developing intelligent systems rather than computers, which have a general-purpose. Embedded systems are generally designed to meet specific needs [61]. BCI systems are increasingly made up of embedded systems to meet the user mobility needs and dedicate all the available resources to the system-specific functions [62].

Most of the components of an embedded system are integrated into the motherboard, such as video and audio cards [63], the GPU [64], modems [65], or a particular card-development [66].

An embedded system can be programmed using the assembly language of the accompanying micro-controller, microprocessor or by using specific compilers such as C or C++ programming languages. In some cases, an interpreted language such as Java is used [67].

Some embedded system specifications are low-acquisition cost, low-power consumption, microprocessor capacity, and substantial size [68].

Current research reveals the following challenges for embedded BCI systems based on EEG signals, despite their growing implementations:

- Adequate signal processing due to their non-linear and non-stationary nature: this practically requires, in addition to electrode selection, the robust and precise structuring of the processing algorithms to be efficiently implemented.
- The users training to reliably reproduce signals according to the simulated tasks, the qualified users' selection for the capture step, the number of sessions necessary to build the database are challenges in terms of time and available resources [69].
- The precision, F1-score, or error metric for signals classification or prediction reflects the

correspondence sharpness between produced signal batches and application executed commands [70].

- Information Transfer Rate (ITR) [71]. In manifold BCI applications, such as in robotics, it is imperative to process a large data flow to control, for example, the robot freedom levels. Therefore, this capital requirement imposes a judicious processing units choice [72]. Signal processing algorithms acceleration for real-time BCI applications, BCI systems in which the response time must be as short as possible undoubtedly constitute a real challenge. [73].
- Universal classification algorithms. One of the major challenges of BCI applications is how to design BCIs whose use can be adapted to a large number of users, depending on the cerebral signals and application executed commands [70].

Here, the hypothetical question is how to design an embedded BCI based on EEG signals using available commercial equipment to implement fast and efficient processing algorithms? The following hypotheses are then raised to propose an answer to this question.

1.2 Hypotheses of the problem

Since the challenges raised in the preliminaries concerning the implementation of the Brain-Computer systems, and considering the availability of non-invasive EEG signal capture equipment, electronic cards equipped with data processing units (CPU-GPU), and numerous BCI applications, particularly in robotics, this doctoral thesis formulates the following hypotheses:

- An embedded-BCI system based on Motor Imagery EEG signals would be made, using an EMOTIV EPOC+ headset, a Cyclone V SoCKit FPGA development card, and a hexapod robot. The EMOTIV EPOC+ headset would capture EEG signals generated at the moment of the right and left fist movements imagination, would send corresponding signals to the SoCKit development card to be processed and converted into hexapod motion commands. Therefore, motions of a hexapod would result from closing-opening fist intentions.
- A private database will be created with seven subjects, in good health, previously trained to reproduce Motor Imagery EEG signals corresponding to closing and opening right-left fists. Subjects would be trained for at least 500 half-second sessions.
- Algorithms based on Deep Learning (DL) would be used for signal processing, explicitly combining CNNs and RNNs (LSTM).
- Signals processing would be accelerated by the rigorous choice of the processing unit resources. The transfer rate would be limited to 10 MB/s for 32-bit signals, the data delay time to 10 ms, and the hexapod response time between 0.50 and 2.50 ms.

1.3 Justification

Several distinctive voices have been amplified to claim for assistive technologies from home to more than a third of people with disabilities [74], not counting social policies and recommendations at the international and local government levels [75].

The designed embedded BCI system seeks to overcome the challenges mentioned above and lay deep foundations for future projects, aiming to control a motorized wheelchair and smart-home accesses using motor imagery EEG signals.

Among recent commercial equipment for capturing EEG signals, the EMOTIV EPOC+ headset is the most used in research [76], due to its low cost, easy manipulation, integrated filters, and also the resolution of the signal at 14-bit (1 LSB=0.51 micro V), connectivity mode (wireless connection at 2.4 GHz) and signal sampling frequency at 128 samples per second. In addition, EMOTIV EPOC+ allows the detection of brain activities generated by facial gestures (blinking, winking, smiling, etc.), emotional and cognitive states from thoughts.

Lotte *et al.* proposed a BCIs categorization according to the reliability, signal capture mode, and operating method [77]. From an operating point of view, the dependent BCIs grant the control power to the user, for example, by looking or by a facial gesture, to manage an application. While independent BCIs do not require any form of user control over BCIs. These BCIs are used in severe motor disability situations, as in the case of a stroke.

Among the dependent BCIs, those based on Motor Imagery (MI) are the most used because they give users total control by imagining body limb movements [78]. The subject can control BCIs voluntarily with specific words by effective thought training.

For its part, the FPGA Cyclone V SoCKit card was selected as the signal processing unit to constitute an embedded system in which all resources would be dedicated to the application control. SoCKit is an enhanced FPGA technologies version involving an ARM cortex-A9 processor and various application development tools. It is expected to reduce the application response time considerably by taking advantage of parallel signal processing in the FPGA part and at the processor level.

Algorithms based on deep learning have amply demonstrated their efficiency in processing MI EEG signals using artificial neural networks [79]. Implementing a cascade of convolutional and recurrent neural networks in the thesis project, seeks to optimize the signal processing in time and in terms of efficiency, binarizing the weight patterns for training and signals classification.

Finally, the hexapod robot has been used in various works due to its movement comfortability on unstructured surfaces and its multiple degrees of freedom [80]. These specific criteria motivated its selection as the project application.

1.4 Motivations

The prime motivation for the topic selection comes from the considerable interest to propose a concrete solution to a social problem scientifically, specifically here with the increasing number of people with motor disabilities, according to the official statistics [81].

Another critical motivation derives from my Master's academic research on the equipment interconnection built from different technologies, the specific case of interconnecting the EMOTIV EPOC headset, FPGA, Raspberry or NVIDIA Jetson TX2 cards with the hexapod, quadruped, or bipedal robots. These preliminary works paved the path for the present thesis by studying the electronic modalities of the coupling functioning.

This doctoral thesis fills out a crucial stage in this ambitious project development. It is projected to control the home-user automation environment. Therefore, our motivation goes beyond the present thesis objective, making people with motor disabilities independent in their communication with the surrounding environment based on motor imagery EEG signals.

1.5 Objectives

1.5.1 General Objective

The general objective of this doctoral thesis is to design and implement an embedded Brain-Computer Interface (BCI) based on Motor Imagery EEG signals to control the hexapod robot motions voluntarily.

1.5.2 Particular Objectives

To reasonably achieve the general objective set out above, we present the following intermediate goals:

- Carry out a state-of-the-art analysis to gather recent information on BCIs in general and those based on MI EEG signals in particular, EEG signal acquisition systems, development cards (FPGA, Raspberry, Jetson TX2), and walking robots.
- Perform the subject's training and EEG signals capture, to create a local database.
- Configure the BCI hardware components and implement the signal processing algorithms.
- Carry out the successful BCI implementation and functioning tests.
- Interpret and validate the results comparing with those of the state-of-the-art.

1.6 Thesis organization

This thesis is presented as follows:

Chapter 2 addresses the general concept of Brain-Computer interfaces, their evolution over time, their categorizations, and functional structure. An emphasis is made on BCIs based on MI EEG signals to understand better the BCI structure proposed in this thesis. A short introduction is made on EEG signals to highlight the useful characteristics built for many BCI.

As a principal processing method used in this doctoral thesis, the deep learning approach based on recurrent and convolutional neural networks is presented in Chapter 3. This chapter provides fundamental concepts and neural network architectures related to general signals processing, especially for electroencephalographic signals.

Chapter 4 presents the proposed method, that contemplates the principal steps in the BCI realization, from the motor imagery EEG signals capture to a hexapod motions control. Aspects as equipment used, algorithms implemented, and the BCI prototype presentation is developed in this chapter.

In Chapter 5, experimental results obtained with the local database are compared with those achieved with two public databases, to evaluate the implemented algorithm effectiveness. These public datasets are selected according to the BCI paradigm similarities.

The thesis's conclusion, presented in Section 5.4, reports the analysis of the results regarding those of the state-of-the-art, highlighting the thesis's particular contributions to meet the previous hypotheses.

Chapter 2

Brain-Computer Interfaces

This chapter covers the theory and development of a general Brain-Computer Interface (BCI), as shown in Figure 2.1. Fundamental aspects such as the EEG signals nature and categorization, etymology of the BCI concept, evolution over time and the BCI operating principle are explored in this part. Also, Brain-Computer Interfaces based on motor imagery EEG signals are discussed before concluding the chapter.

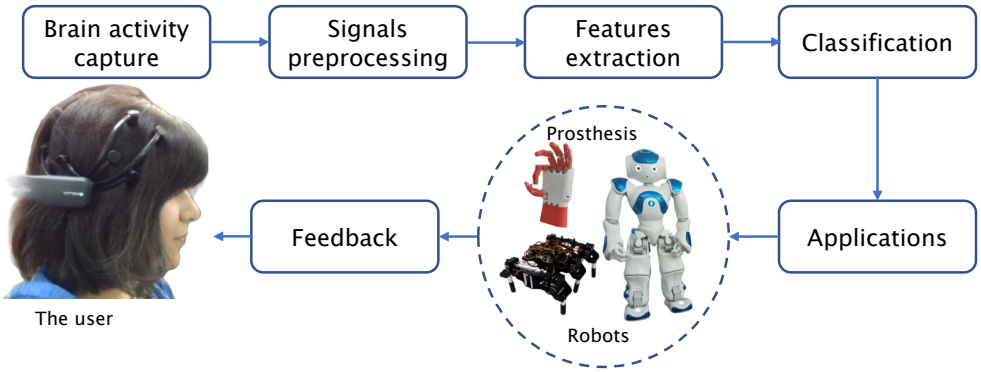

Figure 2.1: The operating principle of a general BCI in robotics and human assistance.

2.1 The electroencephalography (EEG)

Electroencephalography measures the brain electrical activity over time through the electrodes placed on the scalp. Besides, it allows the diagnosis of certain diseases that affect brain activity from signal registers previously established with healthy subjects. It is the case with epilepsy, sleep disorders, Alzheimer's, and other cognitive diseases.

2.1.1 Introduction

Researchers are unanimous in recognizing the German neuropsychiatrist Hans Berger for the electrical activity firstly recorded on the human brain (1924). Earlier, the brain's electrical functioning constituted the main focus of Adolf Beck's research [82]. Besides, the British Richard Caton had already made EEG recordings in animals [83], depending on the wakefulness, sleep, anesthesia or death state.

Hans Berger described two dominant EEG rhythms, the alpha rhythm (10 cycles per second) and the beta rhythm [25]. Therefore, broad research on EEG signals and their clinical use started. From Hans Berger's own words in 1929:
"The electroencephalogram represents a continuous curve with continuous oscillations in which ... one can distinguish larger first order waves with an average duration of 90 milliseconds and smaller second order waves of an average duration of 35 milliseconds [Beta waves]. The larger deflections measure at most 150 to 200 microvolts...."

Two years later, Berger made some revelations about the EEG. For example, in patients induced by cocaine and general anesthesia or in sleep, ALPHA waves had low values compared to subjects in a normal state. Similar results were observed in patients with severe intracranial pressure. However, in epileptic patients, Berger noted that ALPHA waves had large amplitudes. His research revealed that Alzheimer's disease and multiple sclerosis markedly modify EEG recordings.

Taking advantage of Berger's advances, the Foundation Carl Zeiss provided an oscillography and electronic amplifier, which allowed it to observe the plane waves after a seizure in epileptic patients but that the similar waves had growing peaks while they regained consciousness.

In 1934, Forester and Altenburger [84] recorded brain activities using selective electrodes placed directly on the cerebral cortex (intraoperative EEG recordings), named the Electrocorticography (ECoG). Four years early, with Canadian neurosurgeon Wilder Penfield published an expanded map of the human cortex locating the motor, sensory, acoustic, and visual cortices [85].

Numerous advances in the study of EEG signals for medical purposes were developed between the 30s and 40s, due notably to the cases of epilepsy that occurred during the two world wars. It is worth mentioning the works of Rasmussen and Penfield [86], Schott [87], Jasper [88], Hayne [89], and Talairach [90].

The invention of color television in the 1950s and transistors in the 1960s helped various computerized electroencephalography techniques to flourish. The utility of intraoperative (invasive) techniques decreased significantly in the 1980s with computed tomography and magnetic resonance imaging inventions. They only proceeded with invasive techniques in specific cases of severely altered epilepsies.

At the same time, research on assistance to people with disabilities advanced with technology. So, Vidal formalized in 1973 the concept of Brain-Computer Interface [91], understood as a system that processes the patterns of brain activity to convert them into commands for a given application. The objective was to

communicate between a user and his local surroundings through brain signals.

Since the 90s, many trends of research and applications based on EEG signals continue to advance and constitute a research field with much more prospects.

2.1.2 The Brain Structure

We begin this section with the Vilayanur S. Ramachandran famous citation:
"There are 100 billion neurons in the adult human brain, and each neuron makes something like 1,000 to 10,000 contacts with other neurons in the brain. Based on this, people have calculated that the number of permutations and combinations of brain activity exceeds the number of elementary particles in the universe"[1].

2.1.2.1 The brain anatomy

According to its members, the human body is symmetric: one eye on the left and the other on the right, one leg on the left and the other on the right. Therefore, we assume a virtual vertical axis passing through the human center from the head to between the two legs, as represented by Leonardo da Vinci in the Vitruvian Man. In particular, Figure 2.2 shows the right and left hemispheres divided into distinct lobes, whose complex function depends on the effective coordination between several neural networks distributed in the brain.

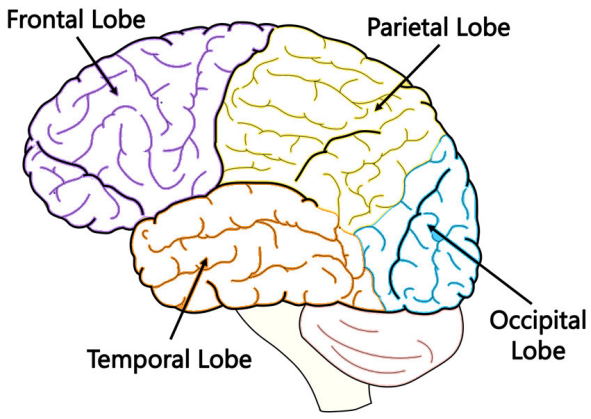

Figure 2.2: Cerebral lobes. The frontal (F), parietal (P), temporal (T), and occipital (O) brain lobes.

The frontal lobe is located at the front of the cerebral hemispheres. The primary motor cortex, the upper, middle, and lower frontal gyruses are the four convolutions that constitute the frontal lobe, and each one has its specificity [92]:

[1] "The neurons that shaped civilization". TEDIndia Talk, www.ted.com. November 2009.

- The primary motor cortex manages voluntary movements. The superior frontal gyrus plans behavior. The middle frontal gyrus controls superior executive functions and decision-making processes [93].
- Broca's area, located in the inferior frontal gyrus, is involved in language production, processing and comprehension [94].

The developmental maturity of the human frontal lobe occurs between 25 and 30 years. It is the largest of all the brain lobes. Various cognitive functions depend on the frontal lobes such as judgment, memory, appropriate or no social behavior, planning and problem-solving.

The parietal lobe is located between the temporal and occipital lobes and is composed of the superior and inferior parietal lobules, separated by the intraparietal groove. The parietal lobe manages sensory information (temperature, pain, pressure), visual data in addition to learning mathematics [95].

The temporal lobe controls sound and speech processing, essentially the left one, with a phonological representation purpose [96]. The left gyrus handles functions such as color processing, word, face and number recognition [97].

The occipital lobe is placed at the back of the brain, posterior to the parietal and temporal lobes. It is the smallest cerebral lobe responsible for the vision and its interpretation. It receives visual information, processing and dispatching it to other brain areas for analysis, representing the visual cortex's primary function [98].

With this brain anatomy comprehension, we are going to analyze how specific information is communicated from one cerebral cortex to another by means of neurons.

2.1.2.2 Neurons

The brain is basically made up of neurons and glial cells. A neuron is a cell possessing electrical and chemical properties that allow it to propagate nerve impulses, specialized in inter-neural communication. There are about 30 billion neurons available to the brain at birth, which can vary depending on the subject up to 89 billion [99].

Figure 2.3 illustrates the fundamental structure of a neuron. The existence of an electrical potential in the nerve cell and a chemical process that warrants communication from one neuron to another ensures the formation of small and then vast neural networks.

The neuron typically receives signals through dendrites or even through its molecular body and produces as an organic reaction, electrical potentials whose frequency is proportional to the input signals. These potentials are then propagated through the nerve fiber. Multipolar inter-neurons (see Figure 2.3(a)) have a single long axon with very dense branches at its end. Figure 2.3(b) shows a motor neuron that generally interacts with a muscle cell and, in mammals, has the axon almost covered by fat (myelin). As illustrated in Figure 2.3(c), the nerve impulse is carried by two axons with different ends in the sensory neuron. The

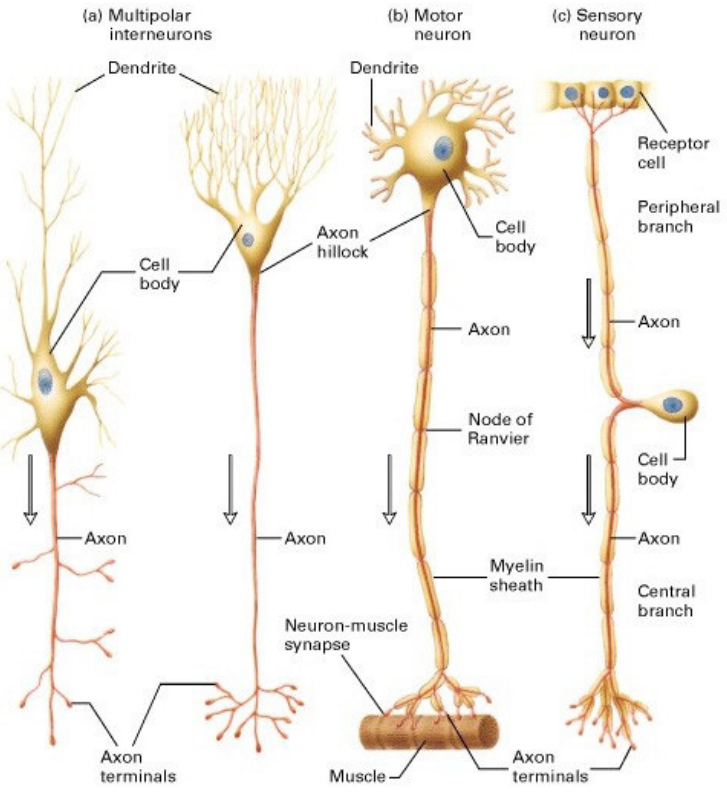

Figure 2.3: The typical mammalian neurons structure. The electrical potential in the cell is unidirectional; its propagation direction in the axons is shown by the arrows [1].

first connects the recipient cell to the molecular body located in the dorsal root ganglion. The second axon establishes the connection between the molecular body and the spinal cord or brain.

The synapse formed by the termination, the synaptic cleft, and the next neuron dendrite (postsynaptic), interconnects two neurons. The neurotransmitter is the chemical released by the synapse when it receives action potentials. Moreover, the postsynaptic neuron undergoes an excitatory or inhibitory effect depending on the amount and type of neurotransmitters released.

Multiple factors intervene in the communication between neurons. The neurotransmitters amount released by axons, their speed through the synaptic cleft, and the number of postsynaptic receptors, influence the communication power between neurons. The most sustained represents the increase in the synapses number, called ”synaptogenesis”.

Myelination fulfills a significant role in the communication between two neurons: by releasing a neurotransmitter in an electrical pulse nature, the axon assumes the conductor role. Therefore, myelination plays the insulating effect for the axon easing the cerebral electric current circulation.

The human brain is extremely complex functionally. Each brain part is dedicated to a specific assignment with interconnected neurons constituting a network, which can be interconnected to other networks,

especially for similar or identical tasks. Thereby, the areas have very specific functions, as presented in Section 2.1.4.

2.1.3 EEG Signals

There are predominantly two brain signal groups, typically depending on how the subject is stimulated: On one hand, we have brain rhythms whose existence is not induced by external stimulation. Put differently, the existence of these signals is not caused by an external stimulus. These are signals detected during sleep, in a consciousness state, or specific cases of cerebral pathology diagnosis. On the other hand, there are evoked potentials resulting from an external stimulation or an internal event like stress, a directed thought, or a memory. These signals are classified into frequency bands as follows:

- **Delta:** These waves are present in a state of dreamless sleep or meditation. These are slow waves due to their frequencies below 4 Hz.
- **Theta:** With frequencies between 4 and 8 Hz, these waves appear in a state of drowsiness and help in learning, and memory consolidation. Attention deficits accompanied by hyperactivity in adults can be seen through *Theta* rhythm picks. The frustration or disappointment state is also observable through *Theta* waves.
- **Alpha:** These waves produce frequencies between 8 and 13 Hz and are observed during an alertness state, superficial meditation, or mental activity coordination.
- **Beta:** Waves produced by an attention engaged state through cognitive tasks such as solving a problem or during an external stimulus. Their frequencies vary between 14 and 30 Hz. This waveband is frequently divided into low and high Beta-band for signal processing.
- **Gamma:** These waves contain frequencies above 30 Hz and are observed during intense attention or sustained concentration states. They also intervene during the information synchronization provided by several cerebral lobes at the same time.

In summary, *Delta* waves are associated with the deep sleep state, *Theta* with the drowsiness state, *Alpha* with relaxation, *Beta* with sustained attention, and *Gamma* with the excited state.

For their part, the Steady-State Evoked Potentials are classified into Steady-State Visual Evoked Potentials (SSVEP) [100], Steady-State Auditory Evoked Potentials (SSAEP) [101], Steady-State Somatosensory Evoked Potentials (SSSEP) [102], Steady-State Cognitive Evoked Potentials (SSCEP) [103] and Steady-State Motor Evoked Potentials (SSMEP) [104]. A subject periodically stimulated by a scintillating photo or an amplitude modulated sound produces a Steady-State Evoked Potentials (Visual and Auditory) whose stimulation frequency equals the EEG signal periodicity [105].

Event-Related Potentials (ERP) are EEG waveforms associated with sensory, cognitive, or motor stimulation [106]. The instant between the stimulus presentation and the appearance of the wave representing

an ERP understood as the event triggering time carries out to define particular signals, for instance, P300 signals which appear 300 milliseconds after the stimulus is presented. Somatosensory Evoked Potentials (SSEP) generated by sensory stimuli such as pain or touch sensation, and Error stimulation Potentials (ErrP) are other types of ERP signals [107].

The evoked potentials typically appear as a potential difference between electrode pairs for a given external stimulation. They are defined according to their occurrence time (milliseconds), their polarity (negative for n and positive for p), their spatial location, and the used protocol (mismatch negativity for MMN).

Event-Related Desynchronization (ERD), as well as Event-Related Synchronization (ERS), is typically associated with cognitive tasks such as Motor Imagery (MI) or the physical movement execution, mental calculation, or the imaginary rotation of geometric figures [108].

For a classic example, The left-hand movement imagination produces in the right sensory motor cortex, an EDR of 8 to 12 Hz in the μ band and 16 to 24 Hz in the β band, an ERS follows after the movement imagination [109].

Capturing EEG signals, first of all, refers to the signal definition and the brain cortex. Detection equipment can be located on the cortex that employs an invasive or non-invasive approach in the given task.

2.1.4 EEG signals Capture Systems

Neurons' excitation causes ionic current to flow through synaptic junctions and cells, causing brain activity. Electric potentials are therefore generated from these particle movements.

The EEG uses electrodes often made of silver chloride (AgCl) to capture electrical potentials generated by brain activity. An EEG system is called non-invasive when these electrodes are placed on the scalp. A conductive paste is used on dry electrodes to maximize the electrical current flow to the electrode. The electrode is placed directly over the interest cortex in an invasive system by surgery (see Figure 2.4). Invasive systems are predominantly employed in diagnosing cases or treating specific diseases [110].

The electrodes can be active or passive depending on whether or not they are equipped with an internal pre-amplification system, considering that the electrical potentials generated by brain activity are of the order of 100 μV at most and must be amplified from 10 to 50 thousand times.

The electrode mounting can be unipolar or bipolar. In a unipolar mounting, one electrode is active, and the other is taken as a reference for the potential difference to be measured. However, in a bipolar arrangement, both electrodes are active. Generally, EEG headsets consist of 1 to 256 electrodes.

Faced with the difficulty of organizing the cerebral cortex coverage by electrodes to detect neuronal activity properly, the international 10-20 electrode placement system (see Figure 2.5a) was proposed by the International Federation of Societies for Electroencephalography and Clinical Neurophysiology (IFCN) in

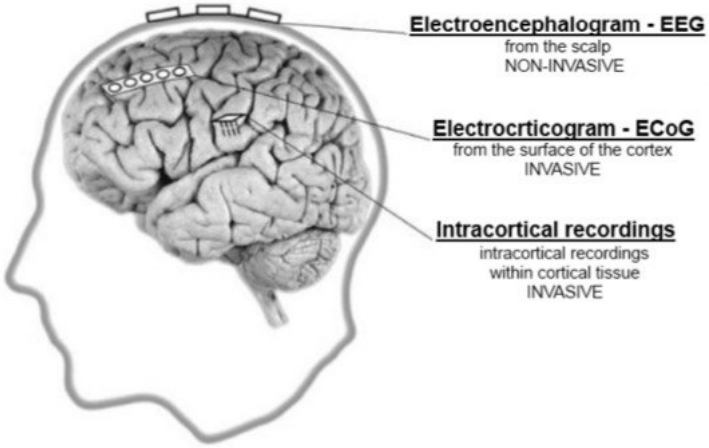

Figure 2.4: Invasive and non-invasive brain electrical activity recordings [2].

1958 [111].

The 10-20 system reflects the distances between adjacent electrodes, which must be 10% of the skull's circular length (front-back) and 20% of its longitudinal distance. The 10-20 system employs uppercase letters to locate the brain hemisphere, as shown in Table 2.1. The central lobe does not actually exist as seen

Table 2.1: 10-20 System Electrodes nomenclature according to the brain lobes.

Lobe location	**Electrode**
Frontal	F
Temporal	T
Central	C
Parietal	P
Occipital	O

in Section 2.1.2, the letter C is used only for the usage purpose.

Therefore, the electrode designation begins with capital letters indicating the cerebral cortices which carry them. In the second position come either the lowercase letter "z" for the electrodes located on the skull longitudinal axis or a number. The numbers (2,4,6,8) show the right-hemisphere electrode location while the odd numbers (1,3,5,7) refer to the left-hemisphere electrode placement.

The International 10-20 system for electrodes placement was defined for twenty-one electrodes. For the research sake into brain functioning, the 10-10 (1985) and 10-5 (2001) systems were proposed later to increase spatial resolution by extending the number of electrodes [112].

Figure 2.5b representing the 10-10 System, shows electrodes added to those of 10-20 system. Since the electrodes mosaic is denser, the 10-10 system (with up to 64 electrodes) makes it possible to cover almost

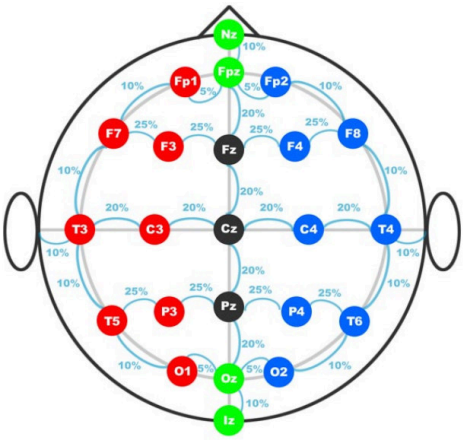

(a) The International 10 - 20 System Electrodes configuration.

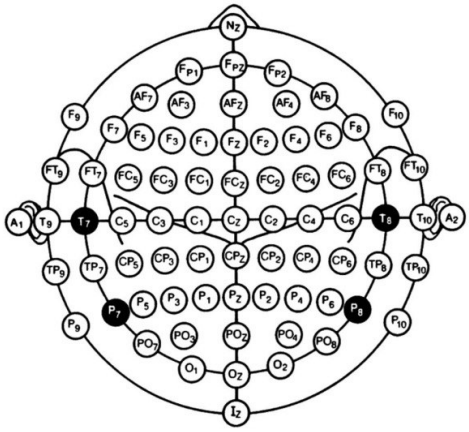

(b) The 10 - 10 System electrodes configuration [112].

Figure 2.5: The 10-20 and 10-10 electrode placement systems for recording EEG signals. **(a)** The initial 10-20 system was proposed in 1959 and **(b)** the 10-10 system was introduced in 1985.

Table 2.2: System 10-10 added electrodes nomenclature.

Between Electrodes	MCN Code	Location
Fp and F	AF	Anterior Frontal
F and C	FC	Frontocentral
F and T	FT	Frontotemporal
C and P	CP	Centroparietal
P and O	PO	Parieto-occipital
T and P	TP	Temporal-posterior

all the cerebral cortices and, therefore, provide the spatial resolution improvement of EEG signals.

With the increase of electrodes, the Modified Combinatorial Nomenclature (MCN) was agreed to name each electrode [113], especially the added ones. The system provides odd numbers between 1 and 9 equivalent to 10, 20, 30, 40, and 50% of the left-hemisphere considering the nasion-inion distance, to place intermediate electrodes. The MCN system nomenclature provides the codes listed in Table 2.2.

The electrodes T3, T4, T5, and T6 of the 10-20 system are replaced by the electrodes T7, T8, P7 and P8 in the designation MCN. The letter P is decoded in two ways: P means Parietal when it is followed by a number less than or equal to 6. For a number greater than 6, P is translated as posterior temporal.

Table 2.3 relates the electrodes terminology of the 10-20 system to the brain signals type to be detected considering a given stimulus. But in practice, various approaches have been developed to locate the discriminating electrodes for a defined stimulus [114].

Table 2.3: Nomenclature and functions for the electrodes in the international $10-20$ system [6].

Brain region	Electrode	Function
Frontal	Fp1	Attention
	Fp2	Judgment restrains impulses
	F7	Verbal expression
	F3	Motor planning
	F4	Motor planning of left-upper extremity
	F8	Emotional expression
Temporal	T3	Verbal memory
	T4	Emotional memory
	T5	Verbal understanding
	T6	Emotional understanding and motivation
Central	C3	Sensorimotor integration (right)
	Cz	Sensorimotor integration (midline)
	C4	Sensorimotor integration (left)
Parietal	P3	Cognitive processing special temporal
	Pz	Cognitive processing
	P4	Math word problems, Non-verbal reasoning
Occipital	O1	Visual processing
	Oz	Incontinence
	O2	Visual processing

Based on the neural network interconnections spanning multiple cortices, as explained in Section 2.1.2, the probability of the same stimulus producing discriminant EEG signals in more than one cerebral cortex is greater. Hence, the practical difficulty of deciding exactly the electrodes discriminating the EEG signals produced by a given stimulus.

2.2 Brain-Computer Interfaces based on EEG

Brain-Computer Interfaces (BCI) allow communication between a given user and his/her immediate surroundings through brain signals. These systems are based on the electrical characteristics of cerebral signals, as explained in Section 2.1.2. BCIs based especially on EEG signals are widely used in medical research [115] as in various modern applications [116] due to the technological advances of the capture equipment and their low acquisition cost. Brain-computer systems have captured the researchers' attention

for two decades. Escolano *et al.* have developed a dry EEG system to allow BCI home use for spinal cord injury patients [117]. For its part, Banach *et al.* designed a wheelchair fully controlled by an algorithm using alpha waves [118]. Solid knowledge of neuroscience, psychology, engineering, computer science, and signal processing are required to design a BCI system. The following section explains the working principle of a BCI system based on EEG signals.

2.2.1 Principles

Figure 2.6 resumes the six steps contemplated in the BCI system's functioning. The first step consists of the brain activity capture. The user intentionally varies his brain state according to the given task while the capture equipment records corresponding signals to control the application. For the capture of EEG signals,

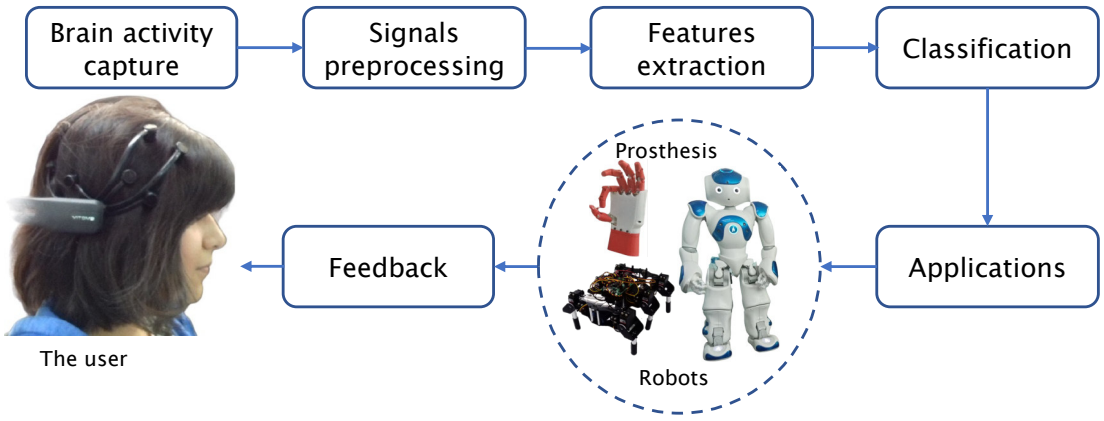

Figure 2.6: General structure of BCI based on EEG signals. This model approach is developed in this thesis.

non-invasive systems are more commonly used than invasive systems, which prevent surgery for placing the electrodes. In fact, according to electrodes type, BCIs are classified into invasive and non-invasive systems.

One problem when dealing with EEG signals is that they are inherently non-stationary. This phenomenon is because brain processes change due to brain state changes, *e.g.*, mental fatigue [119]. For this purpose, in the preprocessing step, raw EEG signals are cleaned and denoised to enhance the relevant information [120].

By obtaining noise-free EEG signals from the preprocessing phase, the extraction process of relevant features is required, which varies depending on the type of signals [121].

In the next stage, EEG features are classified using linear and nonlinear Bayesian, Artificial Neural Networks (ANN), and k Nearest-Neighbors (k-NN) classifiers [122]. Each class represents the brain activity pattern generated for the task, *i.e.*, the right-hand finger movements.

Each feature class is associated to a command controlling an application which could be a robot, a wheelchair, a prosthesis or any other application. Explicitly, the right-hand finger movements could be

translated into commands to move the NAO robot forward, backward, to the right, to the left, or to stop.

The feedback step allows the user to be informed about the features class recognized by the application. The purpose is to modulate brain activity if the application's control changes. Each step mentioned above requires an adequate calibration of the equipment and processing algorithms according to the nature of the EEG signals recorded. This leads to very varied approaches to BCI systems based on EEG signals.

2.2.2 EEG Capture Systems

Various equipment for capturing EEG signals has been used in non-invasive BCI systems. Taking into account low-cost, capacity, portability, resolution, sampling rate, compatibility, reliability, and scalability criterion, the most prominent BCI systems are [123]:

- The g.tec BCI called *g.BCIsys*, is made in Austria. This equipment records simultaneously Electroencephalogram (EEG), electromyogram (EMG), electrooculogram (EOG), and electrocardiogram (ECG) signals [124].
- The EEG Powerlab Data Acquisition System, a New Zealand product, records signals on 32 cortical sites [125].
- The Emotiv Epoc Headset, is made in Australia. This is a portable, high resolution, and 14-channel EEG system for practical research applications only [126].
- The Neurosky Mindwave equipment is made in the USA, consisting of a headset, an ear-clip, and a sensor arm [127].

Figure 2.7 shows the EEG non-invasive equipment mentioned above. However, various other capture devices are not included in the above list, but they are used in some BCI applications. The case of the EEG-1200 JE-921A medical equipment used in [128] and of the system using the ADS1299 chip implemented by Rai *et al.* [129].

2.2.3 EEG Signals Preprocessing

EEG signals are commonly analyzed in temporal, frequency, or/and spatial domains. In time-based representations, for instance the case of event-related potentials (ERP), EEG signals are extracted from a time-window. In contrast, spectral powers are considered in the EEG signal processing for frequency-based representations. The latter is originally classified according to frequency; consequently, the frequency domain is inherent in the processing process, constituting a signals prefilter. Spatial representations are based on the electrodes topography according to their functions as described in Table 2.3, Section 2.1.4. Active cortical areas according to a defined task could be reconstructed by spatial filters (Laplacian filters) to evaluate the signal-to-noise ratio (SNR) between signals from neighboring electrodes. Considering the

(a) The *gBCIsys* equipment.

(b) The *Neurosky Mindwave* equipment.

(c) The *EMOTIV EPOC* headset.

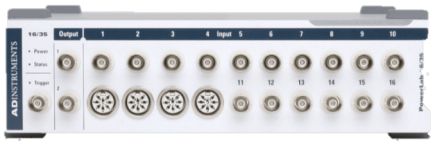

(d) The PowerLab DAQ system.

Figure 2.7: The prominent EEG capture equipment for noninvasive BCIs.

non-stationary property of EEG signals and the differences between frequency bands activation, approaches based on two or three combined representations are frequently used in practice [130].

The preparation of the EEG data matrix for the preprocessing process depends on the considered representation domain and generally includes signal frequency bands, the length and number of the signals time-window (samples), the number of selected sensors, and the number of test subjects.

Because variations in the electrical potential of the EEG signal are on the magnitude of tens of microvolts (μV), preprocessing of EEG signals, also referred to as signal enhancement, is required after signal acquisition to remove noise from the effective signal and preserve useful information. Artifacts, which are muscular activities of body parts not involved in the task, such as eye blinking, eye movements (EOG), and heartbeat (ECG) added to EEG signals, are one source of the noise. Besides, because the recording equipment is essentially electrical, interference from electric lines is added to the EEG signals. As a result, the raw EEG signals should be preprocessed beforehand [131].

Various approaches have been developed to eliminate artifacts from EEG signals, in particular, approaches based on Common Spatial Patterns (CSP) [132], Independent Component Analysis

(ICA) [133], Principal Component Analysis (PCA) [134], Common Average Referencing (CAR) and Surface Laplacian [135], Robust Kalman Filtering (RKF) [136], Common Spatio-Spectral Patterns (CSSP) [137], Adaptive Filtering [138], Ensemble Empirical Mode Decomposition [139] and deep learning approaches [140]. Each approach offers advantages and disadvantages, and the specific method to be used is determined mainly either by the nature of the EEG data available or the downstream processing stages. Moreover, some methods are improvements of others, the case of The CSSP that deal with the CSP limitations by applying spectral filters to the raw EEG signal before using the spatial filtering [137].

2.2.4 EEG Features extraction Algorithms

The feature extraction step aims to reduce the dimensionality of the EEG signals preprocessed, in terms of relevant information, summarizing the essential properties of the signals defined by the task. Either to extract features k_i and k_j, belonging to distinctive classes $\mathbb{X}$ and $\mathbb{Y}$ contained in the signal $\mathbb{S}$. Features must tend to maximize and minimize variances depending on whether they belong to the same class or not, as follows,

$$k_i \Rightarrow min\{Cov(k_i)\}, \quad \forall\, k_i \ \varepsilon\ \mathbb{X}, \tag{2.1}$$

$$k_j \Rightarrow min\{Cov(k_j)\}, \quad \forall\, k_j \ \varepsilon\ \mathbb{Y}, \tag{2.2}$$

$$k_i \Rightarrow max\{Cov(k_i)\}, \quad \forall\, k_i \ \varepsilon\ \mathbb{Y}, \ and \tag{2.3}$$

$$k_j \Rightarrow max\{Cov(k_j)\}, \quad \forall\, k_j \ \varepsilon\ \mathbb{X}. \tag{2.4}$$

With $\mathbb{X} = [k_1, k_2, \ldots, k_i]^\intercal$ and $\mathbb{Y} = [k_1, k_2, \ldots, k_j]^\intercal$ feature vectors of each class. To assure their classification in the following stage, features of the same class must be closer and those of different classes must be evaluably dissimilar.

The temporal, spatial, or spectral information can be exploited depending on the signal enhancement-method. A variety of algorithms are employed to extract features from EEG data, such as Genetic Algorithms (GA) [141], Wavelet Packet Decomposition (WPD) [142], Adaptive Auto-Regressive parameters (AAR) [143], Fast Fourier Transformations (FFT), Wavelets transformations (WT) [144], deep learning approaches, among others.

CSP algorithms and their variants are also used to extract EEG discriminant features [145], and ICA that separates blind sources from EEG signals [146]. For its part, Empirical Mode Decomposition (EMD) allows obtaining features in the time-frequency domain decomposing an EEG signal into several Intrinsic Mode Functions (IMF) [147].

Several EEG signal-based feature extraction techniques are being developed and current challenges include maximizing the efficiency of the training structure using a reduced feature set.

2.2.5 EEG Feature Classification Methods

In the classification stage, each feature vector $v_i = [v_1, v_2, ..., v_n]^\intercal$ is associated with its respective class c_i, after training on the subset of feature vectors. The training aims to optimize a function f that associates to each feature vector v_i a class c_i, such as $c_i = f(v_i)$.

Generally, in the classification step, training features set associated with their respective classes is processed to assign new objects to only one of these classes. The binary classification contemplates two classes, while a multi-class classification is evoked for more than two classes. A multi-class classification can be carried out using binary classification: one against one in pairs [148], one against all [149], hierarchical classifiers similar to a binary decision tree [150], or interpretable multi-class classifiers [151].

In the literature, linear classifiers, nearest-neighbors classifiers (NNC), ANN classifiers and nonlinear Bayesian classifiers (NBC) are developed. Linear classifiers are based on a linear function to ensure the classification, among which LDA [152] and SVM (linear kernel) [47] algorithms have improved results for EEG classification.

The nearest-neighbor classifiers as non-linear classifiers consider the closest neighbors to assign a feature vector to a class. The feature vector can be part of the training set, as in the case of $k-NN$ classifiers, or be taken outside the training set. Therefore, k is a parameter that allows considering k neighbors of a training sample in the features space [153].

Bayesian classifiers are based on Bayes' posterior probability rule to assign a features vector to a class. Naïve Bayesian Classifiers [154] and Hidden Markov Models (HMMs) are examples of non-linear Bayesian classifiers and offer satisfactory results in the classification of EEG signals [155].

Recently, various classifiers based on deep learning models have been developed using complex artificial neural networks. From Multi-Layer Perceptron Neural Network (MLPNN) [156] to recent specialized EEG deep neural network [157], classifier challenges are how to design hidden layers making them more efficient to predict classes from the learning features.

The accuracy metric is one of the statistical metrics used to evaluate classification performance. It provides the correct recognition percentage and varies depending on defined classes. When a feature vector is erroneously classified to class A given that it corresponds to class B, classification errors occur. The confusion matrix or other methods could be used to examine such types of errors [158]. Some classification performance metrics could be computed: given a positive class P where a feature vector is assigned, True Positives (TP) are all features assigned correctly to the class P. In constrast, other classes are seen as negative.

Assigning class P features to another class is called False Negative (FN) while True negatives (TN) are called to all features of other classes than P not assigned to class P, False Positives (FP) being all features erroneously assigned to class P. Therefore, it can be defined the following statistical measures for

the classification evaluation,

$$Accuracy = \frac{TP+TN}{TP+TN+FP+FN}, \tag{2.5}$$

$$Sensitivity = \frac{TP}{TP+FN}, \tag{2.6}$$

$$Specificity = \frac{TN}{TN+FP}, \tag{2.7}$$

$$Precision = \frac{TP}{TP+FP}, \tag{2.8}$$

$$F-score = \frac{2 \times precision \times sensitivity}{precision + precision}. \tag{2.9}$$

High classification accuracy is currently used to evaluate the EEG-based BCI performance. One subset can be used to train the model for large datasets. However, for small datasets, a k-folds cross-validation technique is recommended that splits a whole dataset into k folds, taking iteratively one-fold as test set and the others as a training set.

There are several methods of classifying EEG signals and numerous evaluation metrics, for instance using strong class association rules based on overall coverage of the learning sets [159] or merging the Apriori algorithm, Harmony Search, and Classification-Based Association (CBA) method to build a rule-based classifier [160]. The use of either technique will depend on the project requirements and on the specificity of the available signals.

2.2.6 BCI applications based on EEG Signals

BCI applications based on EEG signals are numerous and continue to flood the field of scientific research and modern applications for public use [161]. For general purpose use, classified feature vectors are transformed into commands:

- to communicate using devices and software such as neuroprostheses, adapted computers, or word processors [162];
- to control the surrounding environment as intelligent home systems, telemedical systems, desk assistants, robotic manipulators, or rehabilitative systems [163];
- to control assistive devices such as exoskeletons and wheelchairs for people who have lost their motor functions [164].

The diagnosis and treatment of severe brain injuries or severe movement impairments are among the medical applications of BCI systems [165]. The therapy could include using a rehabilitation neuroprosthesis, which encourages the patient to generate brain signals on purpose to perform a specific task. The therapy cycle is successful once the patient can accurately control the prosthesis and produce commands that correspond to his intention.

The design of an EEG-based BCI application must comply with the code of ethics for its deployment, namely the Helsinki Protocol of 1964, as updated in 2001 [166]. This protocol recommends, among other considerations, the patient's informed consent, personal and shared responsibility within the experiment team, potential risks, and societal implications of the experiment. Figure 2.8 summarizes the most relevant applications of BCI systems based on EEG signals.

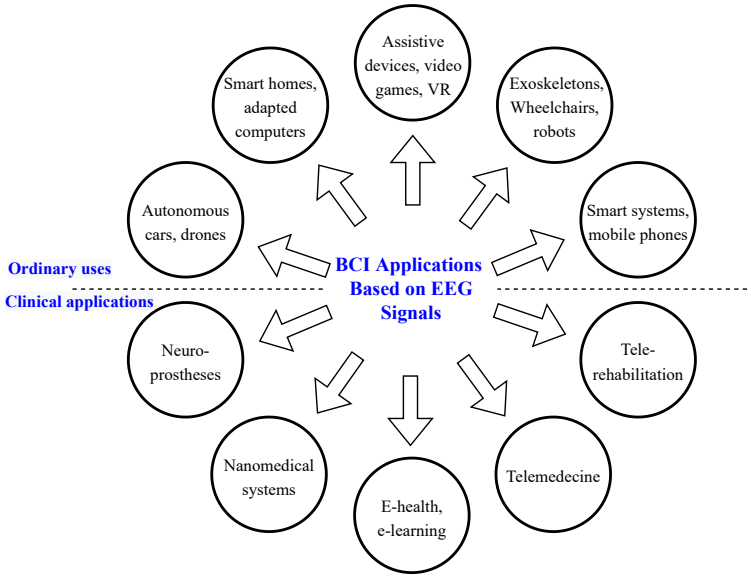

Figure 2.8: Representative BCI Applications based on EEG signals.

2.2.7 Feedback

The feedback delivers information to the application allowing the user to maintain full control of the application, especially for real-time applications. The feedback could be visual, audible, or other depending on the user's functional sensory functions. Thus, the user will adjust brain signals according to the defined tasks to control the application. The user and the application have a master-slave relationship as the feedback. As a result, in addition to the fixed or adaptive signal processing algorithms implemented, the user should be rigorously trained to produce precise brain signals so that the application can decode them.

2.2.8 Chapter Conclusion

This chapter presented the principles, prominent capture equipment and relevant processing algorithms for Brain-Computer interfaces based on EEG signals. The brain structure, EEG signals, and electrode placement systems were introduced to understand the topic best. This chapter constitutes the central node of the understanding, and the development of the thesis. BCIs constituting a vast field evolving from day to day,

the content developed in this chapter pursued the objective of identifying the BCI key concepts for a better thesis understanding.

Chapter 3

Artificial Neural Networks

"When an axon of cell A is near enough to excite a cell B and repeatedly or persistently takes part in firing it, some growth process or metabolic change takes place in one or both cells such that A's efficiency, as one of the cells firing B, is increased."

D.O. Hebb [167]

This chapter describes the operating principle and two artificial neural networks (ANN) types. Before completing the chapter, a brief introduction to the ANN history is presented, and learning algorithms and activation functions.

3.1 Introduction

Artificial neural networks, inspired by the human brain in name and structure, are a sub-field of machine learning and use deep learning algorithms to mimic the functioning of biological neurons. They could well be considered artificial clones of the human brain in how they integrate artificial neurons to solve problems ranging from simple to complex.

Already early on, the ancient Greeks projected the idea of a "thinking machine" [168], for example, with the "Antikythera mechanism" in the eclipse prediction [169]. Warren compared neurons with a binary threshold to Boolean logic at the turn of the century [170]. Rosenblatt developed the first perceptron

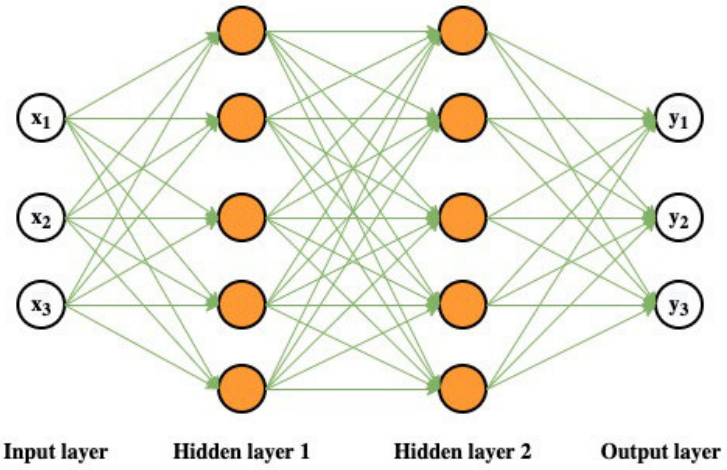

Figure 3.1: Artificial Neural networks structure.

model [171] called **Mark I Perceptron** based on McCulloch and Pitt's work by the 1958s. His first tests with the perceptron allowed him to recognize the cards marked on the left and those marked on the right. Figure 3.2 shows the McCulloch-Pitts neuron structure. The neuron receives the data Input vector

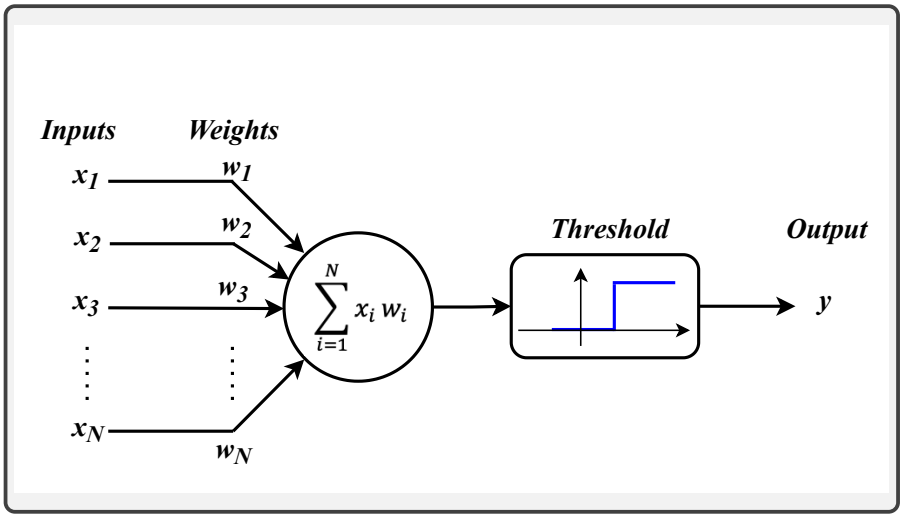

Figure 3.2: The McCulloch-Pitts neuron structure.

$[x_1, x_2, x_3, \ldots, x_N]^\intercal$ including neighboring neurons. The sum of products $x_i w_i$ is compared with the Threshold: the output "y" takes "0" if the sum is below the Threshold and "1" otherwise, activating the neuron or not. The weights W, that is the strength of each neuron's synapse, are modified according to the inputs by minimizing the difference between the actual output and that predicted by the neuron.

The perceptron includes an input called "bias" set to 1 for function computing purposes, compensating for the addition operation, in addition to the data or the output connection

of another nearby perceptron. Rosenblatt's perceptron works as described in Algorithm 1.

Algorithm 1 The operational algorithm of Rosenblatt's perceptron.

Input: Training examples $\{\mathbf{x}_i, y_i\}_{i=1}^{m}$.

Initialize $\mathbf{w}$ and b randomly
while *notconverged* **do**
    ### Loop through the examples.
    for $j = 1, m$ **do**
        ### Compare the true label and the prediction.
        $error = y_j - \sigma(\mathbf{w}^\intercal \mathbf{x}_j + b)$
        ### If the model wrongly predicts the class, update the weights and bias.
        if $error! = 0$ **then**
            $\mathbf{w} = \mathbf{w} + error \times x_j$
            ### Update the bias.
            $b = b + error$
        end if
    end for
    Test for convergence
end while
return *Set of weights* $\mathbf{w}$ *and bias b for the perceptron.*

In the case of binary output, such as y = 1 or y = 0, the threshold that works as an activation function is fairly straightforward. However, studying the neuron firing function in depth is crucial to categorize numerous entries to appropriate labels. Rosenblatt pioneered the machine learning era by implementing the perceptron in hardware with an adapted computer language: he achieved to classify basic 20×20 pixel patterns.

In 1959, Bernard Widrow developed the first artificial neural network configured to solve a real problem, ADALINE employing ADAptive LINear threshold Elements, and MADALINE built specifically to remove noise in phone lines [172]. So we were witnessing the birth of artificial intelligence, with heuristic programming where computers could solve research, learning, pattern-recognition, planning, and induction problems.

"The Winter of Artificial Intelligence" had started with Marvin Minsky's writings [1] towards the end of the 1960s. The problem raised by Minsky was based on multilayer neural networks, as illustrated in Figure 3.3, considering Rosenblatt's unique neuron model: how to optimize the weights of the neurons in each layer so that the number of training iterations will be finite and as small as possible, for a desired output ?.

[1] https://apps.dtic.mil/sti/pdfs/ADA078863.pdf

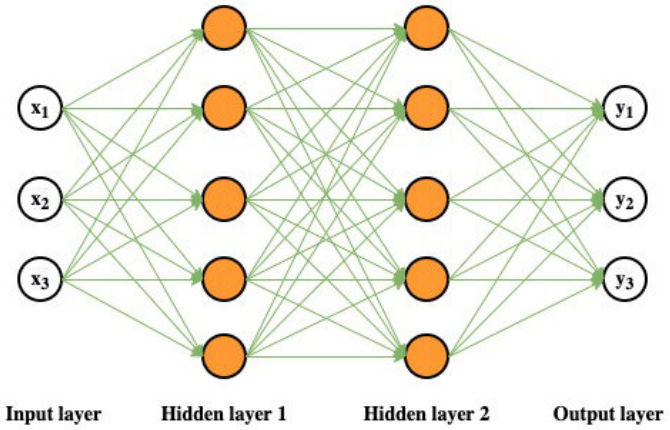

Figure 3.3: The multilayer neural network structure.

Minsky further addressed the idea of employing a large number of random neurons to build one or more hidden layers that interconnect the perceptron's input and output to solve complex problems, with the expectation that each neuron in the hidden layer would deal with a different part of the problem.

The structural problems of Minsky's multilayer perceptron (MLP) generated discouragement and a loss of funding for related research. An attempt to solve the problems of training neural networks came with Paul Werbos' doctoral thesis in 1974, which integrated the "feedback" approach in neural networks [173].

Two mechanisms complement each other in backpropagation: on the one hand, the descent gradient continuously updates the weights and the bias towards the global minimum of the cost function. On the other hand, the backpropagation compares the cost gradient concerning the cost function. As a result, the gradient descent determines the magnitude and direction of the adjustments to be applied to the weights and bias, as illustrated in Figure 3.4.

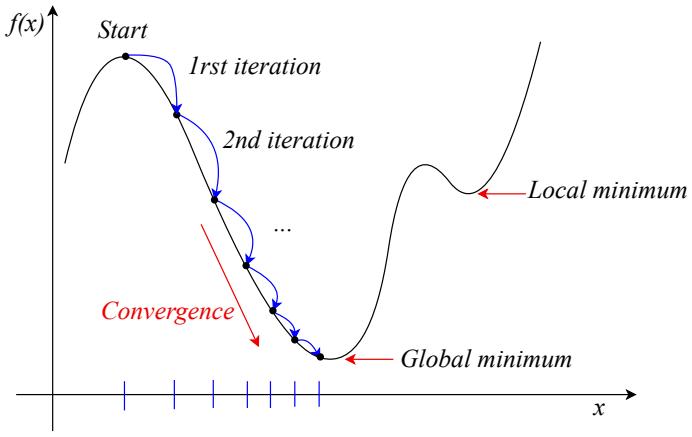

Figure 3.4: Convergence towards the global minimum of a cost function, using Gradient Descent. The jump is determined by the gradient value at the considered point.

Fifteen years later, integration of constraints provided by the task domain in backpropagation neural networks was proposed by Yann Lecun to solve the task of Handwritten Zip Code Recognition [4].

While several meetings were organized to relaunch neural network research in 1982, Jon Hopfield proposed the Hopfield Net [3]. In a Hopfield network, information is propagated in a recurring way, that is to say backwards and forwards. When the information finds a stable state where the information does not vary, the dynamics stops but in the opposite case, the network could continue working infinitely. Figure 3.5 presents the Hopfield Net structure. The Hopfield network is considered as an associative memory of

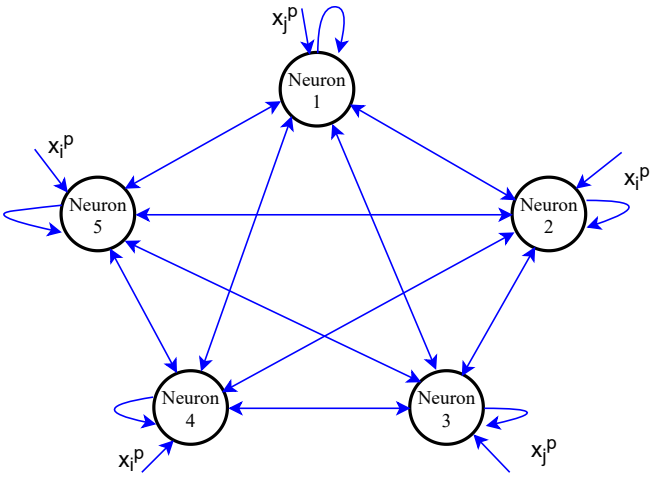

Figure 3.5: The Hopfield Net architecture [3].

addressable content where the matrix of weights W to be determined uses a Lyapunov function. Constructing the weight matrix, W_{ij} elements are found as

$$W_{i,j} = \sum_{i,j} x_i^p \cdot x_j^p, \tag{3.1}$$

where x_i^p and x_j^p represent respectively the element i and j of the input pattern p to be memorized by the network. Since N is the number of neurons, a proportion of $0.15\times$N patterns can be memorized by the network without error in recall, that is, seven neurons per input pattern, according to the empirical experiments.

Since the 1980s, neural networks have been blooming due to the backpropagation algorithm. As a result, the concept of unsupervised machine learning became a fact [174], and ANNs began to be used in various researches [175].

3.2 Convolutional neural Networks (CNN)

3.2.1 The history

Fukushima declared this in 1987 [176]: *"Classical work in visual pattern recognition has demonstrated the advantage of extracting local features and combining them to form higher order features. Such knowledge can be easily built into the network by forcing the hidden units to combine only local sources of information. Distinctive features of an object can appear at various locations on the input image. Therefore it seems judicious to have a set of feature detectors that can detect a particular instance of a feature anywhere on the input place. Since the precise location of a feature is not relevant to the classification, we can afford to lose some position information in the process. Nevertheless, approximate position information must be preserved, to allow the next levels to detect higher order, more complex features (Fukushima 1980; Mozer 1987)."*

The Neocognitron, which was inspired by the architecture of the simple and complex cells of the primary visual cortex, was the first step in today's CNNs. In contrast to what was previously used as fully connected networks, Fukushima proposed alternating layers of convolution and pooling to learn simple and complex features of the input image, as does the visual cortex.

The description and operation of the Neocognitron was supported by the work of Lecun *et al.* [4] which achieved recognition of handwritten digits with the LeNet5 network, and Fukushima succeeded with the Neocognitron in alphanumeric character recognition. The Neocognitron weights are shared in each convolution and the averages are replaced according to average pooling.

In addition to integrating constraints from the task domain, Lecun's modification of backpropagation neural networks aimed to fulfill the need to recognize handwritten digits using data from the US Postal Service, as shown in Figure 3.6. This was the forerunner of today's deep learning techniques. To analyze image attributes, subsets of the input image are considered. Each hidden layer applies convolution having a finite number of units to learn the distinctive features. The combination of information from previously hidden layers are operated until the input digit is interpreted: the first and second hidden layers have 12 layers of 12×64 units and 12 layers of 12×16 units, respectively. The third hidden layer has 30 units, fully connected with the output of 10 digits.

Towards the 90s, after the promotion of CNNs by Lecun, a system for amount recognition was operational commercially for reading checks.

However, the implementation of CNNs to complex problems requiring cascades of convolutions was hampered by technological limits supporting the architectures model training. Also, the lack of robust databases added to the problem of vanishing gradients [177] reduced interest in CNNs in favor of other classification solutions, such as SIFT [178] for example.

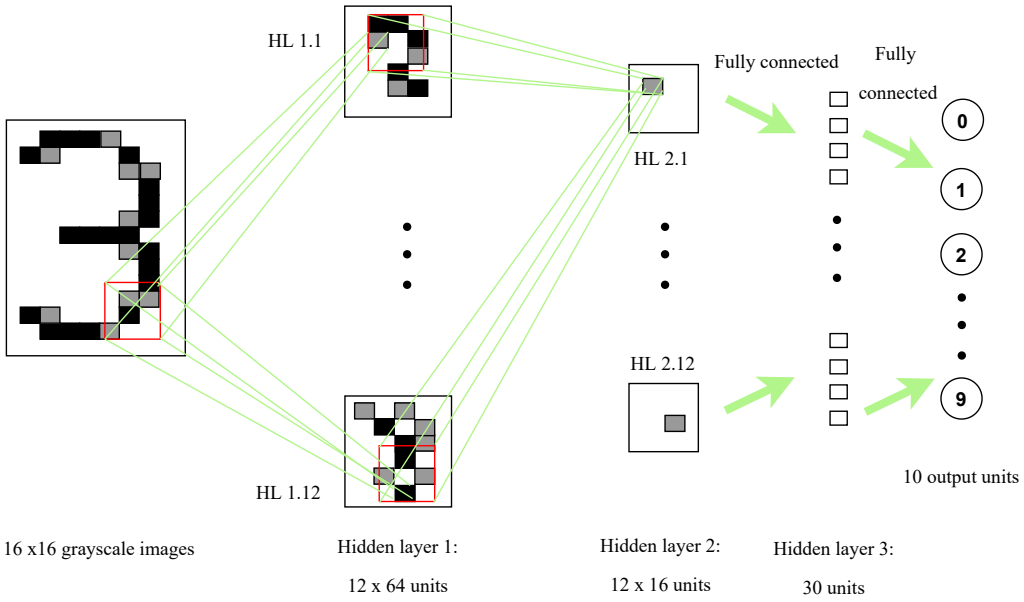

Figure 3.6: LetNe5 architecture illustration [4].

3.2.2 Structure of CNNs

The interesting part of CNNs is how convolutions operate at the hidden layers level to learn local data characteristics. In the mathematical theory, the convolutions of two signals $x_1(t)$ and $x_2(t)$, in time-domain as well as in frequency-domain are given by

$$y(t) = x_1(t) * x_2(t) = \int_{-\infty}^{\infty} x_1(p) \cdot x_2(t-p)dp, \tag{3.2}$$

where $y(t)$ is the continuous convolution of $x_1(t)$ $x_2(t)$ signals, $*$ the convolution operator and p is a dummy variable of integration. The discrete convolution for 1-D signals is given by

$$y[n] = x_1[n] * x_2[n] = \sum_{k=-\infty}^{\infty} x_1[k] \cdot x_2[n-k] \tag{3.3}$$

where $x_1[n]$ and $x_2[n]$ are discrete signals, n is the index number of input sequences and k the input sequence. Therefore, for 2-D signals as images, the Eq. (3.3) can be expressed as

$$(x_1 * x_2)[m,n] = \sum_{i=-\infty}^{\infty} \sum_{j=-\infty}^{\infty} x_1[i,j] \cdot x_2[m-i][n-j] \tag{3.4}$$

where i, j is the pixel spatial location on the map feature.

Convolutional layers use essentially filters, as presented in Figure 3.7. Assuming two successive

convolutions for the RGB image, convolutional filters correspond to the same channel size C_R as the feature maps on which they operate. However, C_B filters convolve for output feature maps of C_B channels. The

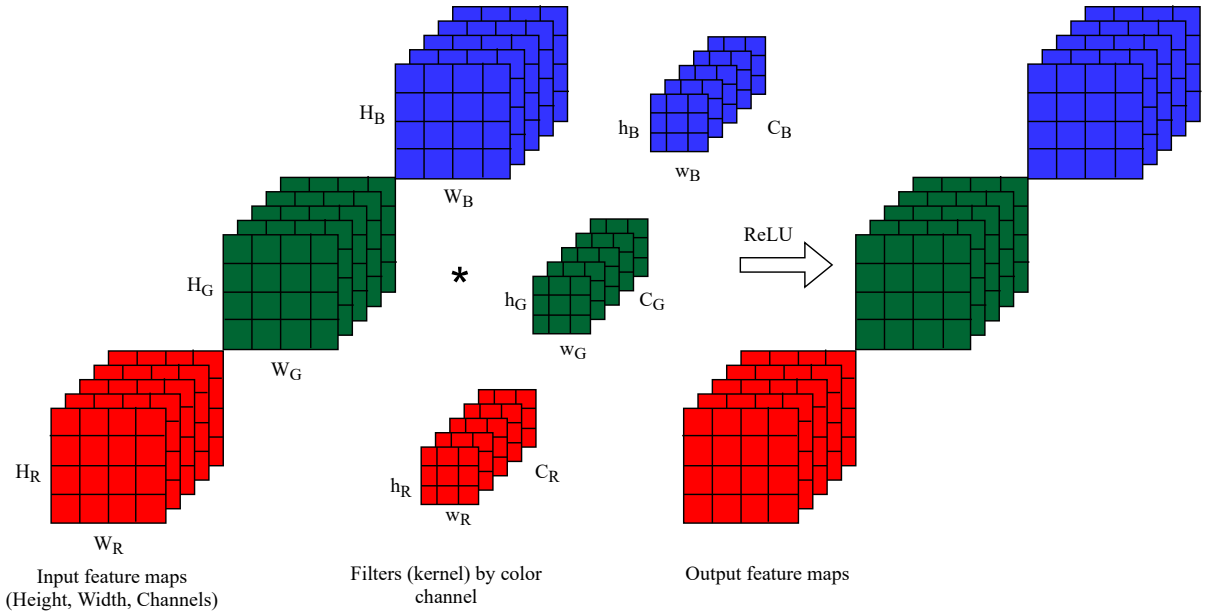

Figure 3.7: Illustration of convolutional filters for 2-D signals.

Rectified Linear Unit (ReLU) is the activation function (see Section 3.5), and in general, the activation function f receives the filter weights W_k, the input feature map x and the bias b_k as arguments, according to

$$h^k_{i,j} = f((W^k * x)_{i,j} + b_k), \tag{3.5}$$

where $h^k_{i,j}$ represents the k^{th} output feature map of the input x at spatial location i, j.

Adopting $\mathbf{X}$ and $\mathbf{Y}$ as the input and the output feature maps, $\mathbf{F}$ as the kernel or convolutional filter. The convolution across the convolutional layer operates as

$$\mathbf{Y}_{i,j,k} = \sum_{l,m,n} \mathbf{X}_{l,j+m,k+n}\, \mathbf{F}_{i,l,m,n}, \tag{3.6}$$

where the scalar elements $i = \{1,2,\cdots,C\}$ is the feature map channel and $j = \{0,1,\cdots,h\}$, $k = \{0,1,\cdots,w\}$ represent the spatial location of the i-th channel pixel. The pair (k,l) represents the row and column offset between the output and input map features, depending on the padding of the input image.

Concretely, the following example illustrates how the convolution takes place for a 4×4 image in gray scale. With a 2×2 kernel initialized randomly as shown in Figure 3.8, moving throughout the image horizontally and vertically, the convolution operation consists of the sum of the dot products between the input image pixels (i, j) and the kernel elements (i, j). The convolution result is a scalar representing the output feature map for the first convolution layer. The operation is repeated until there is no more sliding

available.

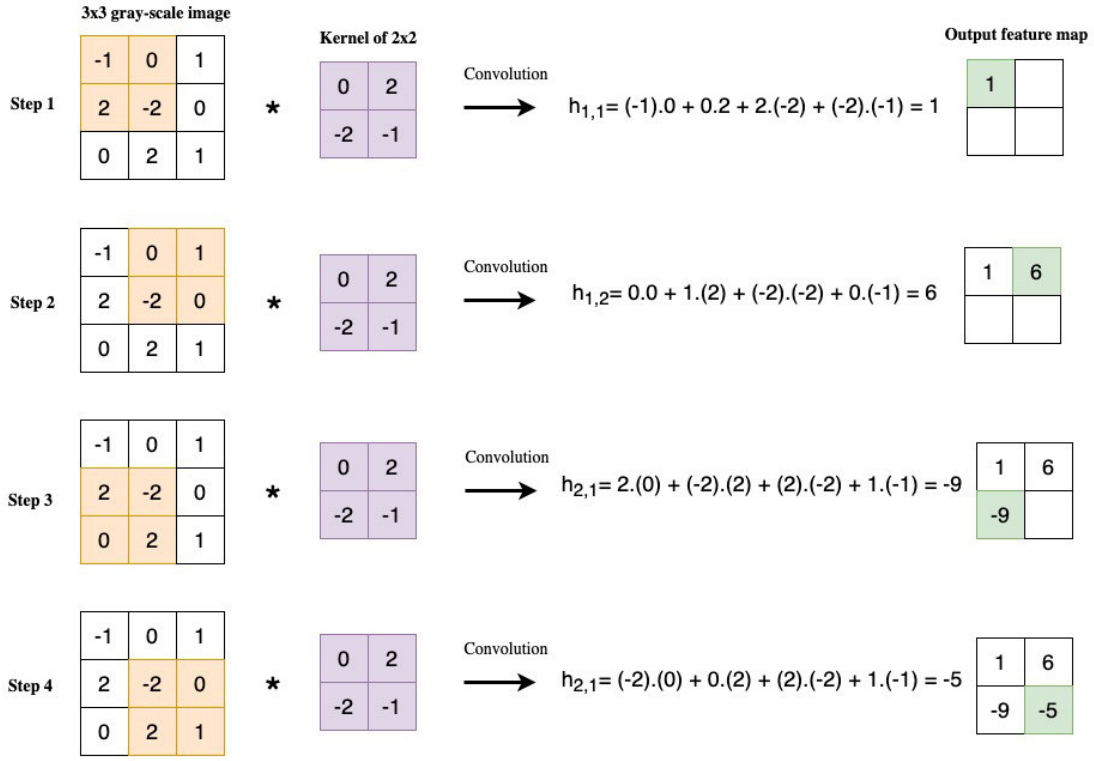

Figure 3.8: How the convolution operation works in the convolutional layer. For the example purpose, the stride is fixed to 1.

3.2.3 Convolution with Strides

The output feature maps, and the computed backpropagation gradients, necessitate that the convolutional layers be computed with enough available memory. As a result, the more convolutional layers in the network, the more memory is required for processing. Large images need a lot of GPU Memory space and can not be trained without using strided convolutions in those cases.

Therefore, the strided convolution reduces the output feature map size by omitting a number of pixels from the input feature map based on their position, lowering the computational training cost. Modifying Eq. (3.6), the strided convolution operation is then given by

$$\mathbf{Y}_{i,j,k} = \sum_{l,m,n} \mathbf{X}_{l,pj+m,pk+n}\, \mathbf{F}_{i,l,m,n}, \tag{3.7}$$

where p represents the strided pixels in row and column directions. The strided convolution operates as illustrated in Figure 3.9. In literature, various stride length estimation approaches have been developed to

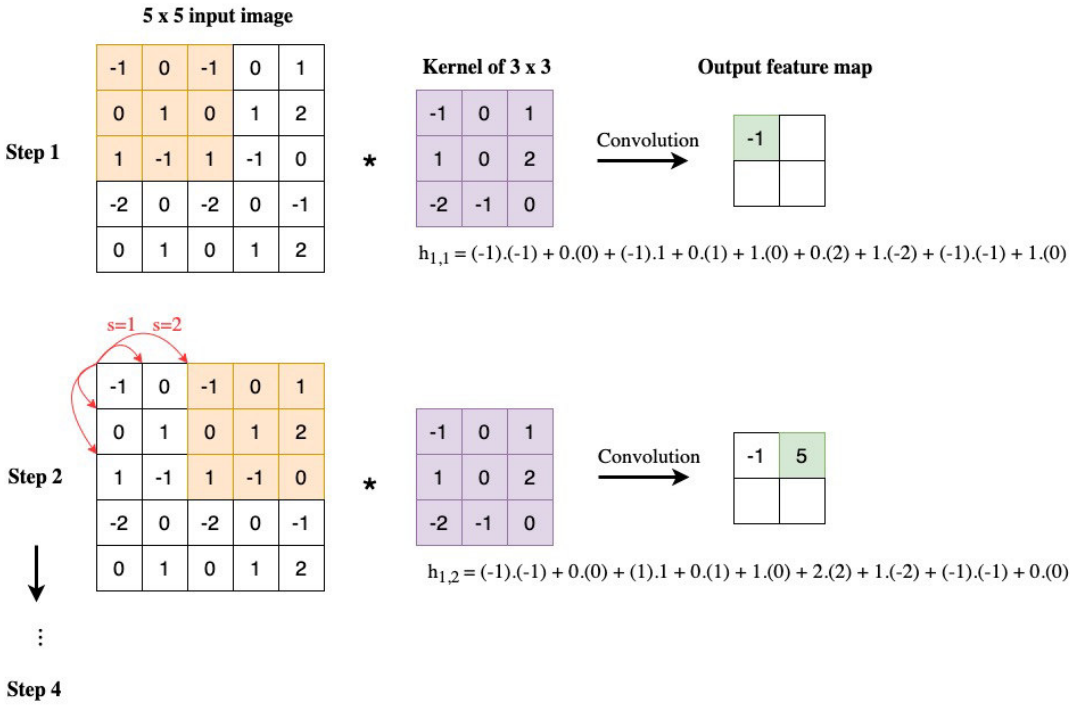

Figure 3.9: The convolution operation with stride = 2.

improve CNN training [179].

3.2.4 Pooling Layers

Pooling allows feature maps to be subsampled, resulting in smaller feature maps that are less susceptible to changes in the spatial position of the input pixels. As a result, each pooling layer preserves significant characteristics. Spatial reduction of feature maps in the pooling layer reduces both space and computational expense in the following convolutional layer, allowing more features to be processed.

Initially, LeNet used average pooling [180], which consists of averaging the pixels mapped by the kernel in the input features map. Currently, Max pooling is used by choosing the pixel with the largest value within the pixels mapped by the kernel. Other pooling methods were developed such as global average pooling (GAP), min pooling and gated pooling depending on the CNN architecture.

Other approaches such as residual networks [181] allow reducing the feature map sizes, operating almost like the pooling layer.

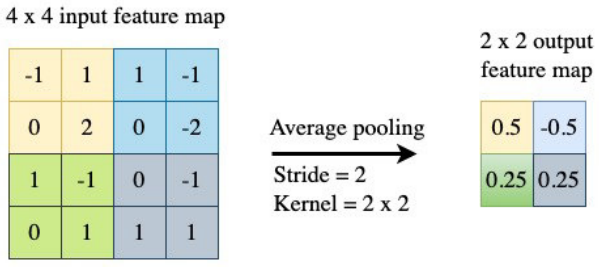

(a) The average pooling.

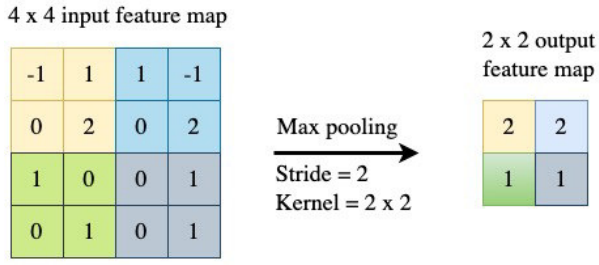

(b) The max pooling.

Figure 3.10: Average and Max pooling operation in a Convolutional Neural Network.

3.3 Recurrent Neural Networks (RNN)

After Lecun's achievement in recognizing handwritten text, he set other goals such as speech recognition and word translation, among others. With CNNs, images can be processed as seen in Section 3.2, since each image feature can be processed by the convolutional layers in a particular way and give the expected output. But with the voice signal, for example, the task becomes complex due to the amount of features to be analyzed and also due to the length of sequences that constitute human speech. Therefore, the challenge was how to modify the network architectures to receive an input data stream (sequences) instead of a compact batch of data such as an image?

A first attempt was Alexander Waibel's work in 1989 on Time Delay Neural Networks (TDNN) [182]. The particularity of TDNNs as opposed to traditional neural networks was that each neuron was responsible for only a subset of the data inflow and the inter-neuronal weights vary according to the inflow delays. A *moving window* is adopted for each input sequence and the neuron processes the data present in the window with different weight sets. The time dimension was subsequently added, comparing to how CNNs work, since the moving window changes and the output depends not on all the data flow but on the sequence present in the moving window.

Another attempt was how to add *memory* in neural networks to overcome the problem raised by sequence processing. Modifying typical network backpropagation such that they not only operate as inputs for the

neurons in the next layers, but also connect the neurons of the first layer with themselves. As a result, the information in the output can be stored in the network, and the network with memory challenge was partially solved. Then, the concept of recurrent neural networks (RNN) was born.

An RNN is a short-term memory unit with a hidden layer in addition to the input and output layers, as shown in Figure 3.11. The concept of recurrence is built by propagating the output layer backwards in time,

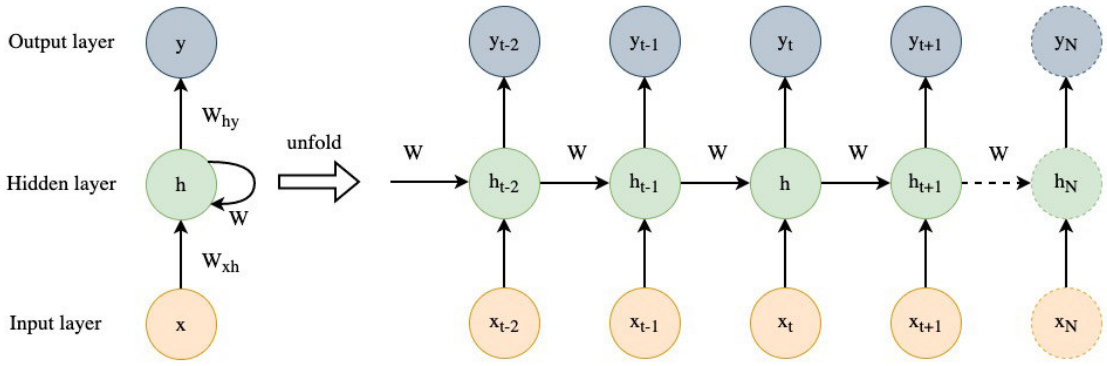

Figure 3.11: The recurrent neural network basic structure.

i.e., propagating the output in previous layers as they receive new sequences. To prevent the output from propagating forever across the network, the network is unfolded into a succession of local loops, with the output of one loop serving as the input of the next. However, in 1994, Bengio [183] raised some concerns regarding RNNs in these terms:

"Although recurrent networks can in many instances outperform static networks, they appear more difficult to train optimally. Our experiments tended to indicate that their parameters settle in a suboptimal solution which takes into account short term dependencies but not long term dependencies. For example in experiments, we found that simple duration constraints on phonemes had not at all been captured by the recurrent network. ... Although this is a negative result, a better understanding of this problem could help in designing alternative systems for learning to map input sequences to output sequences with long term dependencies, i.e., for learning finite state machines, grammars, and other language related tasks. Since gradient based methods appear inadequate for this kind of problem we want to consider alternative optimization methods that give acceptable results even when the criterion function is not smooth."

Next, Bengio *et al.* proposed a neuronal probabilistic language [184] model for natural language processing (NLP), predicting the occurrence frequencies of individual words or combinations of words.

Despite the efforts to process long sequences, the backpropagation applied in the recurrent neural networks did not give good performances, since the backpropagated error in the previous layers disappeared or exploded due to the large number of layers required for long sequences. The "vanishing or exploding gradient problem" arose, as mentioned by Jurgen Schmidhuber [185]:

"A diploma thesis [177] represented a milestone of explicit DL research. As mentioned in Sec. 5.6, by

the late 1980s, experiments had indicated that traditional deep feedforward or recurrent networks are hard to train by backpropagation (BP) (Sec. 5.5). Hochreiter's work formally identified a major reason: Typical deep NNs suffer from the now famous problem of vanishing or exploding gradients. With standard activation functions (Sec. 1), cumulative backpropagated error signals (Sec. 5.5.1) either shrink rapidly, or grow out of bounds. In fact, they decay exponentially in the number of layers or CAP depth (Sec. 3), or they explode."

To solve the problem of "exploding or vanishing gradients" in RNNs training, Schmidhuber and Hochreiter [5] proposed in 1997, the concept of Long Short Term Memory (LSTM):

"The basic LSTM idea is very simple. Some of the units are called Constant Error Carousels (CECs). Each CEC uses as an activation function f, the identity function, and has a connection to itself with fixed weight of 1.0. Due to f's constant derivative of 1.0, errors backpropagated through a CEC cannot vanish or explode (Sec. 5.9) but stay as they are (unless they "flow out" of the CEC to other, typically adaptive parts of the NN). CECs are connected to several nonlinear adaptive units (some with multiplicative activation functions) needed for learning nonlinear behavior. Weight changes of these units often profit from error signals propagated far back in time through CECs. CECs are the main reason why LSTM nets can learn to discover the importance of (and memorize) events that happened thousands of discrete time steps ago, while previous RNNs already failed in case of minimal time lags of 10 steps."

An LSTM Network consists of memory blocks, which are mainly composed of memory units storing the network's temporary states. The flow of sequences is controlled by recurrent connections within the network. Figure 3.12 presents an LSTM memory unit. Denoting by C_j the j^{th} memory unit, in_j and out_j

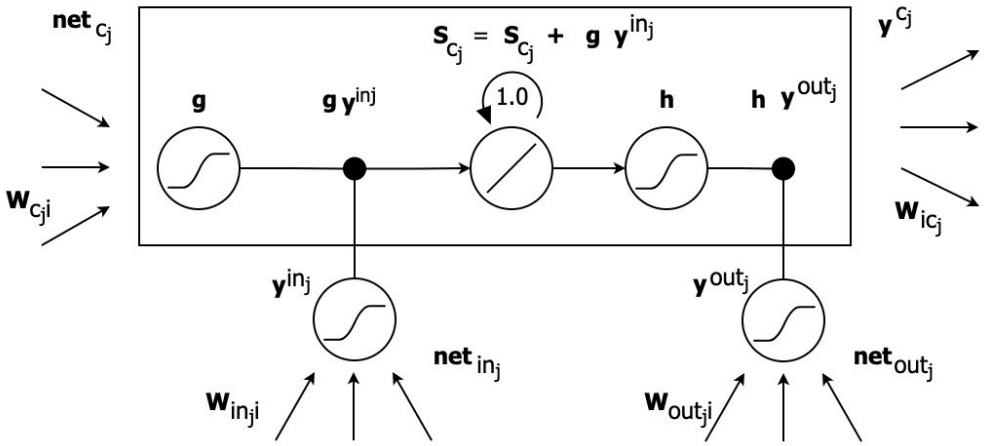

Figure 3.12: The LSTM memory unit C_j architecture as illustrated by Hochreiter and Schmidhuber presenting the LSTM concept [5].

the corresponding input and output gate respectively, activation at time t is presented by $y^{in_j}(t)$ for in_j and $y^{out_j}(t)$ for out_j. C_j receives input from multiplicative units Out_j and in_j, adding Net_{c_j}, to protect the stored information in j from being perturbed by unnecessary inputs. Each memory unit is based on a central linear

unit with a fixed constant error carrousel (CEC), which is specified by the identity function f_j as follows,

$$f_j : f_j(x) = x, \quad \forall x, \;\; W_{jj} = 1.0. \tag{3.8}$$

Therefore, the output gate activation at time t is given by:

$$y^{out_j}(t) = f_{out_j}(Net_{out_j}(t)), \tag{3.9}$$

$$y^{in_j}(t) = f_{in_j}(Net_{in_j}(t)), \tag{3.10}$$

where

$$Net_{out_j}(t) = \sum_u w_{out_j u} y^u(t-1), \tag{3.11}$$

$$Net_{in_j}(t) = \sum_u w_{in_j u} y^u(t-1), \tag{3.12}$$

$$Net_{C_j}(t) = \sum_u w_{C_j u} y^u(t-1), \tag{3.13}$$

considering u as memory units, input, hidden or gate units. Depending on the network topology which defines the recurrent connections ($W_{c_j c_j}$), the output $y^{C_j}(t)$ of C_j at time t is obtained as:

$$y^{C_j}(t) = y^{out_j}(t) h(S_{C_j}(t)), \tag{3.14}$$

where $S_{C_j}(t)$ represents the internal state, given by:

$$S_{C_j}(t) = S_{C_j}(t-1) + y^{in_j}(t) g(Net_{C_j}(t)), \;\; \text{for} \;\; t > 0 \;\; \textit{and} \tag{3.15}$$

$$S_{C_j}(0) = 0. \tag{3.16}$$

LSTM architectures generally depend on how the connections between memory blocks are defined [186], the number of memory unit blocks, the number of memory units per block, and how the weights are initialized. Other parameters regulating over-training or under-training (Dropout, data augmentation, batch normalization) and optimizing learning algorithms (such as Adam, Adagrad, Nadam and momentum) are added to the network architecture to achieve, for example, better classification of sequences.

3.4 Learning algorithms

The learning rate is one of the training hyperparameters of a deep learning neural network. Optimizing a hyper-parameter is one of the current training challenges of neural networks, in the sense that the optimal value is not known a priory for a known problem. In general, hyper-parameters optimal values can be found setting default values or those that worked in similar problems. It can be also found through trial and error.

The learning rate essentially uses the gradient descent algorithm to find the global minimum, thereby reducing the learning error. For a small learning rate it takes a long time to reach the local minimum of the cost function and for a large learning rate it may never reach the local minimum, making it difficult to reduce the learning error. In each training epoch, the network parameters (bias, weights, etc.) are updated while the network must minimize the error by estimating the optimized output. Therefore, the parameter update step size is defined as the learning rate and the training epoch as the repetition of the training data set taking into account the network parameter update.

The network parameter update is operated by the gradient of the cost function: a first-order derivative is calculated with respect to the privileged parameter, which is updated in the opposite direction of the gradient to minimize the error. The parameter update by the gradient is fed back to all the previous layer neurons.

The gradient descent-based algorithms for updating weights work as shown in Algorithm 2.

Algorithm 2 The descent gradient-based algorithms functioning.

Input: $E = epochs\_number$
Input: $b = batch\_size$
Input: $D = data$
Input: $L = loss\_func$
Input: $p = param$
Input: $W = weight\_act$
Output: $weight\_act$
random weights W
$i = 0$
for b *in* D **do**
  $grad\_param = evaluate\_gradient(L, b, p)$
  $weight\_act = past\_weight - learning\_rate * grad\_param$
  $i = i + 1$
end for

3.4.1 The Delta rule

The Delta rule, consisting of calculating the derivative of weights with respect to the output error in order to update the weights and make the training converge towards the local minimum, was first used to train single-layer neural networks using the gradient descent approach.

For a given training dataset $\mathbb{X} = \{\mathbf{X^1}, \mathbf{X^2}, \cdots, \mathbf{X^n}\}$, where $\mathbf{X^k} = [x_0^k,\ x_1^k,\ \cdots,\ x_N^k]^\intercal$ represents a training sample vector. The single-layer neural network output y_j^n is found as following:

$$y_j^n = f(a_j^n), \tag{3.17}$$

where a_j^n is the net activation given by:

$$a_j^n = \sum_i w_{ji} x_i^n, \tag{3.18}$$

with $w_{ji} \in \mathbf{W} = (w_{j0},\ w_{j1},\ \cdots,\ w_{jM})$ the weight to be updated. Assuming t_j^n as the expected output and the bias to 1, the prediction error between the real output y_j^n and the expected output t_j^n is done by:

$$err_j^n = y_j^n - t_j^n. \tag{3.19}$$

For a single sample, the global error is calculated summing the squared errors of each output:

$$E^n = \sum_j (err_j^n)^2, \tag{3.20}$$

Instead, the global error function can be rewritten, since its derivation does not change [187]:

$$E^n = \frac{1}{2} \sum_j (err_j^n)^2 \tag{3.21}$$

Then, the partial derivative of the global error of the network can be calculated as follows:

$$\frac{\partial E^n}{\partial w_{ji}} = \frac{\partial E^n}{\partial err_j^n} \frac{\partial err_j^n}{\partial y_j^n} \frac{\partial y_j^n}{\partial a_j^n} \frac{\partial a_j^n}{\partial w_{ji}}. \tag{3.22}$$

Calculating the 1^{st}, 2^{nd}, 3^{rd} and the 4^{th} differential factors of the right member in Eq. (3.22),

$$\frac{\partial E^n}{\partial err_j^n} = \frac{\partial (\frac{1}{2} \sum_j (err_j^n)^2)}{\partial err_j^n} = err_j^n, \tag{3.23}$$

$$\frac{\partial err_j^n}{\partial y_j^n} = \frac{\partial (y_j^n - t_j^n)}{\partial y_j^n} = 1, \tag{3.24}$$

$$\frac{\partial y_j^n}{\partial a_j^n} = \frac{\partial f(a_j^n)}{\partial a_j^n} = f'(a_j^n), \quad \text{and} \tag{3.25}$$

$$\frac{\partial a_j^n}{\partial w_{ji}} = \frac{\partial}{\partial w_{ji}} (\sum_i w_{ji} x_i^n) = x_i^n. \tag{3.26}$$

Therefore, Eq. (3.22) can be written as

$$\frac{\delta E^n}{\partial w_{ji}} = err_j^n f'(a_j^n) x_i^n. \tag{3.27}$$

The expression Δ_j^n defined by

$$\partial_j^n \equiv \frac{\partial E^n}{\partial a_j^n} = \frac{\partial E^n}{\partial err_j^n}\frac{\partial err_j^n}{\partial y_j^n}\frac{\partial y_j^n}{\partial a_j^n} = err_j^n f'(a_j^n), \tag{3.28}$$

represents the **error**, the **Delta** or the **local gradient**. Rewriting Eq. (3.27) with the **Delta** expression, Eq. (3.29) is found:

$$\frac{\partial E^n}{\partial w_{ji}} = \Delta_j^n x_i^n. \tag{3.29}$$

The weights w_{ji} are adjusted in the layers according to the Delta rule given by

$$\Delta w_{ji} = -\gamma\frac{\partial E^n}{\partial w_{ji}} = -\gamma\Delta_j^n x_i^n, \tag{3.30}$$

where γ is the learning rate or the step size.

3.4.2 The Momentum algorithm

The momentum, introduced by Polyak *et al.* [188] improved the gradient descent curvature minimizing the gradient variation. The weight update using the momentum algorithm accumulates multiple iterations gradients into a velocity gradient given by

$$\mathbf{V}_{t+1} = \alpha\mathbf{V}_t - \gamma\nabla E(\mathbf{W}), \text{ and} \tag{3.31}$$

$$\triangle\mathbf{W} = \mathbf{W}_t + \mathbf{V}_{t+1}, \tag{3.32}$$

where ∇E is the gradient, $E(\mathbf{W})$ the error surface of the weight vector $\mathbf{W}$, γ the fixed learning rate for iteration t, and α a factor modifying the actual velocity. The momentum uses the gradients calculated in past iterations to dampen the effect of a new gradient in the global-minimum direction of the cost function.

3.4.3 The Batch Gradient Descent (BGD) algorithm

For N training samples, weights are updated in each batch training and the gradient is found as:

$$\triangle w_{ij} = -\frac{\gamma}{N}\sum_{n=0}^{N}\frac{\delta E^n}{\delta w_{ji}} \tag{3.33}$$

The BGD method offers a fairly tight gradient in minimizing the error, despite being very costly to calculate over all training samples after each weight update.

3.4.4 The Stochastic Gradient Descent (SGD) algorithm

Instead of considering the entire training set to calculate the gradient at each weights update as with the BGD method, SGD uses a significant mini-batch of the dataset $\mathbf{X}$.

$$\triangle w_{ij} = -\frac{\gamma}{|\mathbf{X}_k|} \sum_{\{n|\mathbf{x}^n \varepsilon \mathbf{X}_k\}} \frac{\delta E^n}{\delta w_{ji}}, \tag{3.34}$$

where the mini-batch $\mathbf{X_k}$ has an adequate size to cover the training set distribution statistics. Note that a significant number of the classes in the training set should be captured by the mini-batch for a classification issue.

3.4.5 The Adaptive Gradient Algorithm (AdaGrad)

The AdaGrad algorithm adapts the learning rate to the weights, drastically updating weights that change occasionally while introducing minor modifications to weights that change frequently. AdaGrad greatly improves SGD robustness by training large-scale neural networks on Google [189].

Let $g_{t,i}$ be the gradient of the weight function with parameter ϕ_i in the time interval t,

$$g_{t,i} = \nabla_{\phi_t} J(\phi_{t,i}). \tag{3.35}$$

Therefore, the AdaGrad algorithm updates each parameter ϕ_i in time steps t as follows,

$$\phi_{t+1,i} = \phi_{t,i} - \eta g_{t,i}, \tag{3.36}$$

where η represents the general learning rate at each time step t. $G_t \in \mathbb{R}^{d.d}$ is the diagonal matrix where each diagonal element *i,i)* represents the gradients sum of past weights ϕ_i at time step t [190]. The small value parameter ε avoids divisions by 0. Hence, Eq. (3.36) becomes

$$\phi_{t+1,i} = \phi_{t,i} - \frac{\eta}{\sqrt{G_{t,ii} + \varepsilon}} g_{t,i}. \tag{3.37}$$

3.4.6 The Adaptive Learning Rate Method (Adadelta)

Instead of accumulating all past squared gradients, the Adadelta algorithm restricts the window of accumulated past gradients to a fixed size W. Therefore, it is defined as the decreasing average of the squared gradients after the sum of the gradients. The decaying average $E[g^2]_t$ of the gradient history depends on the previous average and the current gradient is:

$$E[g^2]_t = \gamma E[g^2]_{t-1} - (1-\gamma) g_t^2. \tag{3.38}$$

Recalling the diagonal matrix G_t with the decreasing average over past squared gradients $E[g^2]_t$,

$$\Delta\phi_t = -\frac{\eta}{\sqrt{E[g^2]_t + \varepsilon}} g_t = -\frac{\eta}{RMS[g]_t + \varepsilon} g_t, \tag{3.39}$$

where RMS is the mean square root given by

$$RMS[\Delta\phi]_t = \sqrt{E[\Delta\phi^2]_t + \varepsilon}. \tag{3.40}$$

Therefore, Eq. (3.38) becomes

$$E[\Delta\phi^2]_t = \gamma E[\Delta\phi^2]_{t-1} - (1-\gamma)\Delta\phi_t^2. \tag{3.41}$$

The Adadelta weights update rule is found as

$$\Delta\phi_t = -\frac{RMS[\Delta\phi]_{t-1}}{RMS[g]_t} . g_t, \tag{3.42}$$

$$\phi_{t+1} = \phi_t + \Delta\phi_t. \tag{3.43}$$

3.4.7 The Adaptive Moment Estimation (Adam)

The Adam algorithm also computes adaptive learning rates as Adadelta for each parameter and store an exponential decaying average of the past squared gradients v_t,

$$m_t = \beta_1 m_{t-1} + (1-\beta_1) g_t, \tag{3.44}$$

$$v_t = \beta_2 v_{t-1} + (1-\beta_2) g_t^2, \tag{3.45}$$

where m_t and v_t represent respectively the mean and the non-centered variance estimations of the gradients, from which the name of the algorithm comes. The first and second moments are estimated as

$$\hat{m}_t = \frac{m_t}{1-\beta_1^t}, \tag{3.46}$$

$$\hat{v}_t = \frac{v_t}{1-\beta_2^t}. \tag{3.47}$$

Then, using Adam algorithm, weights are updated as follows,

$$\phi_{t+1} = \phi_t - \frac{\eta}{\sqrt{\hat{v}_t} + \varepsilon} \hat{m}_t, \tag{3.48}$$

with $\beta_1 = 0.9$, $\beta_2 = 0.999$, and $\varepsilon = 10^{-8}$ as recommended by authors [191].

3.4.8 The Cyclical Learning Rates (CLR)

Developed by Smith [192] in 2017 as an alternative to accelerate convergence to the global minimum and avoid local minima, this method allows the learning rate to vary cyclically between reasonable limit values. The strategy used here is to allow the learning rate to vary cyclically within a range of values instead of adopting a stepping or exponentially decreasing fixed value, as with the algorithms discussed above. A

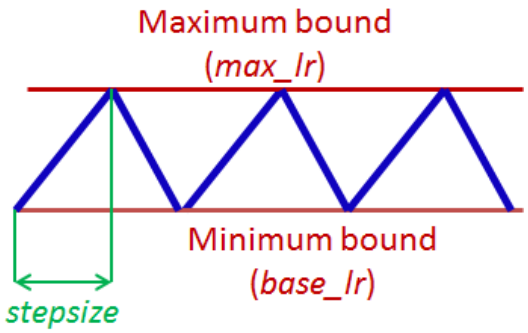

Figure 3.13: The triangular learning rate. The blue lines represent the learning rate values that change between chosen limits. The input parameter *stepsize* is the number of iterations in half a cycle.

triangular window was adopted because the triangular function increases and decreases linearly, which better implements this algorithm that seeks to vary the learning rate between two limits. The stepsize parameter and the cycle duration are defined based on the number of iterations per epoch, obtained by dividing the training data by the batch size.

The minimum and maximum values of the learning rate are estimated by training the constructed network with few iterations, and the range with the most values is chosen according to the Accuracy metric or the range with the least values of the rate with the Loss metric. The cyclic algorithm was implemented in Torch 7 as follows:

Algorithm 3 The Cyclical Learning Rates algorithm.

Input: epochCounter, stepsize, maxLR, opt_LR
Output: local_lr

13 local $cycle$ = math.floor$(1 + epochCounter/(2 * stepsize))$:
local $_x$ = math.abs$(epochCounter/stepsize - 2 * cycle + 1)$
local lr = opt_LR + $(maxLR - opt\_LR)$ * math.max(0, (1 - x))
return *local_lr*

where opt_LR is the minimum learning rate, $epochCounter$ the number of training epochs and lr the calculated learning rate.

3.5 Activation functions

Considering such a perceptron presented in Figure 3.14, the threshold or the activation function drives the neuron output to obtain a binary prediction or classification. The output in this case is given by:

$$y = f(Neur_j + bias_j), \tag{3.49}$$

where the neuron activation $Neur_j$ could be written as following:

$$Neur_j = \sum_{i}^{N} w_{ji} x_i. \tag{3.50}$$

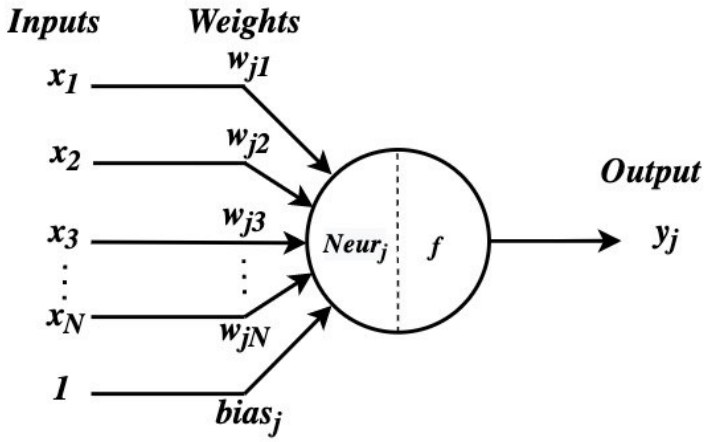

Figure 3.14: The activation function of the single-layer neural network.

Considering the input vector $\mathbf{x} = (x_1, x_2, \cdots, x_N)$, the weights vector linked to the neuron j, $\mathbf{w}_j = (w_{j1}, w_{j2}, \cdots, w_{jN})$, and the bias b_j, Eq. (3.49) can be written as:

$$y = f(\mathbf{w}_j^T \mathbf{x} + b_j), \tag{3.51}$$

where f represents the activation function and b_j the bias. For the Perceptron, the activation function is the Heaviside step function,

$$f(x) = \begin{cases} 1 & \text{if } x \geq 0 \\ 0 \ (or -1) & \text{Otherwise.} \end{cases} \tag{3.52}$$

The activation function can be linear and as the number of neurons increases, the compound activation function remains linear since the composition of the linear functions remains linear. To allow the multi-layer

neural network to learn complex non-linear cost functions, the activation function needs to be non-linear. Among the activation functions used in neural networks, are:

- **Sigmoid function**: this activation function maps positive inputs to positive outputs and negative inputs to negative outputs with a smooth transition around $x = 0$. Eq. (3.53) represents the logistic sigmoid function and Eq. (3.54) the hyperbolic tangent function.

$$f(x) = \frac{1}{1+e^{-x}} \tag{3.53}$$

$$f(x) = \frac{e^{x} - e^{-x}}{e^{x} + e^{-x}} \tag{3.54}$$

- **Rectifed Linear Activation Function (ReLU)**: proposed by Glorot *et al.* for neural networks [193], this activation function avoids the saturation of sigmoid functions and requires fewer computational resources, offering gradients between 0 and 1.

$$f(x) = max(0,x) \tag{3.55}$$

- **Leaky ReLU**: The Leaky ReLU activation function supports even negative inputs, ignored by the ReLU function. Its mathematical representation is as follows:

$$f(x) = \begin{cases} x & \text{if } x > 0 \\ mx & \text{if } x \leq 0, \end{cases} \tag{3.56}$$

  with m set to a small value.

3.6 Chapter Conclusion

This chapter presented a synthesized history of artificial neural networks as an introduction, recalling the great steps taken over time with them. The content focused mainly on two types of network structures: the CNN and the LSTM networks, used in this doctoral project.

Some learning algorithms and frequent activation functions were presented to understand the training mechanism of artificial neural networks. The next chapter introduces the methods used in this doctoral proposal to achieve the stated objectives.

Chapter 4

Proposed Methodologies

"True progress is what makes technology available to everyone".

Henry Ford

This chapter presents the three methods developed in this doctoral thesis: Method-one develops an embedded BCI system based on the EMOTIV EPOC+ capture system, the FPGA Cyclone V SoC developer board and the hexapod robot, as shown in Figure 4.1. Method-two and method-three focus on EEG signal processing using the same public database but developing two different approaches. A conclusion summarizing the three methods is presented at the end of the chapter.

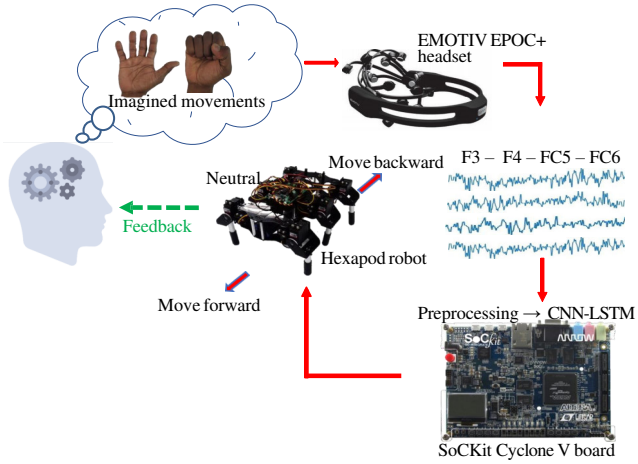

Figure 4.1: The proposed Method-one flowchart.

4.1 Proposed method-one

This method develops a BCI system by interconnecting an EMOTIV EPOC+ headset, an Altera SoCKit Cyclone V SoC board, and a hexapod robot as an application. For this purpose, a database of robot basic movements (forward, backward, and stop) with four test subjects was created. The recognition process was carried out using a CNN-LSTM architecture. The constituted BCI system transforms the continuous MI-EEG signals into command instructions to control a hexapod robot's locomotion.

4.1.1 The method-one framework

The EEG signal acquisition system is chosen following pragmatic criteria such as market accessibility, portability, resolution, sampling rate, compatibility, and scalability [194]. An EMOTIV EPOC+ headset consists of sixteen electrodes to be placed on the scalp according to the 10-20 international system of EEG electrode placement. Figure 4.1 shows the proposed method's flowchart using an EMOTIV EPOC+ for capturing EEG signals and a CNN-LSTM architecture implemented on the SoCKit to control robot movements.

The robot perception and control are conceived to operate in real-time. Simultaneously, data are stored on the SoCKit. The zoomorphic robot used has two degrees of freedom in each leg. The EEG signals for the imagined closing-opening right and left fists are captured by $F3$, $F4$, $FC5$, and $FC6$ electrodes and sent to the SoCKit platform. The CNNs process the EEG data and extract feature sequences. Finally, a recurrent neural network followed by a dense layer classifies these feature sequences into robot locomotion commands. In total, twelve servomotors quickly achieve static and kinematic stability.

4.1.2 The BCI Dataset

The test subjects provided written consent to capture the EEG signals after carefully reading the experimental protocol to protect confidentiality. The specialized equipment used in the experiment was entirely commercial, not presenting any potential risk to the participants. Seven subjects were initially selected for the training process, and after addressing the defined paradigm, only four followed an individual schedule.

Before and during each training session, the Emotiv Software Development Kit (Emotiv Xavier) monitored the subject's cognitive and emotional performances [195]. Hence, a dataset was created selecting four test subjects between 23 and 36 years old, trained and supervised to collect signals during several experimental tasks lasting three seconds each. According to the given task, subjects were instructed to stay still during the capture and invited to imagine closing and opening the right or the left fist focused on a stimulus video (Figure 4.2).

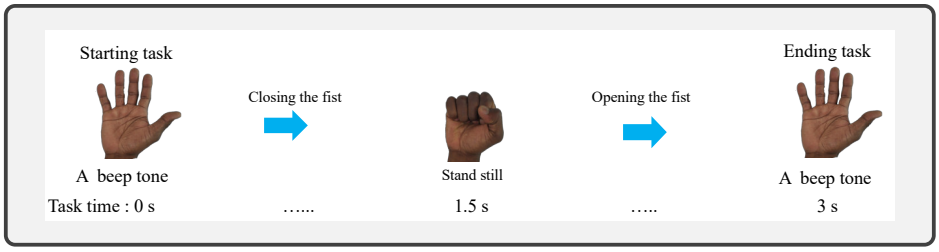

Figure 4.2: The MI task video serving as a subject stimulus. The task starts with a beep tone by closing the fist completely and opening the same fist until the end beep appears. Each task lasts 3 s.

The stimuli video of the fist closing-opening movements was played on the screen according to the temporal task sequence shown in Figure 4.3.

In the capture sequence, the first five seconds served to prepare the test subject, ending this phase with the audible Beep 1, followed by Task 1, related to the left fist MI action. The Beep 2 tone concludes this period and marks a pause of 3 s. Beep 3 triggers the end of this static period and starts a second preparation phase of 2 s. Beep 4 starts Task 2, related to the right fist MI task, ending with Beep 5. Therefore, the developed dataset consists of 2400 trials performed by four subjects (600 trials from each subject), representing 2400 $\times$ 19 s (12.67 h) of data capture. For each session duration, only signals of 3 s corresponding to Task 1 (left fist MI), 3 s to Task 2 (right fist MI), and 3 s to neutral action were gathered to build the dataset.

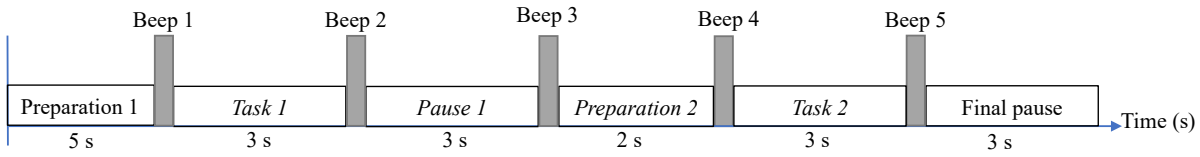

Figure 4.3: Time sequence of each trial. The total trial duration was established at 19 s, where 6 s were used for the related MI tasks: the left fist as Task 1 (3 s) and the right fist as Task 2 (3 s). The neutral or reference action was taken as the final pause (3 s) to have an equal number of samples per class.

4.1.3 Data Preprocessing

Signals from the F3, F4, FC5, and FC6 sensors were processed in the MI recognition process [196]. The Emotiv EPOC+ headset was configured with three filters: a low-pass filter with a cutoff frequency at 85 Hz, an operational bandwidth between 0.16 and 43 Hz, and a band-rejection filter with a stop-band between 50 and 60 Hz [195].

According to the International EEG Waveform Society, the project paradigm is based on the *mu rhythm* processing, which occupies frequencies between 8 and 12 Hz [197]. Such sensors were located in the rear portion of the frontal lobe, as shown in Figure 4.4.

(a) Emotiv EPOC+ headset. (b) Electrode headset location.

Figure 4.4: Electrodes' arrangement and nomenclature. The letter expresses the part of the brain where the sensor is placed, frontal (F), central (C), parietal (P), occipital (O), temporal (T), and frontoparietal (FP). Even numbers are used for the right hemisphere, while odd numbers for the left hemisphere.

The mu rhythm is the most used pattern in BCI systems considering the nature of the MI movements [48]. Thus, the mental imagery of body members' mobility can be perceived through the mu rhythm variations at the sensorimotor cortex, avoiding any real movement of the body limbs [198]. Lotze et al. determined that the left and right hands' physical movements cause an Event-Related Desynchronization (ERD) of the mu rhythm power, captured in different motor cortex areas [199].

Consequently, the $F3$ and $FC5$ electrodes were selected for the left hemisphere, whereas $F4$ and $FC6$ for the right hemisphere on the sensorimotor cortex. Such a choice takes into account the sensor's closeness to the primary motor cortex location associated with the imagined and physical movements of the left and right hands [196].

4.1.4 SoCKit board Configuration

The SoCKit Cyclone V FPGA card powered by an ARM Cortex® A9 Hard Processor System (HPS) was used to implement the EEG signal processing algorithms and the classifier. Figure 4.5 shows the basic SoCKit functional blocks.

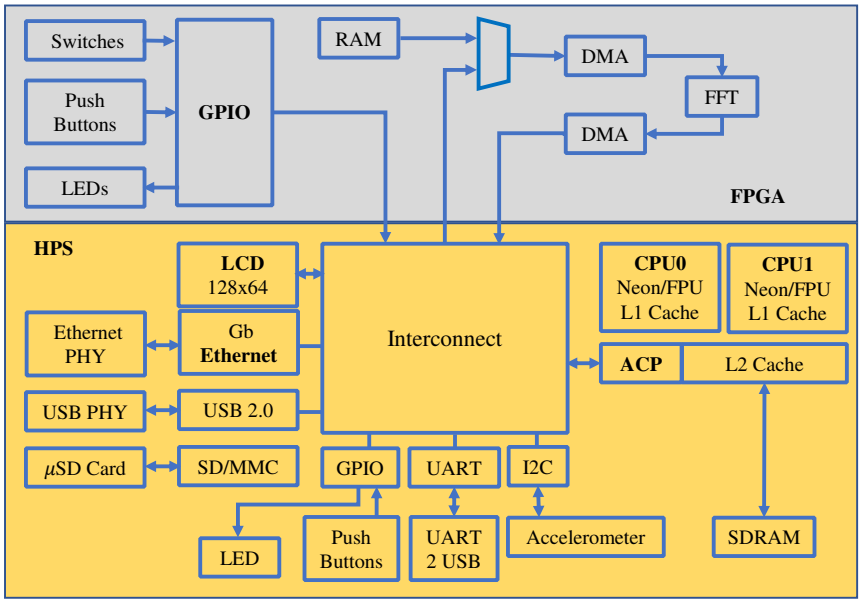

Figure 4.5: The SoCKit functional diagram consists of two main parts: the basic FPGA module and a Hard Processor System (HPS). Main modules include the Floating Point Unit (FPU), Accelerator Coherency Port (ACP), Secure Digital MultiMedia Card (SD/MMC), and Direct Memory Access (DMA).

The algorithms' implementation was designed and tested under Xillybus for SoCKit Linux distribution (Xillinux) [1] based on Ubuntu 12.04 LTS.

Communications were established between the processor and the FPGA core by configuring the Xillybus Intellectual Properties (IPs) Core, as showed in Figure 4.6.

Emotiv EPOC+ data writing (rd-en) is enabled as First-In, First-Out (FIFO) when it is empty. After reading the data, the Xillybus communicates with the processor core using the Advanced eXtensible Interface (AXI) bus, generating Direct Memory Access (DMA) requests on the central CPU bus. Simultaneously, the low-level FIFO (FPGA) is released (the full-en signal is low), and Xillybus carries the data from the processor core to the FPGA to control the hexapod.

The project Xillybus IPs Core was designed to use four FIFOs, two focused on reading and two others on writing data. Each FIFO was configured to a 32 bit data width, a data transmission latency of 5 ms, a bandwidth of 10 MB/s, and a buffering time to autoset.

[1] https://www.terasic.com.tw/wiki/images/e/ef/Xillybus_getting_started_sockit.pdf (accessed on 7 February 2019)

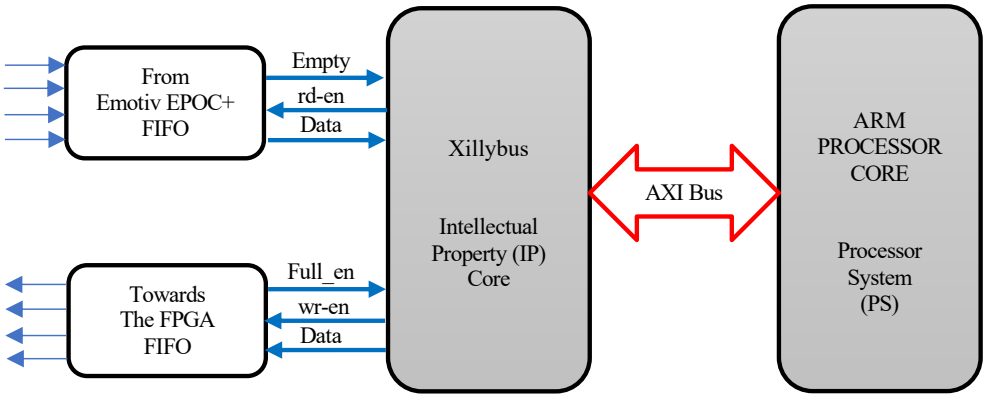

Figure 4.6: The Xillybus IPs Core was used as a data transport mechanism and configured to interconnect the processor core with the FPGA. The primary control signals include the write enable (wr-en), read enable (rd-en), and FIFO full enable (Full-en). Adapted from Xillibus Ltd.

The FPGA is internally forced to control the buffer RAM distribution for continuous reading and writing operations by configuring the buffering time to autoset and specifying the planned period for the maximal processor deprivation. The following equation gives the RAM size required for the DMA buffers' flow:

$$RAM = t \times BW \tag{4.1}$$

where t is the buffering time and BW is the expected data bandwidth. For reading, all FIFOs must be empty, and the enable signals (rd-en) activated. Thus, EEG data can fill the FIFOs until they all are full and the empty signal is disabled.

Since FIFOs work with 32 bit and considering that the Emotiv EPOC+ device has a 14 bit resolution, a zero-padding operation was applied to each signal at the Most Significant Bit (MSB) position. As in the previous procedure, writing is enabled (wr-en at the high level) when all write FIFOs are empty (low level). Therefore, a finite state machine was designed to control the FIFOs' filling and emptying processes. The EEG signal reading, processing, and classification algorithms were written in Python, the Verilog Language, the ANSI-C language (Nios® II Embedded Design Suite), and the Open Computing Language (OpenCL Standard) [200], which were tested and evaluated on the SoCKit. Table 4.1 summarizes the SoCkit resources used in the implemented experiments. FPGA outputs were wire-connected to the hexapod servo-control board. The Central Pattern Generator (CPG), based on discrete-time neural networks, was adapted to move the hexapod robot [201]. The locomotion law defined by the CPGs and derived from the discrete-time spiking neuronal model [202] is mathematically described by:

$$V_i[k] = \gamma(1 - Z_i[k-1])\,V_i[k-1] + \sum_{j=1}^{12} W_{ij} Z_j[k-1] + I_i^{ext}, \tag{4.2}$$

where Z_i is the firing state of the i^{th} neuron at time k, V_i is the potential membrane, W_{ij} is the synaptic

Table 4.1: SoCKit resources and materials deployed for the project implementation. HPS, Hard Processor System.

Label	Characteristics
SoCKit board	Altera Cyclone V SoC ARM, 5CSXFC6D6F31C8NES model, dual-core, ARM Cortex-A9 (HPS), 6 fractional Phase-Locked Loops (PLLs), 3.125G transceivers
FPGA memories	1 GB (2×256 MB $\times 16$) DDR3 SDRAM
HPS memories	1 GB (2×256 MB $\times 16$) DDR3 SDRAM, 64MB Quad Serial Peripheral Interface (QSPI) Flash
Display	24-bit VGA DAC; 128×64 dots LCD module
SD card image	64 GB, speed: Class 4
FPGA FIFO	Word length of 32 bit, transfer rate of 10 MB/s, filling time of 0.2 ms
Number of FIFOs	Four: two for downstream and two for upstream
DMA buffer memories	Autoset internals (automatic memory allocation)
Emotiv to FPGA streams	Delay time of 10 ms
Xillybus IPs Core latency	5 ms
FPGA to hexapod streams	Delay time of 10 ms
Clock frequencies	25, 50, and 100 MHz
FPGA configuration	Quad serial configuration device EPCQ256
Power consumption	1.023 W (internal power evaluation)
SSC-32 V2.0 card (Figure 4.7)	Channel servo controller, from 0.50 to 2.50 ms
USB-TTL adapter	USB to UART converter module

influences (weights), I_i^{ext} is the external current, and γ is a dimensionless parameter. Mainly, $Z_i[k]$ is defined as a thresholded Heaviside function.

Moreover, considering that twelve servomotors control the hexapod movements, twelve neurons were required in this model; the input current was not needed (i.e., $I_i^{ext} = 0$), and $\gamma = 1$ to emulate a linear integrator.

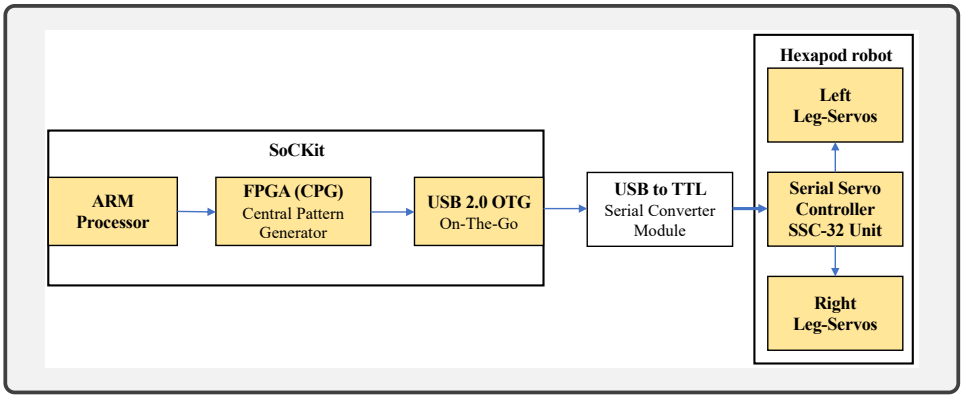

Figure 4.7: SoCKit-hexapod robot interconnection using a USB-TTL adapter and an SSC-32 V2.0 board.

4.1.5 MI-EEG Signals Classification Based on a CNN-LSTM Architecture

Recurrent neural networks (e.g., LSTM networks) are composed of memory units that temporarily store information [203]. Such a network's layer structure is not unique because the interconnections between neurons are not based on a transportable (mutable) logic. The feature extraction and classification of EEG signals are done by combining two neural schemes, the CNN and LSTM. Figure 4.8 presents the CNN-LSTM architecture integrated into the SoCKit to decode robot commands. The overall network consists of a sequence of layers: a convolutional layer (CNN1), an LSTM layer (LSTM1), a convolutional layer (CNN2), followed by a max-pooling layer, a convolutional layer (CNN3), an LSTM layer (LSTM2), and a dense layer.

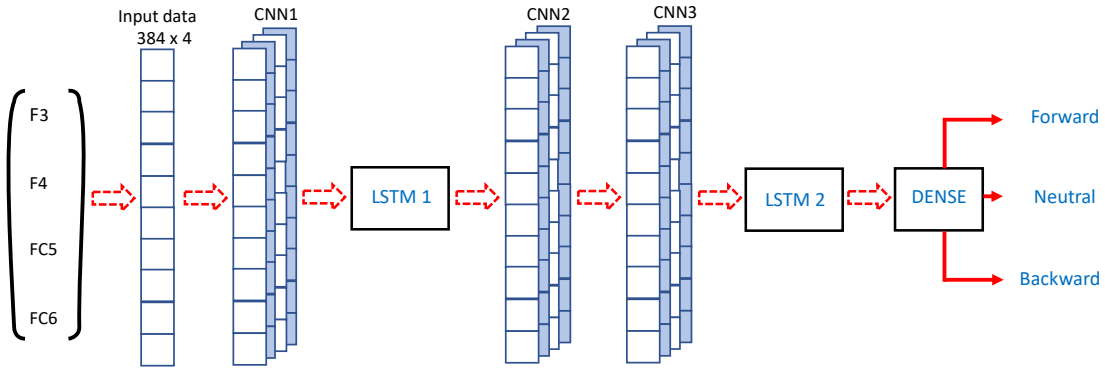

Figure 4.8: The proposed CNN-LSTM network architecture. A convolutional layer extracts features from preprocessed data, followed by an LSTM layer and two CNN layers, directly connected to a second LSTM layer and a dense layer to classify MI-EEG signals into the robot commands.

A 384×4 matrix was applied as the input to the CNN1 layer, which performed 32 convolutions with a 3×3 size kernels. In each convolutional layer (CNN1, CNN2, and CNN3), the padding parameter was

configured to have the same temporal dimensions between input and output data. Weights were initialized according to a uniform distribution using the *He* initialization algorithm [204]. Dropout was applied to each convolutional layer with parameters tuned to 0.4, 0.2, 0.2, and 0.1 for the CNN1, CNN2, CNN3, and LSTM2 layers, respectively. According to the deep learning software package Keras [205], for a dropout rate of 0.1, only 10% of the neurons are disconnected during the training phase, which reduces overfitting (overtraining).

On the other hand, LSTM layers contain 32 and 150 cells and receive feature matrices from convolutional layers for processing. The model was implemented in Keras and TensorFlow using the categorical cross-entropy loss function to evaluate the error between the estimated outputs and the ground-truth. The network was trained for 8000 epochs to meet the max accuracy, using the Nesterov-accelerated Adaptive Moment Estimation (NADAM) optimizer with a batch size of 512.

A cyclical learning rate with a step-size of nine and minimum and maximum learning rates of 0.000001 and 0.0005, respectively, was used to speed up training [192]. The convolutional layers used the leaky Rectified Linear Unit (ReLU) as the activation function with $\alpha = 0.005$. This allowed obtaining a small non-zero gradient when a neuron has a negative net input. The leaky ReLU activation function $f(\alpha;x)$ is defined by:

$$f(\alpha;x) = \begin{cases} \alpha x & \text{if } x < 0 \\ x & \text{otherwise} \end{cases} \tag{4.3}$$

where α is a small positive constant [206].

However, *SoftMax* was used as the activation function of the fully connected layer following the LSTM2 layer to normalize the outputs, such that they may be interpreted as class probabilities [207].

The convolutional layer CNN1 has only 416 parameters, while the CNN2 and CNN3 layers have 3104 parameters each. It must be highlighted that CNNs do not require a specially designed feature extraction stage because they can perform adaptive feature extraction directly on raw input data. Therefore, there were 125,197 parameters necessary for all layers. The output used a fully connected layer with *SoftMax* as the activation function, which produces the three class probabilities. During the neural network training, the neuron weights were randomly initialized using the *He* initialization algorithm. Table 4.2 depicts the principal parameters of the proposed network model.

Table 4.2: Summary of the parameters of the CNN-LSTM architecture.

Layer	Filters/Cells/Rate	Output Shape	Parameters
CNN1	32	(None, 384, 32)	416
Dropout1	0.4	(None, 384, 32)	0
LSTM1	32	(None, 384, 32)	8320
CNN2	32	(None, 384, 32)	3104
Dropout2	0.2	(None, 384, 32)	0
Max-pooling	32	(None, 192, 32)	0
CNN3	32	(None, 192, 32)	3104
Dropout3	0.2	(None, 192, 32)	0
LSTM2	150	(None, 150)	109,800
Dropout 4	0.1	(None, 150)	0
Dense	1	(None, 3)	453

4.2 Proposed method-two

EEG signals measured by non-invasive systems are difficult to classify because of noise added in the sensors, which leads to a low Signal-to-Noise Ratio (SNR). Besides, the electrodes placed physically over the scalp produce a loss of signal potential due to volume conduction effects [208]. In all, the processing and classification of MI-EEG signals generated during the imagined finger movements present other significant technical challenges. Large limb movements imply a substantial number of inter-neuronal connections because the involved muscles require a more significant amount of energy than the fingers [209]. Therefore, the classification of imagined finger movements becomes complex because the fingers move closely together, and specific individual moving features merge.

This approach aims to process and classify MI-EEG signals of individual finger movements from one hand by addressing the problem of noisy signals using a method based on EMD and using more powerful sequence classification architectures, including BiLSTM Recurrent Neural Networks (RNN).

4.2.1 Overall flowchart

The channels $C3$, Cz, $P3$, and Pz were selected to decode the right-hand finger movement in MI-EEG signals. This choice considers channels focused on the primary motor cortex (M1) and the cerebellum, involved in the motor imagery signals generation [199].

The fact that right-hand finger imagery movements activate the left cerebral hemisphere and the left-hand finger imagery movements activate the right one, $P3$ and $C3$ electrode signals are processed, including

those from Cz and Pz for the cortex activation maps during the predefined tasks [209, 210]. In addition, the $\{C3, Cz, P3, P3\}$ combination revealed a better decoding accuracy among the $\{C3, Cz\}$, $\{C3, P3\}$, $\{C3, P3, Cz\}$, $\{C3, P3, Cz\}$, and $\{T3, C3, Cz\}$ combinations evaluated in the electrode preselecting step.

Figure 4.9 shows the head positioning configuration of the corresponding electrodes, which are the most representative and discriminant electrodes in the proposed tasks. Furthermore, Figure 4.10 shows the

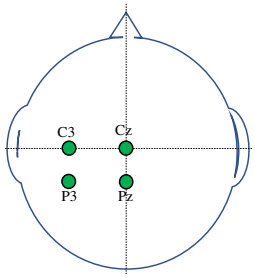

Figure 4.9: Sensors selection from a Nihon Kohden-Japan EEG-1200 JE-921A equipment. MI-EEG signals from four sensors on the left sensorimotor and cognitive cortex were selected (see Table 2.3).

flowchart of the proposed approach.

4.2.2 The EEG Dataset

The employed dataset was built by Kaya *et al.* [128], considering five interaction paradigms related to motor imagery. In particular, the focus of interest in this approach relies on the MI of five right-hand fingers, corresponding to paradigm #3 (5F). The subset of the dataset corresponding to the finger movement imagery consisted of MI-EEG signals from eight subjects captured with the Nihon, Kohden-Japan EEG-1200 JE-921A equipment. Two women and six men aged between 20 and 35 produced 19 file sessions of 4,600 MI-EEG samples per subject. This dataset provided 45 minutes of MI-EEG for all subjects divided into three interaction segments; each segment consisted of the presentation of about 300 MI symbols. The equipment uses 22 electrodes; 19 are active and distributed according to the international standard 10-20 for EEG electrode positioning, shown in Table 2.3. In the creation protocol of the dataset, the developers assert that the test subjects were declared in good physical and mental health at the capture time.

A recliner chair, suited for all participants, was placed at 200 cm from a monitor and slightly above the reference eye. Later, an eGUI displays the five fingers of the right hand. When a number from one to five is displayed just above a finger as a signal for starting the task, the test subject executes the corresponding imagery movement for one second.

Hence, digits 1, 2, 3, 4, and 5 correspond to the thumb, index finger, middle finger, ring finger, and pinkie finger, respectively. The task involves the imagination of the flexion from a finger up and down. This paradigm does not have a neutral state since signals related to this task were not considered in the original dataset.

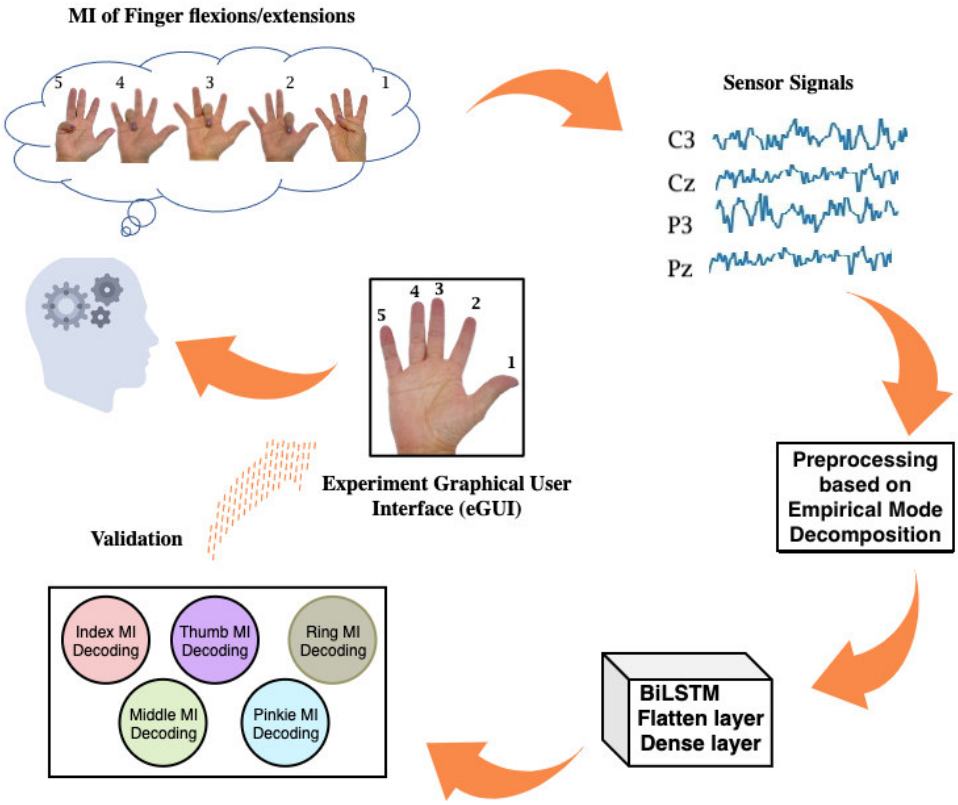

Figure 4.10: MI-EEG signal processing flowchart. The stimulus appears on the experimental Graphical User Interface (eGUI) represented by a number from 1 to 5 directly above the finger. During this period, the MI flexion-extension of the corresponding finger is generated. Next, captured MI-EEG signals from $C3$, Cz, $P3$, and Pz electrodes are processed for each individual.

MI-EEG signals were recorded at 200 and 1000 Hz, where the latter is referred to as a High Frequency (HFREQ). The 5F dataset contains thirteen HFREQ files and six files at 200 Hz collected between 2015 and 2016. Software Neurofax [211] served to bandpass filter the raw MI-EEG signals from 0.53 to 70 Hz for 200 Hz and from 0.53 to 100 Hz for HFREQ signals. Signals from each sensor are arranged into a matrix as follows

$$\mathrm{EEG(t)} = \begin{pmatrix} x_{1,1} & \cdots & x_{1,m} \\ \vdots & \ddots & \vdots \\ x_{n,1} & \cdots & x_{n,m} \end{pmatrix}, \tag{4.4}$$

where n and m are the number of samples and the number of signals, respectively. All 19 files (13 HFREQ and six files at 200 Hz) from the 5F dataset containing the captured signals (lasting from 3582 to 4040 seconds) were retrieved to be directly utilized in the proposed signal processing framework. It is because a preliminary preprocessing was applied during and after capturing in the creation of the dataset [128].

4.2.3 EEG signal preprocessing based on EMD

One problem when dealing with EEG signals is that they are inherently non-stationary. This phenomenon is because brain processes change due to brain state changes, *i.e.*, mental fatigue [212]. This non-stationarity has severe implications for the generalization ability of deep neural network architectures [213].

Current approaches for dealing with non-stationarity are mainly based on trend removal. The main trend removal approaches are high-pass filtering, moving average removal, polynomial fitting, and empirical mode decomposition.

Among high-pass filtering approaches, empirical mode decomposition is one of the most reliable methods in terms of efficiency and simplicity [214]. The EMD method decomposes a signal into an Intrinsic Mode Functions (IMFs) sum.

The IMFs obtained from natural EEG signals provide analytical features (amplitudes, frequency, and phase), which improve the BiLSTM learning algorithm. It is a specific benefit of the EMD approach targeted with this signals preprocessing method.

Empirical Mode Decomposition (EMD) is a signal processing tool proposed by Huang *et al.* to analyze nonlinear and non-stationary signals [215]. IMFs must fulfill the following constraints:

1. The number of local extrema and zero crossings must be equal or differ by at most one on the entire signal.
2. The mean value between the lower and upper envelope must be zero.

EMD can be used to denoise 1-D EEG signals because of the frequency-decreasing property of IMFs [216]. The IMFs represent the oscillation modes in the signal, so the first IMF contains the highest frequency, and the last IMF contains the lowest frequency. Algorithm 4 shows the steps performed by the EMD algorithm. Once completed the sifting process, the original MI-EEG signal can be recovered as follows

$$\text{EEG} = \text{IMF}_1 + \text{IMF}_2 + \cdots + \text{IMF}_N + R_N, \tag{4.5}$$

where N is the number of computed IMFs from the original EEG signal, and $R_N(t)$ is the final residue. EMD operates similarly to a filter bank of bandpass filters for modes with indexes greater than 1 and a high-pass filter for mode 1 [217]. Therefore, Eq. (4.6) describes the signals relations obtained when the first EMD step is applied to the EEG signal,

$$\text{EEG}(t) = C_1(t) + \text{IMF}_1(t), \tag{4.6}$$

where $C_1(t)$ represents the low-frequency components of the signal.

Huang *et al.* developed a method that allows determining the number of iterations to stop the sifting process [218]. This method is based on two criteria:

1. All local maxima are strictly positive, while all local minima are strictly negative; and

Algorithm 4 MI-EEG Signal Decomposition using EMD.

1: Let x_t be an EEG signal.
2: Find the $\max(x_t)$ and $\min(x_t)$.
3: Use the Cubic Spline interpolation to construct the upper $e_u(t)$ and lower $e_l(t)$ envelopes connecting all $\max(x_t)$ and $\min(x_t)$ points separately.
4: Calculate the local Mean: $mean(t) = \frac{1}{2}\{e_u(t) + e_l(t)\}$.
5: Obtain $R(t) = x(t) - mean(t)$.
6: Conclude the i^{th} IMF order if $R(t)$ satisfies the given IMF conditions with $IMF_1(t) = R(t)$, otherwise repeat steps 1 to 5 ($x(t) = R(t)$).
7: Find the remaining $IMF_i(t)$ component by subtracting $e_u(t)$ - $IMF_1(t)$ and repeating the sifting process until to obtain a constant residue $r_N(t)$ (no more oscillations).
8: The decomposed signal $x(t)$ is given by: $x(t) = \sum_i^N IMF_i(t) + r_N(t)$

2. The number of extrema points remains unchanged.

Moreover, the sifting process also stops when the standard deviation of the difference between two successive sifting steps is smaller than a threshold [215]. This last sifting stoppage criterion is given by

$$\frac{\sum_{i=1}^{N} |C_{i-1}(t) - C_i(t)|^2}{\sum_{i=0}^{N} |C_i(t)|^2} \leq SSC, \tag{4.7}$$

where SSC is a predefined threshold.

On the other hand, if IMFs do have different frequencies at the analyzed time, their analytic form (AIMF) can be expressed as

$$\text{AIMF}_i(t) \approx \sum_{i=1}^{N} A_i(t) \cos\theta_i(t), \tag{4.8}$$

where $A_i(t)$ and $\theta_i(t)$ are the instantaneous amplitude and phase of each IMF_i, respectively. These parameters can be estimated using the Hilbert transform [218] as follows

$$A_i(t) = \sqrt{R^2(t) + \hat{R}^2(t)}, \quad \theta_i(t) = \tan^{-1}\left(\frac{\hat{R}(t)}{R(t)}\right), \tag{4.9}$$

where $R(t)$ represents both the corresponding IMF component and the real term of AIMF,

$$\text{AIMF}(t) = R(t) + \text{j}\hat{R}(t), \tag{4.10}$$

and $\hat{R}(t)$ is the Hilbert Transform (HT) of $R(t)$ given by

$$\hat{R}(t) = \text{HT}\{R(t)\} = \frac{1}{\pi} R(t) * \frac{1}{t}, \tag{4.11}$$

where $*$ is the convolution operator. Consequently, the analytic form for the i-th IMF becomes

$$\mathrm{AIMF}(t) = A_i(t)\,\mathbf{e}^{\mathrm{j}\,\theta_i(t)}. \tag{4.12}$$

Zhang *et al.* found that the first four IMFs account for most of the cumulative variance contribution rate [219]. Thus, in our approach, the sum of only the first four IMFs will be used as the preprocessed EEG signal. Figure 4.11 illustrates the empirical mode decomposition of an EEG signal. So, the last IMFs and the residue capture the signal trend. Figure 4.12 shows an example of the preprocessed EEG signal using

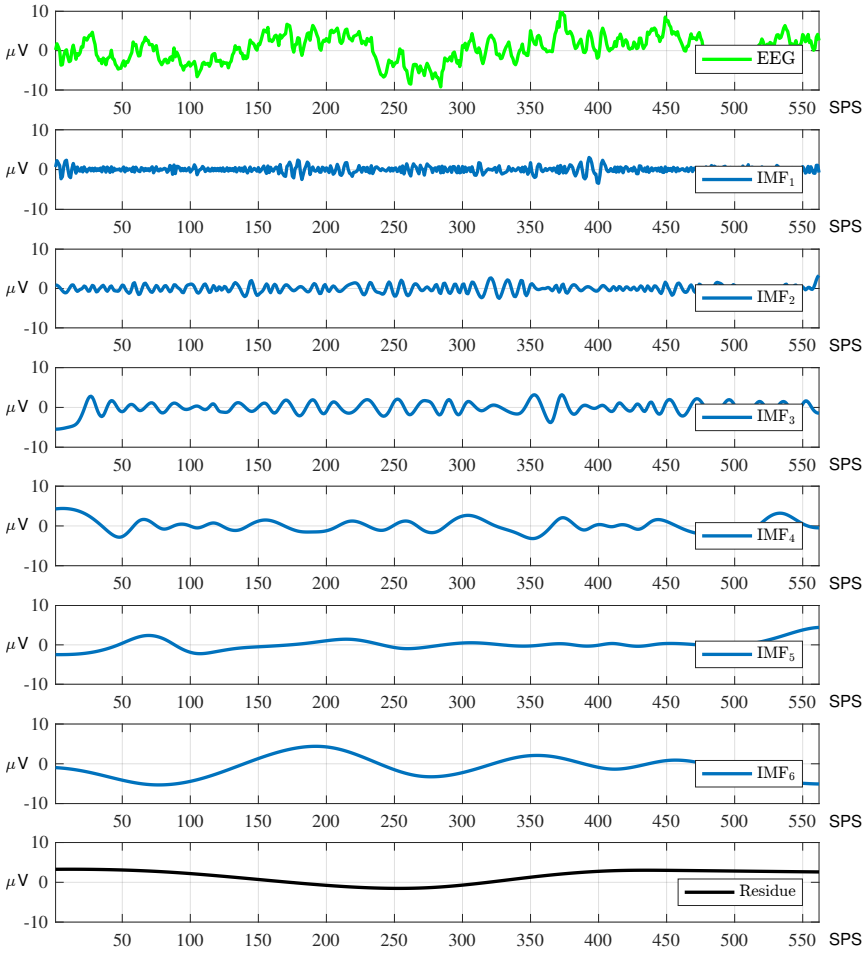

Figure 4.11: Empirical mode decomposition for an EEG signal. Top to bottom: Original signal, IMF_1–IMF_6, residue. The amplitudes are measured in μV and the horizontal axis in Samples Per Second (SPS).

the sum of the first four IMFs. Notice how the residue captures the trend of the signal.

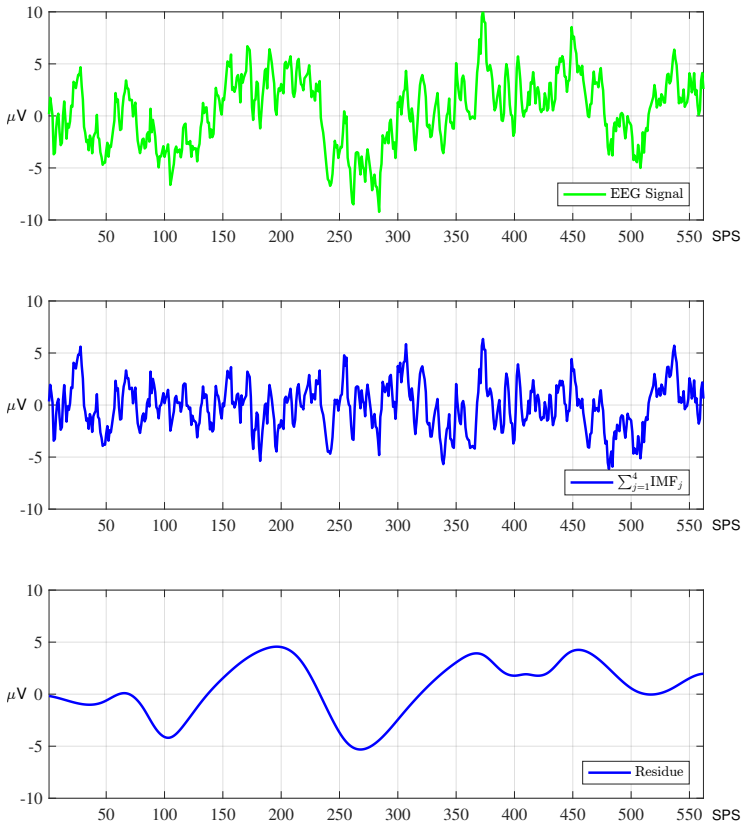

Figure 4.12: Example of an EEG signal preprocessing based on EMD. Top to bottom: an EEG signal, the resulting preprocessed signal, and the residue. The amplitudes are measured in μV and the horizontal axis in Samples Per Second (SPS).

4.2.4 The Bidirectional LSTM (BiLSTM) architecture

Long-Short Term Memory networks are a type of recurrent neural network initially designed to solve the vanishing gradient problem of recurrent neural networks when dealing with long sequences [220].

An LSTM network's architecture consists of a layer of LSTM units followed by a standard feedforward network. Figure 4.13 shows a single functional block of an LSTM unit.

In a general perspective, an LSTM unit operates as follows: let x_t be the current input at time t, the output of the input gate is as follows,

$$i_t = \sigma(W_i^x x_t + W_i^h h_{t-1} + b_i), \tag{4.13}$$

where W_i^x and W_i^h are weight matrices, h_{t-1} is the previous hidden state of the unit, and b_i is the bias vector. The function $\sigma(x) \in (0,1)$ is a sigmoid function used for gating.

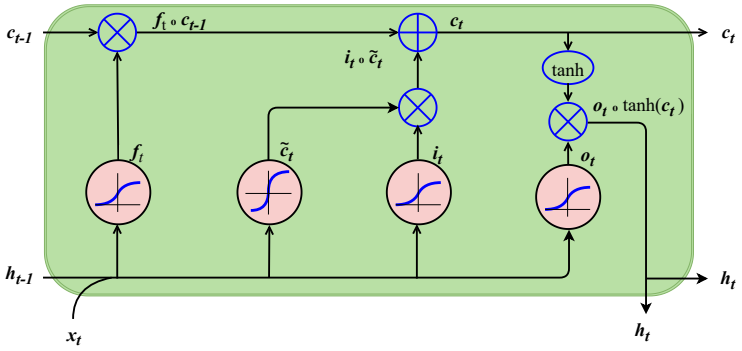

Figure 4.13: Architecture of a Long Short-Term Memory (LSTM) unit.

Similarly, the output of the forget gate f_t is computed as

$$f_t = \sigma(W_f^x x_t + W_f^h h_{t-1} + b_f). \tag{4.14}$$

Finally, the outputs of the output gate o_t and cell state c_t are as follows,

$$c_t = i_t \odot \tanh(W_c^x x_t + W_c^h h_{t-1} + b_c) + c_{t-1}, \tag{4.15}$$

$$o_t = \sigma(W_o^x x_t + W_o^h h_{t-1} + b_o), \tag{4.16}$$

$$h_t = o_t \odot \tanh(c_t), \tag{4.17}$$

where $\odot$ is the Hadamard product.

A BiLSTM consists of two parallel LSTM layers: one for the forward direction and one for the backward direction [220]. Because the input is processed twice, BiLSTMs extract more information from the input. Thus, improving contextual information to make better predictions than LSTMs. Therefore, BiLSTMs present faster convergence and accuracy than LSTMs [221].

Figure 4.14 presents the BiLSTM architecture consisting of two LSTM layers, keeping past and future context at any time of the sequence. The outputs of each LSTM are combined according to the following equation:

$$y_t = W_{\overrightarrow{h}y} \overrightarrow{h_t} + W_{\overleftarrow{h}y} \overleftarrow{h_t} + b_y, \tag{4.18}$$

where $\overrightarrow{h_t}$ and $\overleftarrow{h_t}$ are the outputs of the forward and backward LSTMs.

4.2.5 The proposed BiLSTM Architecture

A feature matrix $\in \mathbb{R}^{W \times 4}$ constituted by each preprocessed EEG signal is applied to the input of the first BiLSTM layer. A stacked architecture has been chosen to learn the complexity of the features extracted by

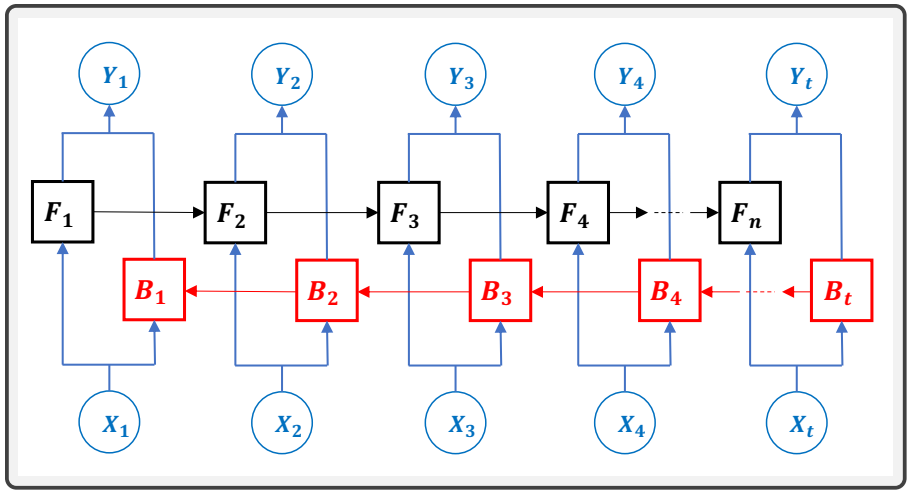

Figure 4.14: A Bidirectional LSTM (BiLSTM) Network unfolded in time. It combines the outputs of two LSTM layers in parallel, processing the input sequence in opposite directions.

the BiLSTM network.

Several experiments were completed for 2, 3, and 4 stacked layers to determine the number of BiLSTM layers to implement, and the configuration with 3 stacked BiLSTM layers provided the highest accurate classification.

Each BiLSTM layer consists of 12 memory units, as illustrated in Figure 4.15. The output of the stacked BiLSTMs is a matrix $\in \mathbb{R}^{W\times 12}$. This matrix is then converted into a vector of size $W \times 12$, *i.e.*, $\mathbb{R}^{12W\times 1}$. The value of W is 170 for 200 Hz signals, whereas for 1000 Hz signals, it is 850. This vector is the input to a dense layer.

The dense layer uses the *SoftMax* activation function to classify the representative features into the class labels.

The batch size for all network training was set to 330. The model was implemented in Python 3.6 using Keras and TensorFlow. The loss function was defined as the Categorical Cross-Entropy, the learning algorithm was defined as the *Nadam* optimizer, and the additional metrics to be computed during training were only the *Accuracy* metric.

Moreover, the Cyclical Learning Rate (CLR) [192] method was used to accelerate the convergence of the training algorithm. Another reason for using CLR is that it can help the training algorithm escape from local minima. So, the minimum and maximum learning rates were set to 10^{-9} and 10^{-3}, respectively. The step size was 8 times the number of iterations per epoch.

The complete model was trained for 300 epochs on a Windows 10 desktop equipped with an NVIDIA RTX 2080 GPU; each training was repeated at least twice.

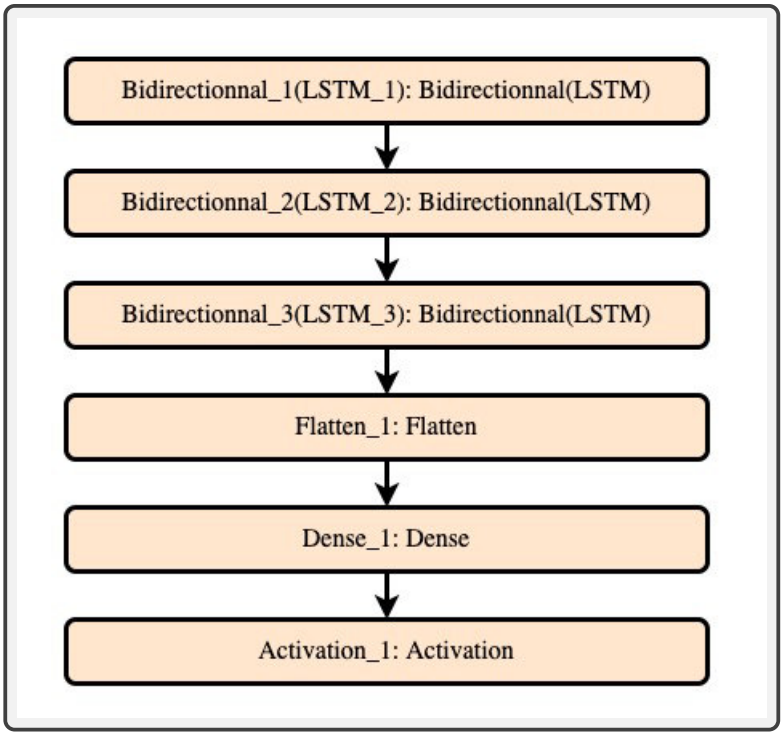

Figure 4.15: Proposed BiLSTM architecture. It consists of three BiLSTM layers, one flatten and one dense layers.

4.3 Proposed method-three

This strategy uses the same database and neural network architecture as Method-two, also the same EMD preprocessing but with a different classifier inspired from models provided in [148], with the same purpose of removing the trend from the EEG signals.

The method-three framework shown in Figure 4.16 is fundamentally based on the MI-EEG signals paradigm. The digits 1, 2, 3, 4, and 5 appear above the fingers on the Experimental Graphical User Interface (eGUI) as the task start. During the stimulus appearance, the test subject produces the imagined movement of the corresponding finger. Finally, EEG signals from the sensors $C3$, Cz, $P3$, and Pz are processed to be decoded using EMD and a BiLSTM architecture. So, this approach aims to decode movements from the right-hand finger using signals from the EEG-1200 C3, C4, P3, and Pz channels since those are close correlated with the predefined task [199]. Table 4.3 presents the fingers combination logic developed and implemented in this work to accomplish such a task.

Figure 4.17 shows the right-hand five fingers displayed on an eGUI. Regularly, digit from 1 up to 5 appears on each finger to guide the subject under tests to imagine the up and down finger flexion movements. At the same time, the EEG-1200 equipment captures and registers the corresponding signals via Neurofax recording software [211].

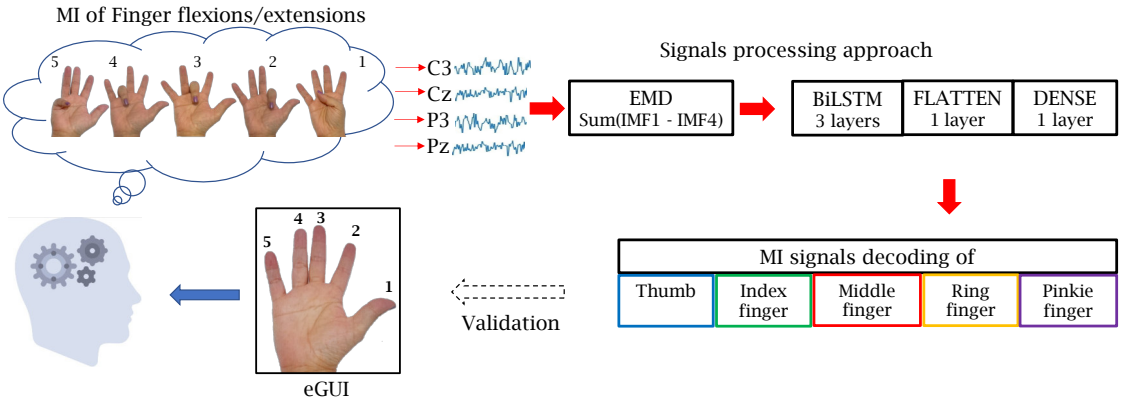

Figure 4.16: The Method-three flowchart.

Table 4.3: The fifteen finger combinations are considered in this study. The used fingers nomenclature consists of Thumb (T), Index Finger (IF), Middle Finger (MF), Ring Finger (RF), and Pinkie Finger (PF).

Combination	**Fingers**	**Stimuli succession**
1	T vs. IF	1 - 2
2	T vs. MF	1 - 3
3	T vs. RF	1 - 4
4	T vs. PF	1 - 5
5	T vs. {IF, MF, RF, PF}	1 - {2, 3, 4, 5}
6	IF vs. MF	2 - 3
7	IF vs. RF	2 - 4
8	IF vs. PF	2 - 5
9	IF vs. {T, MF, RF, PF}	2 - {1, 3, 4, 5}
10	MF vs. RF	3 - 4
11	MF vs. PF	3 - 5
12	MF vs. {T, IF, RF, PF}	3 - {1, 2, 4, 5}
13	RF vs. PF	4 - 5
14	RF vs. {T, IF, MF, PF}	4 - {1, 2, 3, 5}
15	PF vs. {T, IF, MF, RF}	5 - {1, 2, 3, 4}

4.4 Chapter conclusion

This chapter presented, the three methods developed in this doctoral thesis. The first method consisted in developing an embedded BCI system based on EEG motor imagery signals. The system was designed to work in real time, which is why the local database was first set up to provide EEG signals. Therefore, the SoCKit development board was configured to process these signals controlling the hexapod robot

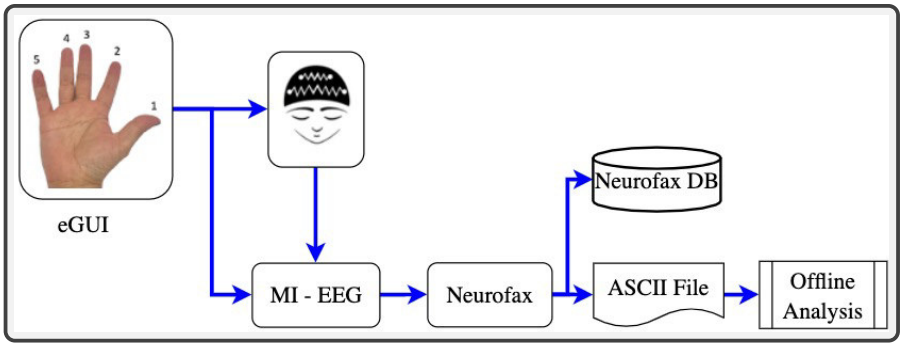

Figure 4.17: 5F dataset capturing experiment sequence. The digits 1, 2, 3, 4, and 5 symbolically represent the imaged movement of the thumb, index finger, middle finger, ring finger, and pinkie, respectively, displayed on the eGUI guiding the subject to start the corresponding task.

movements. The second and third methods focused on the EEG signals preprocessing using the empirical mode decomposition method to improve the classifier performance, on the one hand with the CNN-LSTM multi-classifier for method-two, and on the other with the BiLSTM binary classifier used as a multi-class classifier for method-three.

Chapter 5

Experimental Results

"The real problem is not whether machines think but whether men do".

B. F. Skinner

The results for Method-one, Method-two and Method-three (see Figure 5.1) are presented in this chapter. The results of Method-one being essentially operational, qualitative and quantitative evaluations are presented to corroborate the objectives assigned to the doctoral thesis. The results of Method-two and Method-three articulate on the preprocessing of EEG signals, which constitutes a major challenge for BCI applications.

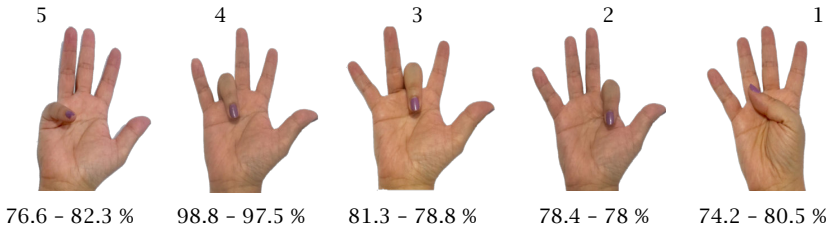

Figure 5.1: Summary results in decoding the fingers flexion-extension imagined movements for MI-EEG signals.

5.1 Results relative to Method-one

The proposed method performance was evaluated according to the operative interconnection of the EMOTIV EPOC+ headset, the SoCKit board, and the hexapod robot. It is worthy to note that recognition algorithms were integrated into an embedded BCI system. MI-EEG recognition was achieved by implementing a CNN-LSTM architecture and creating, training, and validating an EEG dataset.

5.1.1 Qualitative evaluation

Figure 5.2 shows the servomotor location and associated nomenclature, as well as the diagram of the hexapod locomotion sequence.

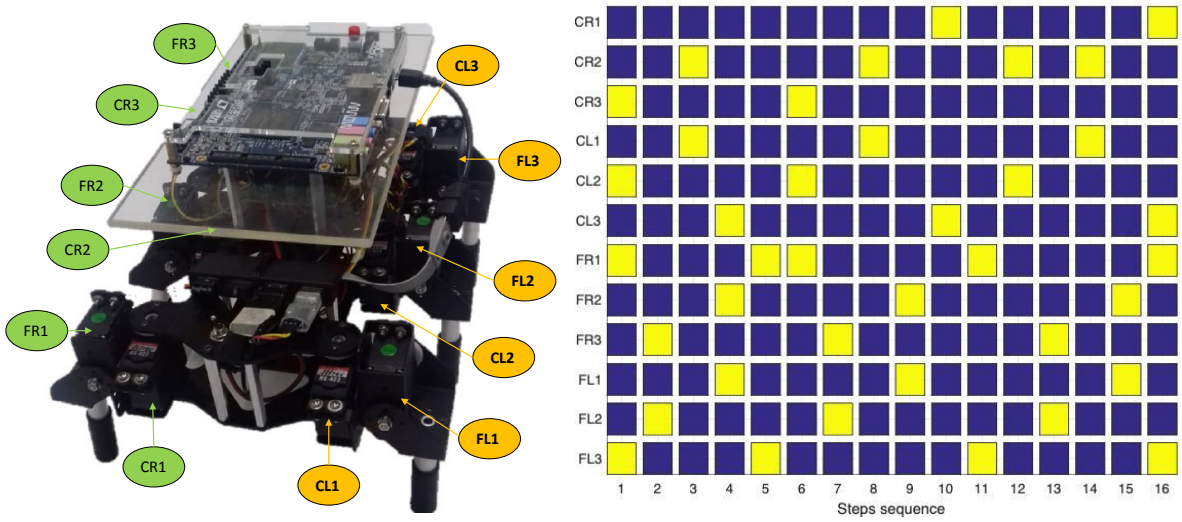

(a) Servomotors nomenclature.

(b) Hexapod locomotion rhythm.

Figure 5.2: (**a**) The SoCKit-hexapod embedded system. The hexapod operates with twelve degrees of freedom using the Coxa (C) and Femur (F) articulations in the Right (R) and Left (L) sides. (**b**) Hexapod locomotion patterns. At any locomotion step, the corresponding servomotor activation is painted in yellow and deactivated in blue.

Figure 5.2(b) illustrates the repeating pattern sequences used to control the servomotors, which are integrated to move the hexapod synchronously. MI-EEG signals for closing-opening right and left fists were processed by the SoCKit and transferred to the hexapod servomotors as commands to move forward, backward, and stop.

A dataset was constituted by signals captured from four chosen subjects, which were trained to reproduce each task pattern until they became familiar with the experience. The Xavier interface of EMOTIV evaluated the subjects' mental-state metrics before each training and capture [222], using cognitive, expressive,

affective, and inertial sensors.

5.1.2 Quantitative evaluation

A total of 2,400 sessions have been validated with four test subjects several times. This process allowed obtaining the representative samples for training and validation datasets. Therefore, 2,160 captures were used as training data, and 240 captures as validation data. The number of classes was three (i.e., Forward, Backward, and Neutral). Moreover, the Stratified k-fold Cross-Validation (CV) was used with $k = 10$ to evaluate the system performance. Table 5.1 summarizes the dataset structure split into training and validation patterns.

Table 5.1: Data partition for training and validation.

Dataset structure		
Stratified k-fold CV	Training (90 %)	Validation (10 %)
$k = 10$	2160 captures	240 captures

The convolutional layer CNN1 used 416 parameters, while the CNN2 and CNN3 layers have 3,104 parameters each. Thus, 125,197 parameters were necessary for all layers.

5.1.2.1 EEG signals dataset

The highlighted parameters in the created dataset are age, gender, and the capture sequence duration. The dataset features are summarized in Table 5.2.

Table 5.2: Local dataset description.

Order	**ID**	**Age**	**Gender**
1	AB	34	Male
2	CD	23	Female
3	EF	36	Male
4	GH	23	Female

Subjects of the dataset required significant mental focus on the stimulus to get reliable signals, which was solved with extensive experimentation for easy adaptation to this experience.

5.1.2.2 Model evaluation

The proposed framework evaluation considers the accuracy of the hexapod movement commands according to the three predefined tasks identified from the MI signals. Simultaneously, the designed BCI must optimize real-time signal processing. The neural network training was repeated five times, achieving an average accuracy of 84.69 % for the three experimental predefined tasks. The highest accuracy of 87.6 % was obtained for the sixth k-fold iteration, whereas the lowest accuracy of 81.88 % was found with the second k-fold iteration. The created database provides signal patterns lasting six hours collected from four test subjects.

Table 5.3 shows the classification accuracy for each test subject, while Table 5.4 summarizes accuracy reached with different subject combinations.

Table 5.3: Classification accuracy for each dataset subject.

Subjects	Training Accuracy	Test Accuracy
AB	95.49 %	82.38 %
CD	94.92 %	80.83 %
EF	99.03 %	83.54 %
GH	97.38 %	85.25 %

Table 5.4: Classification accuracy of subject combinations.

Subjects	Training Accuracy	Test Accuracy
AB-CD	98.9 %	83.7 %
AB-CD	99.2 %	81.3 %
AB-EF	99.8 %	82.7 %
AB-GH	96.5 %	79.5 %
CD-EF	99.4 %	85.7 %
CD-GH	91.1 %	83.6 %
EF-GH	99.5 %	84.2 %
AB-CD-EF	99.7 %	83.4 %
AB-CD-GH	99.8 %	85.4 %
CD-EF-GH	99.6 %	86.1 %

This study was additionally evaluated with the dataset constructed by Kaya *et al.* [128]. This dataset gathers five EEG signal paradigms, captured with the Nihon Kohden Neurofax EEG-1200 electroencephalograph and the JE-921A amplifier. The proposed BCI evaluation is based on left- and

right-hand motor imageries of closing and opening the respective fist once, defined as paradigm #1 [128]. After imagining such actions, the participant remained passive until the next action signal is presented.

Table 5.5 shows that the average accuracy achieved for the 3-task classification was 79.2 % using the evaluated dataset.

Table 5.5: Accuracies achieved with our and Kaya's datasets

Reference	Dataset type	Brain signals	Accuracy
Proposed method	Our dataset (4 subjects)	MI EEG	84.69 %
Kaya et al. [128]	Public dataset (7 subjects)	MI EEG	79.2 %

The proposed network model was trained on a computer with an NVIDIA GeForce® GTX 1080 GPU. Next, the descriptive files (weight files, module files) were migrated to the SoCKit card to optimize the processing latency time of EEG signals. The embedded system took approximately 0.750 s to decide whether the samples present refer to the right-fist, left-fist, or none using FIFO's configuration and the EMOTIV EPOC+ rate of 128 samples per second (SPS). The processing time with the dataset described in [128] (sampled at 200 SPS) was evaluated at 0.279 s with signals from $C3$, $C4$, and Cz electrodes.

Moreover, two closely related embedded BCI approaches [223] were also included to compare the proposed method in Table 5.6, including the signals' processing time and the number of channels.

Table 5.6: Processing time comparison with two additional embedded-BCI systems

Method	Embedded-BCI	Nb. of channels	Pr. time
Lin et al. [224]	BSLEACS	1	2000 ms
Belwafi et al. [223]	3-EGBCI system	22	399 ms
Proposed method (EMOTIV)	SoCKit	4	750 ms
comparison method [128]	SoCKit	3	279 ms

Therefore, this work's contributions are developing an MI-EEG dataset, a CNN-LSTM model implemented in the FPGA SoC board for real-time signals' processing, and the embedded BCI architecture implementation with different technologies.

5.1.3 Discussions

The proposal was implemented on the Altera FPGA SoC environment, building the hardware design modules shown in Table 4.1. A mechanism to read EEG signals in real-time on the SoCKit board was designed with a delay limit of about 10 ms for the EMOTIV EPOC+ capture. A proper buffer module

synchronization guarantees the regularity of data being sent to the processor, where the available memory (DMA) is dynamically allocated.

Quartus II version 13.0 was used to embed the project descriptive architectures, to ensure the processing and classification of motor imagery EEG signals. Real-time signals' processing starts when the EMOTIV EPOC+ system sends EEG signals at 128 samples per second to the SoCKit card. Next, the NIos-II IDE cache memory was previously preloaded with the designed neural network parameters. Therefore, the SoCKit can instantly convert classified EEG signal features into commands to move the hexapod.

Moreover, the SoCKit USB 2.0 OTG port was used to connect the SSC-32 Control board through the USB-TTL adapter. Note that physically, the SoCKit board was embedded in the hexapod and move together.

Table 5.3 shows the achieved variability in accuracy results with each subject confirming intrinsic differences among EEG signal characteristics, besides the close-related faithful reproduction by each subject experience. Table 5.4, different combinations of the subjects' signals were made to appreciate data classification accuracy according to the dataset size variation. Thus, high test accuracy of 85.7 % was reached by combining two signal groups from CD and EF subjects while combining three signal groups from CD, EF, and GH subjects; the highest score achieved was 86.1 %.

5.2 Results relative to Method-two

This approach implements the test subject-dependent approach where signals from a single subject were classified to decode right-hand finger imagery movements. The subject signals were captured using two particular sampling frequencies, 1000 Hz or 200 Hz. EEG signals used in the experiments, corresponding to the electrodes $C3$, Cz, $P3$, and Pz, are presumably involved in the movements from the right-hand fingers [210]. Hence, k-fold CV was used to assess the training performance of the model. Considering that the dataset is relatively small, the value of k was set to 200. So, the dataset was split into 200 disjoint subsets of equal size. Then, one different subset is taken as the test data for each training. At the same time, the remaining subsets 199 are used as learning data. The performance is taken as the average of the 200 testing accuracies. The number of samples in the datasets were between 940 and 1917.

Table 5.7 shows the model accuracy for different subjects and sampling frequencies. As a result, the highest testing accuracy (76.13 %) for signals at 1000 Hz corresponds to subject F, while the lowest accuracy (66.0 %) corresponds to subject I. The highest testing accuracy (82.26 %) for signals at 200 Hz corresponds to subject C, while the lowest accuracy (75.2 %) corresponds to subject B.

Table 5.8 shows the impact of the number of BiLSTM layers on the accuracy of the proposed method. These results show that accuracy reaches a maximum at three BiLSTM layers. Therefore, the configuration of three BiLSTM layers was used in all tests for this study. Table 5.9 shows the number of model parameters for the case of 1000 Hz and 200 Hz signals. Besides, the last BiLSTM layer outputs the whole processed sequence. Therefore, the proposed architecture is different from other architectures because they use only

Table 5.7: Results for subject-dependent finger movement decoding.

Subject	**Training (%)**	**Testing (%)**	**Training (%)**	**Testing (%)**
	1000 Hz		200 Hz	
A	90.76	72.43	85.35	81.84
B	73.47	74.07	79.94	75.2
C	98.69	80.04	88.92	**82.26**
E	80.33	71.93	-	-
F	88.85	**76.13**	88.73	79.70
G	73.59	68.0	-	-
H	91.22	73.33	-	-
I	93.5	66.0	-	-

Table 5.8: Accuracy depending on BiLSTM layers number.

	Subjects							
BiLSTM	**A**	**B**	**C**	**F**	**A**	**B**	**C**	**F**
# Layers	Accuracy (%) at 1000 Hz				Accuracy (%) at 200 Hz			
2	66.25	67.13	75.8	54.95	69.15	67.56	79.8	71.17
3	72.43	74.07	80.04	76.13	81.84	75.2	82.26	79.70
4	63.35	71.83	74.92	67.25	75.55	74.41	78.6	70.9

the last state of the last BiLSTM layer for classification.

Table 5.9: Parameters of the model for training with signals at 1000 Hz and 200 Hz.

Layer Type	**Cells**	**Output shape** 1000 Hz	**Parameters** 1000 Hz	**Output shape** 200 Hz	**Parameters** 200 Hz
Bidirectional	12	(None, 850, 24)	1632	(None, 170, 24)	1632
Bidirectional_1	12	(None, 850, 24)	3552	(None, 170, 24)	3552
Bidirectional_2	12	(None, 850, 24)	3552	(None, 170, 24)	3552
Flatten	–	(None, 20400)	0	(None, 2683)	0
Dense_1	–	(None, 5)	102005	(None, 5)	13418
Activation	–	(None, 5)	0	(None, 5)	0
Total			110,771		22,154

The results obtained by the presented approach outperformed those reported in [128], where an average

accuracy of 43 % was achieved in the decoding of five fingers movements. Besides, the Support Vector Machines (SVM) method was used to classify MI-EEG signals from every single subject using only the $C3$ channel.

The network model was also trained and tested on the samples of all subjects (A, B, C and F) to determine what was the behavior of the accuracy for samples of different subjects. For that purpose, the network model was trained each time using data from four subjects (A, B, C, and F) and for one of two available sampling frequencies: 1000 Hz and 200 Hz.

As a result, the proposed model achieved 80.04 % and 82.26 % accuracy for 1000 Hz and 200 Hz signals, respectively. Those results outperform the results obtained by Kaya *et al.* for five subjects, achieving an accuracy between 40 % and 60 %. They achieved an accuracy between 20 % and 40 % for three subjects, considering all the 13 subjects.

Table 5.10 shows a comparison with other results from the literature for subjects A, B, C, and F, with 200 Hz and 1000 Hz signals.

Table 5.10: Comparison with other state-of-the-art approaches.

Subject	**Sampling frequency**	**Methods**		
		[225] (ADL Network)	Proposed method (EMD+BiLSTM)	[157] (EMD+EEGNet)
A	200 Hz	77.46%	**81.84%**	80.16%
	1000 Hz	**77.75%**	72.43%	75.45%
B	200 Hz	77.82%	75.2%	**80.02%**
	1000 Hz	74.61%	74.07%	**76.07%**
C	200 Hz	81.62%	**82.26%**	80.17%
	1000 Hz	77.49%	**80.04%**	78.90%
F	200 Hz	78.13%	79.70%	**80.01%**
	1000 Hz	**77.20%**	76.13%	75.20%

The choice of subjects is mainly because, for those subjects, the dataset contains both 200 Hz and 1000 Hz signals. Thus, the results obtained by Anam *et al.* with the subject-dependent classification are slightly smaller than the results obtained by our approach for the case of 200 Hz signals [225]. However, in the case of 1000 Hz signals, the method of Anam *et al.* performs better than the proposed framework, except for subject C. This issue can be explained by the number of parameters used for the 1 kHz case, which was about five times the number of parameters for 200 Hz, as shown in Table 5.10. Hence, the proposed model presented overfitting issues for this case. EEGNet [157] was also trained using the proposed preprocessing method for comparison purposes. As a result, the accuracy was very close to the accuracy of the proposed approach. Finally, the EMD-based preprocessing method resulted in about 32.6% faster training convergence for all tests.

5.3 Results relative to Method-three

Two factors have mainly been considered: the stimuli display succession and the fingers' proximity. This choice obeys the particular EEG patterns of each finger [128]. k-fold cross-validation was used, splitting the data into $k = 10$ partitions. Each one served iteratively as the learning data and evaluated with the remainder data; finally, the statistical results are measured.

5.3.1 Subject-dependent classification approach

In this approach, the signals of each subject were processed individually. Several combinations of one finger versus the others were considered, as detailed in Table 5.11. The numerical results were split depending on the sampling frequency.

Firstly, each subject's finger signals at 1.0 kHz were decoded. In such analysis, all subjects performed the ring finger decoding compared to other fingers, obtaining 98.9 %, 99.3 %, 99.1 %, and 98.1 % accuracy for subjects A, B, C, and F.

Figure 5.3 shows that the thumb decoding for its share provided the most limited accuracies, 74.3 %, 73.8 %, 74.9 %, and 74.1 % for subjects A, B, C, and F, respectively.

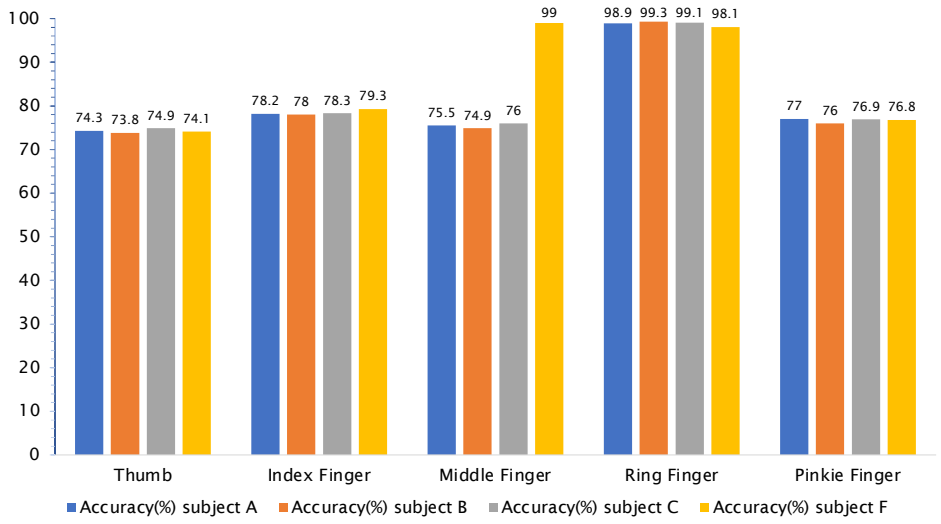

Figure 5.3: The lowest and highest accuracies achieved with signals at 1.0 kHz for the subject-dependent classification approach.

Secondly, subject finger signals at 200 Hz were decoded. At this step, signals at 200 Hz performed better than those at 1.0 kHz in decoding imaginary finger movements. Figure 5.4 shows the results achieved with signals at 1.0 kHz, the ring-finger signals decoding was successful with accuracies of 96.5 %, 96.6 %, 98.0 %, and 99.0 % for subjects A, B, C, and F. The index finger decoding accuracies were lowest for almost

Table 5.11: Accuracies achieved according to the finger combination pairs.

Subjects	Finger cases	Training(%)	Testing(%)	Training(%)	Testing(%)
		1.0 kHz		200 Hz	
A	T vs. {IF, MF, RF, PF}	98.8	74.3	98.2	79.1
	IF vs. {T, MF, RF, PF}	99.1	78.2	98.6	76.5
	MF vs. {T, IF, RF, PF}	98.2	75.5	99.0	76.8
	RF vs. {T, IF, MF, PF}	98.7	**98.9**	99.4	**96.5**
	PF vs. {T, IF, MF, RF}	97.9	77.0	98.6	80.3
B	T vs. {IF, MF, RF, PF}	99.2	73.8	97.3	77.8
	IF vs. {T, MF, RF, PF}	98.9	78.0	98.7	77.3
	MF vs. {T, IF, RF, PF}	98.1	74.9	98.5	77.0
	RF vs. {T, IF, MF, PF}	98.6	**99.3**	92.6	**96.6**
	PF vs. {T, IF, MF, RF}	98.2	76.0	97.3	81.2
C	T vs. {IF, MF, RF, PF}	97.9	74.9	98.8	84.8
	IF vs. {T, MF, RF, PF}	99.2	78.3	99.2	79.6
	MF vs. {T, IF, RF, PF}	98.3	76.0	98.6	82.5
	RF vs. {T, IF, MF, PF}	99.0	**99.1**	94.0	**98.0**
	PF vs. {T, IF, MF, RF}	99.3	76.9	98.9	85.1
F	T vs. {IF, MF, RF, PF}	98.4	74.1	98.1	80.3
	IF vs. {T, MF, RF, PF}	98.9	79.3	91.3	78.6
	MF vs. {T, IF, RF, PF}	99.2	**99.0**	97.8	79.0
	RF vs. {T, IF, MF, PF}	98.5	98.1	99.2	**99.0**
	PF vs. {T, IF, MF, RF}	97.8	76.8	98.7	82.6
Averages ABCF	**Thumb**	**98.5**	**74.2**	**98.1**	**80.5**
	Index-finger	**99.0**	**78.4**	**96.9**	**78.0**
	Middle-finger	**98.4**	**81.3**	**98.4**	**78.8**
	Ring-finger	**98.7**	**98.8**	**96.3**	**97.5**
	Pinkie-finger	**98.3**	**76.6**	**98.3**	**82.3**

all subjects. The highest mean accuracies obtained were 98.8 % and 97.5 % in decoding the ring finger signals at 1.0 kHz and 200 Hz, respectively.

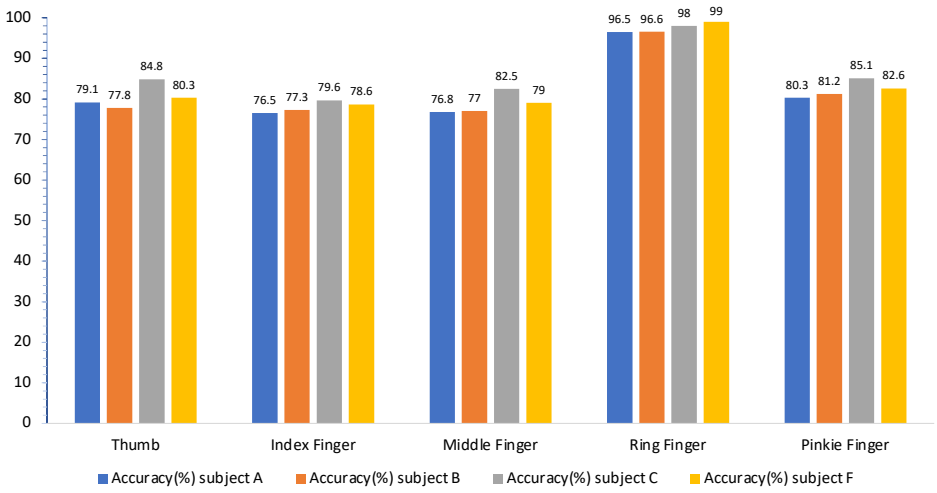

Figure 5.4: Accuracies achieved with signals at 200 Hz for the subject-dependent classification approach.

5.3.2 Finger-independent classification approach

The finger-independent classification approach aims to decode for subjects A, B, C, and F together, signals from respective fingers. This perspective offers an advantage for practical BCI applications in which each finger signal can be used to control BCI application in multi class approach. Therefore, the imaginary movements decoded of each finger concern the subjects A, B, C, and F for signals at 200 Hz and 1.0 kHz.

5.3.2.1 Decoding Thumb Finger Movements

Five thumb combinations were processed to classify thumb signals. The classification models were trained to distinguish among the movements of the thumb finger and the other fingers. The decoding accuracies for signals at 200 Hz were found in the following order: thumb against the pinkie finger (80.08 %), thumb against the ring finger (76.8 %), thumb against the middle finger (73.35 %), and thumb against the index finger (65.2 %). The first block in Table 5.12 shows that the best accuracies of 78.9 % and 80.5 % were achieved by decoding thumb movements at 1.0 kHz and 200 Hz against other fingers.

Table 5.12: Average accuracies (Acc) for all finger combinations at 1.0 kHz and 200 Hz using k-fold cross-validation ($k = 10$).

Finger cases	**Training(%)**	**Testing(%)**	**Training(%)**	**Testing(%)**
	1.0 kHz		200 Hz	
T vs. IF	98.8	65.65	97.6	65.20
T vs. MF	98.1	72.67	99.3	73.35
T vs. RF	98.9	75.18	99.4	76.80
T vs. PF	99.1	76.71	98.9	80.08
T vs. {IF, MF, RF, PF}	98.6	**78.90**	90.6	**80.5**
IF vs. MF	98.4	65.51	99.6	66.03
IF vs. RF	99.5	68.87	98.2	70.92
IF vs. PF	90.1	70.71	98.1	73.54
IF vs. {T, MF, RF, PF}	98.7	**78.9**	98.8	**81.80**
MF vs. RF	96.8	63.64	98.7	65.8
MF vs. PF	98.6	66.43	98.9	68.4
MF vs. {T, IF, RF, PF}	98.7	**77.6**	98.8	**79.8**
RF vs. PF	98.3	67.2	97.5	65.12
RF vs. {T, IF, MF, PF}	98.4	**81.20**	98.6	**80.30**
PF vs. {T, IF, MF, RF}	98.8	**82.9**	98.6	**80.7**

Contrarily, the lowest accuracy (65.20 %) was found for decoding thumb signals against those of the index finger at 200 Hz. These results agree with the results reported by Anam and Kaya, where the thumb and pinkie MI signals were clearly distinguished.

5.3.2.2 Decoding Index-Finger Movements

The second block in Table 5.12 presents the results of four index-finger combinations at 1.0 kHz and 200 Hz. The highest accuracy was achieved decoding index-finger signals against those of other fingers (78.9 %) and (81.8 %) combination at 1.0 kHz and 200 Hz, respectively. These results prove that the discrimination of signals is much more significant when fingers are more separated from each other.

5.3.2.3 Decoding Middle-Finger Movements

Middle-finger movements were decoded using three finger combinations evaluated: the first combination, according to the stimulus progress, compared Middle-Finger signals against Ring-finger, where a notable

accuracy was achieved with signals at 200 Hz (65.8 %). The second combination aimed to decode Middle-Finger signals from those of Pinkie-Finger's, obtaining an accuracy of 68.4 % for signals at 200 Hz. The latest combination decoded the Middle-Finger signals from all fingers, achieved the best accuracy of 79.8 % with signals at 200 Hz, as given in the third block in Table 5.12.

5.3.2.4 Decoding Ring-Finger and Pinkie Finger Movements

Specific ring-finger signals are decoded using the following two finger signal combinations: (1) the ring-finger against the pinkie and (2) the ring-finger against the other fingers set. Table 5.12 in the fourth block presents 80.3 % and 81.2 % accuracy achieved while decoding Ring-Finger signals against those of other fingers, at 200 Hz and 1.0 kHz, respectively.

The last block in Table 5.12 shows accuracies of 80.7 % and 82.9 % reached while decoding Pinkie-Finger for signals at 200 Hz and 1.0 kHz, respectively.

5.3.3 Fingers decoding evaluation

Globally, several performances were observed while decoding finger signals. Firstly, considering the subjects separately (subject-dependent approach), decoding for subjects *C* and *F* was (averages of 86 % and 83 %) more accurate than for subjects A and B (averages of 81 %). Posteriorly, another approach was considered to decode finger signals of all subjects. In this last case, Ring-Finger signals were decoded more efficiently (82.9 % and 80.7 % of accuracy at 1.0 kHz and 200 Hz, respectively) than the Middle-Finger signals (77.6 % and 79.8 % at 1.0 kHz and 200 Hz, respectively). *Middle-Finger* combinations presented the lowest accuracies justified by the closeness of all other fingers, producing noise and signal mixtures. These results express clearly that the more distant fingers are, the better the classification accuracy is. Figure 5.5 summarizes the achieved accuracies for each finger while exploring the finger combinations presented in Table 5.12.

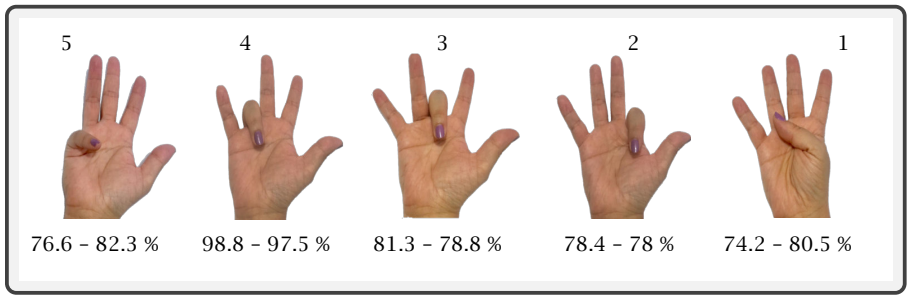

Figure 5.5: Graphical representation of summary results in decoding the fingers flexion-extension imagined movements for MI-EEG signals at 1.0 k Hz and 200 Hz, respectively.

This study also evaluated the EMD as a contribution according to the training convergence speed of

the implemented network model. Table 5.13 shows the improvement by including or excluding EMD in the proposed approach. This comparison is based on analyzing the convergence (number of epochs) and the

Table 5.13: A 2-class global improvement regarding the convergence speed (number of epochs) and the accuracy to decode finger imaginary movements while including or excluding EMD preprocessing.

Finger Cases	**Training** without EMD		**Training** using EMD		**Convergence** Improvement	**Accuracy** Improvement
Combination	1.0 kHz	200 Hz	1.0 kHz	200 Hz	Rel. [%]	Rel. [%]
T vs. All	135	182	97	117	31.9	4.9
IF vs. All	176	198	101	142	35.4	4.0
MF vs. All	150	174.	94	113	36.1	4.0
RF vs. All	157	186.	97	148	29.3	3.6
PF vs. All	142	208.	82	168	30.7	4.4
Average	**152**	189.6	**94.2**	137.6	**32.6**	4.1

accuracy results related to the inclusion (or not) of EMD in the preprocessing of EEG signals.

The relative Convergence Improvement (CI) was calculated regarding the maximum accuracy obtained using raw data, without EMD, as follows

$$\mathrm{CI}_f = \left(1 - \frac{\mu_1}{\mu_0}\right) \times 100, \quad \forall f \in \{200, 1000\}[\mathrm{Hz}], \tag{5.1}$$

where $\mu_1 = \mathbb{E}\{EpD\}$ is the mean value of the Epochs number using EMD, while $\mu_0 = \mathbb{E}\{Ep\overline{D}\}$ is the mean value of the Epochs number using raw data (without EMD), and $\mathbb{E}$ is the mathematical expectation. Therefore, the Average Relative Convergence Improvement (ARCI) using all data, at 200 and 1.0 kHz is given by

$$\mathrm{ARCI} = \frac{1}{2}\left(\mathrm{CI}_{200} + \mathrm{CI}_{1000}\right). \tag{5.2}$$

Similarly, the Relative Accuracy Improvement (RAI) was found considering the maximum number of epochs, which were fixed at 1000, and the neural network was trained with data using (or not) EMD, as follows

$$\mathrm{RAI}_f = \left(1 - \frac{\mu_2}{\mu_3}\right) \times 100, \quad \forall f \in \{200, 1000\}[\mathrm{Hz}], \tag{5.3}$$

where $\mu_3 = \mathbb{E}\{EpD\}$ is the mean value of accuracy using EMD, $\mu_2 = \mathbb{E}\{Ep\overline{D}\}$ is the mean value of accuracy using raw data (without EMD), computed with the total number of epochs. Finding the Accuracy Relative Benefit as follows,

$$\mathrm{ARAI} = \frac{1}{2}(\mathrm{RAI}_{200} + \mathrm{RAI}_{1000}). \tag{5.4}$$

It is noteworthy that, on average, the Convergence and Accuracy Relative improvements were 32.6 %

and 4.1 %, respectively, while preprocessing signals with the EMD method. One final remark on fingers' decoding is focused on the training convergence, which was even faster for all conducted tests while using the EMD preprocessing. From the results in analyzing MI-EEG signals, it was found that EMD adapts better to the non-stationary signals filtering than other traditional filters as moving average removal and polynomial fitting, as it was previously remarked by Lentka *et al.* [226].

5.4 Chapter conclusion

This chapter presented the results achieved with the 3 methods developed in this doctoral thesis. With Method-one, MI EEG signal recognition was carried out using a hybrid CNN-LSTM neural network. By using stratified 10-fold cross-validation, the average task accuracy achieved was of 84.69 %. The digital logical design guaranteed adequate functionality in the integral transmission of data. Hence, FIFOs communicating with FPGA outputs were implemented at 32-bit word-length, running at 10 MB/s. Task recognition delay on the SoCKit was estimated at 755 ms and about 500 ms in executing the hexapod movements, including intrinsic delays in the SSC-32 V2.0 card.

Method-two aimed to decode individual imagined movements of the five right-hand fingers using a public dataset. Numerical results showed that the decoding accuracy depends heavily on the availability of training data. Maximum accuracy of 82.9 % was obtained by using stratified 200-fold CV.

Method-three contemplated two approaches using the same network architecture: in the subject-dependent approach, finger imagined movements were decoded for each subject separately, while for the other approach, the finger movements decoding concerned all the subject's data together. The two approaches offer advantages for specific BCI applications. All subjects performed the finger movement decoding with the first approach, especially for Ring-Finger signals (98.8 % at 1.0 kHz). The second approach achieved the most superior accuracy of 82.9 % decoding Pinkie signals at 1.0 kHz.

General Conclusions

The main objective of this doctoral thesis was to design and implement an embedded Brain-Computer Interface (BCI) based on Motor Imagery EEG signals to voluntarily control the movements of the hexapod robot. Therefore, in Chapters 2 and 3, the concept of brain-computer interfaces was presented, respectively, emphasizing BCI based on EEG signals, and the convolutional neural network (CNN) followed by the recurrent neural network(LSTM). These theories allowed us to get closer to the methodology developed in Chapter 4, which gave the results presented in Chapter 5.

In the first approach, an embedded BCI system based on EEG signals was developed, operating with imagined fist movements, using an EMOTIV EPOC+ headset, and processed in real-time on the SoCKit Cyclone V SoC card to control a hexapod robot. The designed framework allowed controlling the forward and backward movements of a hexapod robot, using two MI tasks: closing and opening the right fist, closing and opening the left fist, and the neutral (reference) action. Likewise, an MI-EEG dataset was created. Using a hybrid CNN-LSTM neural network and stratified 10-fold cross-validation, the average task accuracy of 84.69 % was achieved in the MI EEG signal recognition.

This method proved the active and accurate locomotion of a hexapod robot, exploiting EEG brain signals captured by an EMOTIV EPOC+ headset and processed by a SoCKit card using a pre-trained CNN-LSTM neural network as a classifier. The results and the database referred to this approach were published in [227].

To deal with the non-stationarity of EEG signals, approaches developed in Sections 4.2 and 4.3 based on Empirical Mode Decomposition (EMD) were developed as preprocessing steps to improve the classifier's accuracy based on deep learning. Kaya's dataset was used to decode individual imagined movements of the five right-hand fingers Therefore, preprocessing steps of MI-EEG signals from the $C3$, Cz, $P3$, and Pz sensors were considered. Next, the obtained IMF signals were classified using a recurrent neural network, described as BiLSTM and achieving a maximum accuracy of 82.9 %. Results related to this method were published in [228].

In addition, another approach was developed in Section 4.3 to decode Fingers Motor Imagery EEG signals for Brain-Computer Interfaces. Therefore, the EMD method was employed to filter MI-EEG signals before decoding individual finger features utilizing a BiLSTM network. In the subject-dependent approach, finger imagined movements were decoded for each subject separately, in addition, the finger movements decoding concerning all the subject's data together, respectively achieving accuracies of 98.8 % and of

82.9 % at 1.0 kHz. The advantages of using EMD as a filter to preprocess signals were also evaluated. The improvements achieved using EMD, in terms of convergence epochs and accuracy, have been seen as another method contribution.

Considering the results obtained in the three approaches, the objectives assigned in this doctoral thesis are fulfilled, confirming the hypotheses established in the introduction. An embedded BCI system based on MI EEG signals controlling the hexapod robot movements was designed and implemented. The quality of EEG signals for BCI systems was improved using the empirical mode decomposition method. The next stages basing on the present results are presented in the Section 5.4.

Future Works

The research perspectives of this doctoral these include:

- building a more extensive and robust database with more sophisticated sensing equipment, considering the practical difficulties encountered in capturing of EEG signals such as the perfect contact of the electrodes with the scalp and the rapid oxidation of the electrodes once wet with the saline solution. A larger and more robust database will expand the number of BCI's users,
- increasing the number of modular tasks to control the mobile robot as turning right or left, running, sitting, or climbing to integrate the pragmatics of using BCI,
- using the present results to control an embedded BCI-based on a wheelchair supporting human mobility for the social impact purposes.

Bibliography

[1] H Lodish, Arnold Berk, S Zipursky, P Matsudaira, D Baltimore, and J Darnell. *Molecular Cell Biology, forth edition. Section 21.1, Overview of Neuron Structure and Function*. W. H. Freeman and Company, 01 1999.

[2] Aleksandra Kawala-Sterniuk, Natalia Browarska, Amir Al-Bakri, Mariusz Pelc, Jaroslaw Zygarlicki, Michaela Sidikova, Radek Martinek, and Edward Jacek Gorzelanczyk. Summary of over Fifty Years with Brain-Computer Interfaces: A Review. *Brain Sciences*, 11(1):43, 2021. ISSN 2076-3425.

[3] J.J. Hopfield. Neural networks and physical systems with emergent collective computational abilities. *Proceedings of the National Academy of Sciences of the United States of America*, 79(8):2554–2558, 1982. doi: 10.1073/pnas.79.8.2554.

[4] Yves Lecun, I. Guyon, L.D. Jackel, D. Henderson, B. Boser, R.E. Howard, J.S. Denker, W. Hubbard, and H.P. Graf. Handwritten Digit Recognition: Applications of Neural Network Chips and Automatic Learning. *IEEE Communications Magazine*, 27(11):41–46, 1989. doi: 10.1109/35.41400.

[5] Sepp Hochreiter and JÃŒrgen Schmidhuber. Long Short-term Memory. *Neural computation*, 9: 1735–80, 12 1997. doi: 10.1162/neco.1997.9.8.1735.

[6] Syarifah Syakiylla, Syarifah Syakiylla Sayed Daud, and Rubita Sudirman. Decomposition Level Comparison of Stationary Wavelet Transform Filter for Visual Task Electroencephalogram. *Jurnal Teknologi*, 74(6):7–13, 04 2015. doi: 10.11113/jt.v74.4661.

[7] Tina Stavrinaki. *Optional Protocol to the Convention on the Rights of Persons with Disabilities*, page 1. United Nations, 11 2018. ISBN 9780198810667. doi: 10.1093/law/9780198810667.003.0052.

[8] Sutthichai Jitapunkul, Chaiyos Kunanusont, Wiput Phoolcharoen, Paibul Suriyawongpaisal, and Shah Ebrahim. Determining public health priorities for an ageing population : The value of a disability survey. *The Southeast Asian journal of tropical medicine and public health*, 34:929–36, 01 2004.

[9] Deirdre O'Neill and Daniel Forman. Cardiovascular care of older adults. *BMJ*, 374:n1593, 08 2021. doi: 10.1136/bmj.n1593.

[10] Jacques Ferlay, Murielle Colombet, Isabelle Soerjomataram, Donald M. Parkin, Marion Piñeros, Ariana Znaor, and Freddie Bray. Cancer statistics for the year 2020: An overview. *International Journal of Cancer*, 149(4):778–789, 2021. doi: https://doi.org/10.1002/ijc.33588.

[11] P. B. Jones. Adult mental health disorders and their age at onset. *British Journal of Psychiatry*, 202 (s54):s5–s10, 2013. doi: 10.1192/bjp.bp.112.119164.

[12] Mehran Amiri, Abdollah Ardeshir, Mohammad Hossein Fazel Zarandi, and Elahe Soltanaghaei. Pattern extraction for high-risk accidents in the construction industry: a data-mining approach. *International Journal of Injury Control and Safety Promotion*, 23(3):264–276, 2016. doi: 10.1080/17457300.2015.1032979.

[13] Amin Gharebaghi, Mir Abolfazl Mostafavi, Seyed Hossein Chavoshi, Geoffrey Edwards, and Patrick Fougeyrollas. The Role of Social Factors in the Accessibility of Urban Areas for People with Motor Disabilities. *ISPRS International Journal of Geo-Information*, 7:131, 03 2018. doi: 10.3390/ijgi7040131.

[14] Crispian Scully. 28 - Impairment and disability. In Crispian Scully, editor, *Scully's Medical Problems in Dentistry (Seventh Edition)*, pages 676–686. Churchill Livingstone, Oxford, 7 edition, 2014. ISBN 978-0-7020-5401-3. doi: 10.1016/B978-0-7020-5401-3.00028-X.

[15] Mónica Pinilla-Roncancio, Islay Mactaggart, Hannah Kuper, Carlos Dionicio, Jonathan Naber, G.V.S. Murthy, and Sarah Polack. Multidimensional poverty and disability: A case control study in India, Cameroon, and Guatemala. *SSM - Population Health*, 11:100591, 2020. ISSN 2352-8273. doi: https://doi.org/10.1016/j.ssmph.2020.100591.

[16] Margaret A. Winzer and Kas Mazurek. Exploring the Social Milieu of Disability: Themes of Poverty, Education, and Labour Participation. *Political Science*, 1(3):155–171, 2015. doi: CorpusID:59040489.

[17] Jhon W. McArthur Homi Kharas and Izumi Ihno. *Leave No One Behind: Time for Specifics on the Sustainable Development Goals*, page 333. THE BROOKINGS INSTITUTION, 10 2019. ISBN 08115737831.

[18] Gerard Goggin, Katie Ellis, and Wayne Hawkins. Disability at the centre of digital inclusion: assessing a new moment in technology and rights. *Communication Research and Practice*, 5(3):290–303, 2019. doi: 10.1080/22041451.2019.1641061.

[19] Emma Jolley, Paul Lynch, Bhavisha Virendrakumar, Stacy Rowe, and Elena Schmidt. Education and social inclusion of people with disabilities in five countries in West Africa: a literature review. *Disability and Rehabilitation*, 40(22):2704–2712, 2018. doi: 10.1080/09638288.2017.1353649.

[20] Mark Weber. Reflections on the New Individuals with Disabilities Education Improvement Act. *HeinOnline*, 58(1):8–51, 06 2006.

[21] Alvin Muilenburg and Maurice LeBlanc. *Body-Powered Upper-Limb Components*, pages 28–38. Springer-Verlag, 01 1989. doi: 10.1007/978-1-4612-3530-9_5.

[22] G. Bourhis, O. Horn, Olivier Habert, and Alain Pruski. An autonomous vehicle for people with motor disabilities. *Robotics & Automation Magazine, IEEE*, 8:20 – 28, 04 2001. doi: 10.1109/100.924353.

[23] Daehyung Park, Yuuna Hoshi, Harshal P. Mahajan, Ho Keun Kim, Zackory Erickson, Wendy A. Rogers, and Charles C. Kemp. Active robot-assisted feeding with a general-purpose mobile manipulator: Design, evaluation, and lessons learned. *Robotics and Autonomous Systems*, 124:103344, 2020. ISSN 0921-8890. doi: 10.1016/j.robot.2019.103344.

[24] Fabien Lotte, Chang Nam, and Anton Nijholt. *Introduction: Evolution of Brain-Computer Interfaces*, pages 1–11. Theoretical Advance, Taylor & Francis (CRC Press), 01 2018. ISBN 978-1-4987-7343-0.

[25] H. Berger. Ueber das Elekroenkephalogramm des Menschen. *Archiv für Psychiatrie und Nervenkrankheiten*, 40:527–570, 09 1929.

[26] Majid Aljalal, Sutrisno Ibrahim, Ridha Djemal, and Won ko. Comprehensive review on brain-controlled mobile robots and robotic arms based on electroencephalography signals. *Intelligent Service Robotics*, 13:539–563, 10 2020. doi: 10.1007/s11370-020-00328-5.

[27] Ram Kumar, K. Kumar, T. Rajkumar, Ilayaraja .M, and Dr Shankar. A review-classification of electrooculogram based human computer interfaces. *Biomedical Research (India)*, 29:1078–1084, 04 2018. doi: 10.4066/biomedicalresearch.29-17-2979.

[28] Alexis Burns, Hojjat Adeli, and John Buford. Upper Limb Movement Classification Via Electromyographic Signals and an Enhanced Probabilistic Network. *Journal of Medical Systems*, 44:176, 08 2020. doi: 10.1007/s10916-020-01639-x.

[29] Sergio Ruiz, Niels Birbaumer, and Ranganatha Sitaram. Abnormal Neural Connectivity in Schizophrenia and fMRI-Brain-Computer Interface as a Potential Therapeutic Approach. *Frontiers in Psychiatry*, 4:17, 2013. ISSN 1664-0640. doi: 10.3389/fpsyt.2013.00017.

[30] Erwei Yin, Zongtan Zhou, Jun Jiang, Yang Yu, and Dewen Hu. A dynamically optimized SSVEP brain-computer interface (BCI) speller. *IEEE transactions on bio-medical engineering*, 62:1–10, 04 2014. doi: 10.1109/TBME.2014.2320948.

[31] Martin Spüler and Simone Kurek. Alpha-band lateralization during auditory selective attention for brain computer interface control. *Brain-Computer Interfaces*, 5(1):23–29, 2018. doi: 10.1080/2326263X.2017.1415496.

[32] K. Venkatachalam, Devipriya A., Maniraj J., Sivaram M., Ambikapathy A., and S Amiri Iraj. A novel method of motor imagery classification using EEG signal. *Artificial Intelligence in Medicine*, 103: 101787, 2020. ISSN 0933-3657. doi: 10.1016/j.artmed.2019.101787.

[33] Patrick Ofner, Andreas Schwarz, Joana Pereira, and Gernot Müller-Putz. Upper limb movements can be decoded from the time-domain of low-frequency EEG. *PLOS ONE*, 12:e0182578, 08 2017. doi: 10.1371/journal.pone.0182578.

[34] Andrea Kübler, Femke Nijboer, J Mellinger, Theresa Vaughan, H Pawelzik, Gerwin Schalk, Dennis Mcfarland, N Birbaumer, and Jonathan Wolpaw. Patients with ALS can use sensorimotor rhythms to operate a brain-computer interface. *Neurology*, 64:1775–7, 06 2005. doi: 10.1212/01.WNL.0000158616.43002.6D.

[35] Herbert Ramoser, J Müller-Gerking, and Gert Pfurtscheller. Optimal Spatial Filtering of Single Trial EEG During Imagined Hand Movement. *IEEE transactions on rehabilitation engineering : a publication of the IEEE Engineering in Medicine and Biology Society*, 8:441–6, 01 2001. doi: 10.1109/86.895946.

[36] Bangyan Zhou, Xiaopei Wu, Jing Ruan, Zhao LV, and Lei Zhang. How many channels are suitable for independent component analysis in motor imagery brain-computer interface. *Biomedical Signal Processing and Control*, 50:103–120, 2019. ISSN 1746-8094. doi: 10.1016/j.bspc.2019.01.017.

[37] Xinyang Yu, Pharino Chum, and Kwee-Bo Sim. Analysis the effect of PCA for feature reduction in non-stationary EEG based motor imagery of BCI system. *Optik*, 125(3):1498–1502, 2014. ISSN 0030-4026. doi: 10.1016/j.ijleo.2013.09.013.

[38] Leonard Trejo, Kevin Wheeler, Charles Jorgensen, Roman Rosipal, Sam Clanton, Bryan Matthews, Andrew Hibbs, Robert Matthews, and Michael Krupka. Multimodal neuroelectric interface development. *IEEE transactions on neural systems and rehabilitation engineering: a publication of the IEEE Engineering in Medicine and Biology Society*, 11:199–204, 07 2003. doi: 10.1109/TNSRE.2003.814426.

[39] David Peterson, James Knight, Michael Kirby, Charles Anderson, and Michael Thaut. Feature Selection and Blind Source Separation in an EEG-Based Brain-Computer Interface. *EURASIP Journal on Advances in Signal Processing*, 19:1–14, 11 2005. doi: 10.1155/ASP.2005.3128.

[40] Imali Hettiarachchi, Thanh Nguyen, and Saeid Nahavandi. Multivariate Adaptive Autoregressive Modeling and Kalman Filtering for Motor Imagery BCI. *2015 IEEE International Conference on Systems, Man, and Cybernetics*, 1(15719020):3164–3168, 10 2015. doi: 10.1109/SMC.2015.549.

[41] Christa Neuper, Gernot Müller-Putz, Andrea Kübler, N Birbaumer, and Gert Pfurtscheller. Clinical application of an eeg-based brain-computer interface: A case study in a patient with severe motor impairment. *Clinical neurophysiology : official journal of the International Federation of Clinical Neurophysiology*, 114:399–409, 04 2003. doi: 10.1016/S1388-2457(02)00387-5.

[42] Dongkoo Shon, Kichang Im, Jeong-Ho Park, Dong-Sun Lim, Byungtae Jang, and Jong-Myon Kim. Emotional stress state detection using genetic algorithm-based feature selection on eeg signals. *International Journal of Environmental Research and Public Health*, 15(11), 2018. ISSN 1660-4601. doi: 10.3390/ijerph15112461. URL https://www.mdpi.com/1660-4601/15/11/2461.

[43] Zhaoyang Qiu, Jing Jin, Hak-Keung Lam, Yu Zhang, Xingyu Wang, and Andrzej Cichocki. Improved SFFS method for channel selection in motor imagery based BCI. *Neurocomputing*, 207:519–527, 2016. ISSN 0925-2312. doi: 10.1016/j.neucom.2016.05.035.

[44] Muhammad Hamza Bhatti, Javeria Khan, Muhammad Usman Ghani Khan, Razi Iqbal, Moayad Aloqaily, Yaser Jararweh, and Brij Gupta. Soft Computing-Based EEG Classification by Optimal Feature Selection and Neural Networks. *IEEE Transactions on Industrial Informatics*, 15(10):5747–5754, 2019. doi: 10.1109/TII.2019.2925624.

[45] Catherine M. Sweeney-Reed, Slawomir J. Nasuto, Marcus F. Vieira, and Adriano O. Andrade. Empirical Mode Decomposition and its Extensions Applied to EEG Analysis: A Review. *Advances in Data Science and Adaptive Analysis*, 10(02):1840001, 2018. doi: 10.1142/S2424922X18400016.

[46] Yijun Wang, Zhiguang Zhang, Yong Li, Lian Gao, Xiaorong Gao, and Fusheng Yang. BCI competition 2003-data set IV: an algorithm based on CSSD and FDA for classifying single-trial EEG. *Biomedical Engineering, IEEE Transactions on*, 51:1081 – 1086, 07 2004. doi: 10.1109/TBME.2004.826697.

[47] Abdelhakim Ridouh, Daoud Boutana, and Salah Bourennane. EEG Signals Classification Using Support Vector Machine. *Advanced Science, Engineering and Medicine*, 12:215–224, 02 2020. doi: 10.1166/asem.2020.2490.

[48] R. Fu, Y. Tian, T. Bao, Z. Meng, and P. Shi. Improvement Motor Imagery EEG Classification Based on Regularized Linear Discriminant Analysis. *Journal of Medical Systems*, 43(6):1–13, 2019. doi: 10.1007/s10916-019-1270-0.

[49] Martin Dobiáš and Jakub Šťastný. Movement EEG classification using parallel Hidden Markov Models. *2016 International Conference on Applied Electronics (AE)*, pages 65–68, 09 2016. doi: 10.1109/AE.2016.7577243.

[50] Rashid M, Hasan MJ Bari BS, Musa RM Razman MAM, Ab Nasir AF, and P.P. Abdul Majeed A. The classification of motor imagery response: an accuracy enhancement through the ensemble of random subspace k-NN. *PeerJ Computer Science*, 7:e374, 2021. doi: 10.7717/peerj-cs.374.

[51] Alborz Rezazadeh Sereshkeh, Robert Trott, Aurélien Bricout, and Tom Chau. EEG Classification of Covert Speech Using Regularized Neural Networks. *IEEE/ACM Transactions on Audio, Speech, and Language Processing*, 25(12):2292–2300, 2017. doi: 10.1109/TASLP.2017.2758164.

[52] Kaishuo Zhang, Neethu Robinson, Seong-Whan Lee, and Cuntai Guan. Adaptive transfer learning for EEG motor imagery classification with deep Convolutional Neural Network. *Neural Networks*, 136:1–10, 2021. ISSN 0893-6080. doi: 10.1016/j.neunet.2020.12.013.

[53] Xiao Zheng and Wanzhong Chen. An Attention-based Bi-LSTM Method for Visual Object Classification via EEG. *Biomedical Signal Processing and Control*, 63:102174, 2021. ISSN 1746-8094. doi: 10.1016/j.bspc.2020.102174.

[54] Çiğdem İnan Acı, Murat Kaya, and Yuriy Mishchenko. Distinguishing mental attention states of humans via an EEG-based passive BCI using machine learning methods. *Expert Systems with Applications*, 134:153–166, 2019. ISSN 0957-4174. doi: 10.1016/j.eswa.2019.05.057.

[55] Masaki Nakanishi, Yu-Te Wang, Tzyy-Ping Jung, John Zao, Yu-Yi Chien, Alberto Diniz-Filho, Fábio Daga, Yuan-Pin Lin, Yijun Wang, and Felipe Medeiros. Detecting Glaucoma With a Portable Brain-Computer Interface for Objective Assessment of Visual Function Loss. *JAMA Ophthalmology*, 135:1–8, 04 2017. doi: 10.1001/jamaophthalmol.2017.0738.

[56] Ioulietta Lazarou, Spiros Nikolopoulos, Panagiotis C. Petrantonakis, Ioannis Kompatsiaris, and Magda Tsolaki. EEG-Based Brain Computer Interfaces for Communication and Rehabilitation of People with Motor Impairment: A Novel Approach of the 21st Century. *Frontiers in Human Neuroscience*, 12:14, 2018. ISSN 1662-5161. doi: 10.3389/fnhum.2018.00014.

[57] Michael Bensch, Ahmed Karim, Jürgen Mellinger, Thilo Hinterberger, Michael Tangermann, Martin Bogdan, Wolfgang Rosenstiel, and Niels Birbaumer. Nessi: An EEG-Controlled Web Browser for Severely Paralyzed Patients. *Computational intelligence and neuroscience*, page 71863, 02 2007. doi: 10.1155/2007/71863.

[58] Hongbo Gao, Ling Luo, Ming Pi, Zhijun Li, Qinjian Li, Kuankuan Zhao, and Junliang Huang. EEG-Based Volitional Control of Prosthetic Legs for Walking in Different Terrains. *IEEE Transactions on Automation Science and Engineering*, 18(2):530–540, 2021. doi: 10.1109/TASE.2019.2956110.

[59] Yang Yu, Zongtan Zhou, Erwei Yin, Jun Jiang, Jingsheng Tang, Yadong Liu, and Dewen Hu. Toward brain-actuated car applications: Self-paced control with a motor imagery-based brain-computer

interface. *Computers in Biology and Medicine*, 77:148–155, 2016. ISSN 0010-4825. doi: 10.1016/j.compbiomed.2016.08.010.

[60] Walid Zgallai, John Brown, Afnan Ibrahim, Fatma Mahmood, Khulood Mohammad, Maitha Khalfan, Maryam Mohammed, Maryam Salem, and Noof Hamood. Deep Learning AI Application to an EEG driven BCI Smart Wheelchair. *Advances in Science and Engineering Technology International Conferences (ASET)*, 10(1):1–5, 03 2019. doi: 10.1109/ICASET.2019.8714373.

[61] Thomas Henzinger and Joseph Sifakis. The Embedded Systems Design Challenge. *FM 2006: Formal Methods. FM 2006. Lecture Notes in Computer Science*, 1(1):1–15, 08 2006. doi: 10.1007/11813040_1.

[62] Aleksandra Kawala-Janik, Mariusz Pelc, and Michal Podpora. Method for EEG Signals Pattern Recognition in Embedded Systems. *Elektronika ir Elektrotechnika*, 21:3–9, 06 2015. doi: 10.5755/j01.eee.21.3.9918.

[63] Mana Amornthammarong, Knadej Jareonsutasinee, and Duangjai Nacapricha. Interfacing of spectrophotometric detector to a personal computer via an audio card for a flow injection system. *Laboratory Robotics and Automation - LAB ROBOTICS AUTOMATION*, 12:138–141, 08 2000. doi: 10.1002/1098-2728(2000)12:33.0.CO;2-L.

[64] Dilip Sharma, Vitaliy Malikov, Danila Parygin, Alexey Golubev, Anastasia Lozhenitsina, and H. GPU-Card Performance Research in Satellite Imagery Classification Problems Using Machine Learning. *Procedia Computer Science*, 178:55–64, 01 2020. doi: 10.1016/j.procs.2020.11.007.

[65] Henry S. Dol, Paolo Casari, Timo van der Zwan, and Roald Otnes. Software-Defined Underwater Acoustic Modems: Historical Review and the NILUS Approach. *IEEE Journal of Oceanic Engineering*, 42(3):722–737, 2017. doi: 10.1109/JOE.2016.2598412.

[66] Assia Arsalane, Noureddine El Barbri, Abdelmoumen Tabyaoui, Abdessamad Klilou, Karim Rhofir, and Abdellah Halimi. An embedded system based on DSP platform and PCA-SVM algorithms for rapid beef meat freshness prediction and identification. *Computers and Electronics in Agriculture*, 152:385–392, 2018. ISSN 0168-1699. doi: 10.1016/j.compag.2018.07.031.

[67] Jorge Docampo, Sabela Ramos, Guillermo Taboada, Roberto Expósito, Juan Tourino, and Ramon Doallo. Evaluation of Java for General Purpose GPU Computing. *Advanced Information Networking and Applications Workshops (WAINA)*, 1(13615028):1398–1404, 03 2013. doi: 10.1109/WAINA.2013.234.

[68] Tomasz Chajduga. Embedded Systems Ensuring Safety for People With Disabilities. *System Safety: Human - Technical Facility - Environment*, 3:296–303, 05 2021. doi: 10.2478/czoto-2021-0031.

[69] Federica Turi, Maureen Clerc, and Théodore Papadopoulo. Long Multi-Stage Training for a Motor-Impaired User in a BCI Competition. *Frontiers in Human Neuroscience*, 15:1–13, 03 2021. doi: 10.3389/fnhum.2021.647908.

[70] No-Sang Kwak and Seong-Whan Lee. Error Correction Regression Framework for Enhancing the Decoding Accuracies of Ear-EEG Brain–Computer Interfaces. *IEEE Transactions on Cybernetics*, 50(8):3654–3667, 2020. doi: 10.1109/TCYB.2019.2924237.

[71] Dennis J McFarland, William A Sarnacki, and Jonathan R Wolpaw. Brain-computer interface (BCI) operation: optimizing information transfer rates. *Biological Psychology*, 63(3):237–251, 2003. ISSN 0301-0511. doi: 10.1016/S0301-0511(03)00073-5.

[72] Ke Lin, Shangkai Gao, and Xiaorong Gao. Boosting the information transfer rate of an SSVEP-BCI system using maximal-phase-locking value and minimal-distance spatial filter banks. *Tsinghua Science and Technology*, 24(3):262–270, 2019. doi: 10.26599/TST.2018.9010010.

[73] Martin Spüler. A high-speed brain-computer interface (BCI) using dry EEG electrodes. *PLOS ONE*, 12:1–12, 02 2017. doi: 10.1371/journal.pone.0172400.

[74] Enable Ireland Disability Federation of Ireland. Assistive Technology for People with Disabilities and Older People: A Discussion Paper. https://www.enableireland.ie/sites/default/files/publication/AT%20Paper%20final%20version.pdf, 2016. [Accessed 2-oct-2021].

[75] Governmentof Mexico. PROGRAMA Nacional para el Desarrollo y la Inclusión de las Personas con Discapacidad 2014-2018. https://www.un.org/development/desa/disabilities/wp-content/uploads/sites/15/2019/10/Mexico_Programa-Nacional-para-el-Desarrollo-y-la-Inclusi%C3%B3n-de-las-Personas-con-Discapacidad-2014-2018.pdf, 2014. [Accessed 2-oct-2021].

[76] Nikolas Williams, Genevieve McArthur, Bianca Wit, George Ibrahim, and Nicholas Badcock. A validation of Emotiv EPOC Flex saline for EEG and ERP research. *PeerJ*, 8:e9713, 08 2020. doi: 10.7717/peerj.9713.

[77] Fabien Lotte, Laurent Bougrain, and Maureen Clerc. Electroencephalography (EEG)-based Brain-Computer Interfaces. In *Wiley Encyclopedia of Electrical and Electronics Engineering*, page 44. Wiley, 2015. doi: 10.1002/047134608X.W8278.

[78] Kwon-Woo Ha and Jin-Woo Jeong. Temporal Pyramid Pooling for Decoding Motor-Imagery EEG Signals. *IEEE Access*, PP:1–1, 12 2020. doi: 10.1109/ACCESS.2020.3047678.

[79] Jiexun Liao, Joy Luo, Tao Yang, Rosa So, and Matthew Chua. Effects of local and global spatial patterns in EEG motor-imagery classification using convolutional neural network. *Brain-Computer Interfaces*, 7:1–10, 08 2020. doi: 10.1080/2326263X.2020.1801112.

[80] Mircea Nitulescu, Mircea Ivanescu, S. Mánoiu-Olaru, and Hai Nguyen. *Experimental Platform for Hexapod Locomotion*, volume 46, pages 259–267. New Advances in Mechanisms, Mechanical Transmissions and Robotics, 10 2017. ISBN 978-3-319-45449-8. doi: 10.1007/978-3-319-45450-4_26.

[81] Catherine Okoro, Natasha Hollis, Alissa Cyrus, and Shannon Griffin-Blake. Prevalence of Disabilities and Health Care Access by Disability Status and Type Among Adults - United States, 2016. *MMWR. Morbidity and mortality weekly report*, 67:882–887, 08 2018. doi: 10.15585/mmwr.mm6732a3.

[82] A. Beck. Determination of localization in the brain and spinal cord by means of electrical phenomena. *Presented October 20, 1890. Rozpr. Wydz. mat.-przyr.*, 1:186–232, 01 1973.

[83] A. Coenen and Oksana Zayachkivska. Adolf Beck: A pioneer in electroencephalography in between Richard Caton and Hans Berger. *Advances in cognitive psychology / University of Finance and Management in Warsaw*, 9:216–21, 12 2013. doi: 10.2478/v10053-008-0148-3.

[84] Otto Foerster and Hans Altenburger. Elektrobiologische Vorgänge an der menschlichen Hirnrinde. *Deutsche Zeitschrift für Nervenheilkunde*, 135:277–288, 2005.

[85] Wilder Penfield O. Foerster. The structural basis of traumatic epilepsy and results of radical operation. *Brain*, 53:99–119, 1930.

[86] T. Rasmussen and W. Penfield. The human sensorimotor cortex as studied by electrical stimulation. *Federation proceedings*, 6(1):184, 1947.

[87] G D Schott. Penfield's homunculus: a note on cerebral cartography. *Journal of Neurology, Neurosurgery & Psychiatry*, 56(4):329–333, 1993. ISSN 0022-3050. doi: 10.1136/jnnp.56.4.329.

[88] H H Jasper. Electrical Activity of the Brain. *Annual Review of Physiology*, 3(1):377–398, 1941. doi: 10.1146/annurev.ph.03.030141.002113.

[89] R. Hayne, R. Meyers, and J.R. Knott. Characteristics of electrical activity of human corpus striatum and neighboring structures. *Journal of neurophysiology*, 12(3):185–195, 1949. doi: 10.1152/jn.1949.12.3.185.

[90] J. Talairach, H. Hecaen, and M. David. Recherches sur la coagulation thérapeutique des structures sous-corticales chez l'homme. *Rev Neurol*, 81:4–24, 1949.

[91] J.J. Vidal. Toward Direct Brain-Computer Communication. *Annual review of biophysics and bioengineering*, 2:157–80, 02 1973. doi: 10.1146/annurev.bb.02.060173.001105.

[92] Philippe Chouinard and Tomas Paus. The Primary Motor and Premotor Areas of the Human Cerebral Cortex. *The Neuroscientist : a review journal bringing neurobiology, neurology and psychiatry*, 12:143–52, 05 2006. doi: 10.1177/1073858405284255.

[93] K. Neulinger, Joanne Oram, Helen Tinson, John O'Gorman, and David Shum. Prospective memory and frontal lobe function. *Neuropsychology, development, and cognition. Section B, Aging, neuropsychology and cognition*, 23:1–13, 07 2015. doi: 10.1080/13825585.2015.1069252.

[94] Adeen Flinker, Anna Korzeniewska, Avgusta Shestyuk, Piotr Franaszczuk, Nina Dronkers, Robert Knight, and Nathan Crone. Redefining the role of Broca's area in speech. *Proceedings of the National Academy of Sciences*, 112:1–5, 02 2015. doi: 10.1073/pnas.1414491112.

[95] Carsten Klingner and Otto Witte. Somatosensory deficits. *Handbook of clinical neurology*, 151:185–206, 01 2018. doi: 10.1016/B978-0-444-63622-5.00009-7.

[96] Jeffrey R Binder. Current Controversies on Wernicke's Area and its Role in Language. *Current neurology and neuroscience reports*, 17(8):1–10, August 2017. ISSN 1528-4042. doi: 10.1007/s11910-017-0764-8.

[97] Robert Clark. *Current Topics Regarding the Function of the Medial Temporal Lobe Memory System*, volume 37, pages 13–42. Current topics in behavioral neurosciences, 01 2017. ISBN 978-3-319-78755-8. doi: 10.1007/7854_2017_481.

[98] Emmanouil Froudarakis, Paul Fahey, Jacob Reimer, Stelios Smirnakis, Edward Tehovnik, and Andreas Tolias. The Visual Cortex in Context. *Annual Review of Vision Science*, 5:317–339, 09 2019. doi: 10.1146/annurev-vision-091517-034407.

[99] Suzana Herculano-Houzel. *The Human Advantage: A New Understanding of How Our Brain Became Remarkable*. The Human Advantage: A New Understanding of How Our Brain Became Remarkable, 04 2016. ISBN 9780262034258. doi: 10.7551/mitpress/9780262034258.001.0001.

[100] Bradley J. Edelman, Jianjun Meng, Nicholas Gulachek, Christopher C. Cline, and Bin He. Exploring Cognitive Flexibility With a Noninvasive BCI Using Simultaneous Steady-State Visual Evoked Potentials and Sensorimotor Rhythms. *IEEE Transactions on Neural Systems and Rehabilitation Engineering*, 26(5):936–947, 2018. doi: 10.1109/TNSRE.2018.2817924.

[101] Stephen Fairclough and Kiel Gilleade. *Advances in Physiological Computing*. Springer, 01 2014. ISBN 978-1-4471-6391-6. doi: 10.1007/978-1-4471-6392-3.

[102] G.R. Muller-Putz, R. Scherer, C. Neuper, and G. Pfurtscheller. Steady-state somatosensory evoked potentials: suitable brain signals for brain-computer interfaces? *IEEE Transactions on Neural Systems and Rehabilitation Engineering*, 14(1):30–37, 2006. doi: 10.1109/TNSRE.2005.863842.

[103] Yi-Feng Wang, Gang-Shu Dai, Feng Liu, Zhi-Liang Long, Jin Yan, and Hua-Fu Chen. Steady-state BOLD Response to Higher-order Cognition Modulates Low-Frequency Neural Oscillations. *Journal of cognitive neuroscience*, 27:1–10, 08 2015. doi: 10.1162/jocn_a_00864.

[104] Danielle Langeloo, Arjan Lelivelt, Louis Journee, Robert Slappendel, and Marinus De Kleuver. Transcranial Electrical Motor-Evoked Potential Monitoring During Surgery for Spinal Deformity. *Spine*, 28:1043–50, 06 2003. doi: 10.1097/01.BRS.0000061995.75709.78.

[105] Cédric Gouy-Pailler, Sophie Achard, Bertrand Rivet, Christian Jutten, Emmanuel Maby, Antoine Souloumiac, and Marco Congedo. Topographical Dynamics of Brain Connections for the Design of Asynchronous Brain-Computer Interfaces. *Conference proceedings : ... Annual International Conference of the IEEE Engineering in Medicine and Biology Society. IEEE Engineering in Medicine and Biology Society. Conference*, 2007:2520–3, 02 2007. doi: 10.1109/IEMBS.2007.4352841.

[106] Mamunur Rashid, Norizam Sulaiman, Anwar P. P. Abdul Majeed, Rabiu Muazu Musa, Ahmad Fakhri Ab. Nasir, Bifta Sama Bari, and Sabira Khatun. Current Status, Challenges, and Possible Solutions of EEG-Based Brain-Computer Interface: A Comprehensive Review. *Frontiers in Neurorobotics*, 14: 25, 2020. ISSN 1662-5218. doi: 10.3389/fnbot.2020.00025.

[107] Bernardo Seno, Matteo Matteucci, and Luca Mainardi. Online Detection of P300 and Error Potentials in a BCI Speller. *Comp. Int. and Neurosc.*, 2010:1–5, 01 2010.

[108] Elisabeth V.C. Friedrich, Reinhold Scherer, and Christa Neuper. Long-term evaluation of a 4-class imagery-based brain-computer interface. *Clinical Neurophysiology*, 124(5):916–927, 2013. ISSN 1388-2457. doi: 10.1016/j.clinph.2012.11.010.

[109] Maureen Clerc Fabien Lotte, Laurent Bougrain. Electroencephalography (EEG)-based BrainComputer Interfaces. *Wiley Encyclopedia of Electrical and Electronics Engineering*, 1(1):44, 2015. doi: 10.1002/047134608X.W8278.

[110] Samden Lhatoo, Nuria Lacuey, and Philippe Ryvlin. *Principles of Invasive EEG*, pages 19–25. Oxford University Press, 11 2018. ISBN 9780198714668. doi: 10.1093/med/9780198714668.003.0002.

[111] H.H. Jasper. The 10-20 electrode system of the International Federation. *Electroenceph Clin Neurophysiol*, 10:370–375, 01 1958.

[112] Jayant Acharya, Abeer Hani, Janna Cheek, Parthasarathy Thirumala, and Tammy Tsuchida. American Clinical Neurophysiology Society Guideline 2: Guidelines for Standard Electrode Position Nomenclature. *The Neurodiagnostic Journal*, 56:245–252, 10 2016. doi: 10.1080/21646821.2016.1245558.

[113] Margitta Seeck, Laurent Koessler, Thomas Bast, Frans Leijten, Christoph Michel, Christoph Baumgartner, Bin He, and Sándor Beniczky. The standardized EEG electrode array of the IFCN. *Clinical Neurophysiology*, 128(10):2070–2077, 2017. ISSN 1388-2457. doi: 10.1016/j.clinph.2017.06.254.

[114] Jair Montoya-Martínez, Alexander Bertrand, and Tom Francart. Effect of number and placement of EEG electrodes on measurement of neural tracking of speech. *PloS one*, 16(2):e0246769, 02 2021. doi: 10.1371/journal.pone.0246769.

[115] L. Chen, B. Gu, Z. Wang, L. Zhang, M. Xu, S. Liu, F. He, and D. Ming. EEG-controlled functional electrical stimulation rehabilitation for chronic stroke: system design and clinical application. *Frontiers of Medicine*, 15(5):740–749, 2021. doi: 10.1007/s11684-020-0794-5.

[116] S.F. Abd Gani, M.F. Miskon, R.A. Hamzah, K.A. A. Aziz, A.F. Kadmin, A.Z. Jidin, M.F. Md Basar, M. Kamalrudin, E.N.S. A. Razak, and M.A.S. Md Ali Shah. Electrical appliance switching controller by brain wave spectrum evaluation using a wireless EEG headset. *International Journal of Emerging Technology and Advanced Engineering*, 11(10):109–117, 2021. doi: 10.46338/IJETAE1021_14.

[117] C. Escolano, E. López-Larraz, J. Minguez, and L. Montesano. Brain-Computer Interface-Based Neurorehabilitation: From the Lab to the Users' Home. *Biosystems and Biorobotics*, 28(IV):569–573, 2022. doi: 10.1007/978-3-030-70316-5_91.

[118] K. Banach, M. Małecki, M. Rosół, and A. Broniec. Brain-computer interface for electric wheelchair based on alpha waves of EEG signal. *Bio-Algorithms and Med-Systems*, 17(3):165–172, 2021. doi: 10.1515/bams-2021-0095.

[119] P. Von Bunau, F.C. Meinecke, S. Scholler, and K.-R. Muller. Finding stationary brain sources in EEG data. In *Annual International Conference of the IEEE Engineering in Medicine and Biology Society. IEEE Engineering in Medicine and Biology Society. Annual International Conference*, volume 2010, pages 2810–2813. Annu Int Conf IEEE Eng Med Biol Soc, 2010. doi: 10.1109/IEMBS.2010.5626537.

[120] Y. Dai, F. Duan, F. Feng, Z. Sun, Y. Zhang, C.F. Caiafa, P. Marti-Puig, and J. Solé-Casals. A fast approach to removing muscle artifacts for eeg with signal serialization based ensemble empirical mode decomposition. *Entropy*, 23(9):1170, 2021. doi: 10.3390/e23091170.

[121] P. Patel, R. Raghunandan, and R.N. Annavarapu. EEG-based human emotion recognition using entropy as a feature extraction measure. *Brain Informatics*, 8(1):1–13, 2021. doi: 10.1186/s40708-021-00141-5.

[122] P.P. Mini, T. Thomas, and R. Gopikakumari. EEG based direct speech BCI system using a fusion of SMRT and MFCC/LPCC features with ANN classifier. *Biomedical Signal Processing and Control*, 68:102625, 2021. doi: 10.1016/j.bspc.2021.102625.

[123] Juan Arango, J.C. Mazo, and A. PeñaPalacio. Rehabilitation system for phantom limb syndrome using brain-computer interface and augmented reality. *Revista Ibérica de Sistemas y Tecnologías de Información*, 2013:1000–1008, 01 2013.

[124] E. Mikołajewska and D. Mikołajewski. Neuroprostheses for increasing disabled patients' mobility and control. *Advances in Clinical and Experimental Medicine*, 21(2):263–272, 2012.

[125] S. Kate, V. Malkapure, B. Narkhede, and R. Shriram. Analysis of Electroencephalogram During Coloured Word Reading Interference. *Lecture Notes in Electrical Engineering*, 750:253–262, 2021. doi: 10.1007/978-981-16-0336-5_21.

[126] R. Abid, F. Hamden, M.A. Matmati, and N. Derbel. Fuzzy Control of an Intelligent Electric Wheelchair Using an EMOTIV EPOC Headset. *Smart Sensors, Measurement and Instrumentation*, 39:261–286, 2021. doi: 10.1007/978-3-030-71221-1_12.

[127] S. Narayana, R.V. Prasad, and K. Warmerdam. Mind your thoughts: BCI using single EEG electrode. *IET Cyber-Physical Systems: Theory and Applications*, 4(2):164–172, 2019. doi: 10.1049/iet-cps.2018.5059.

[128] Murat Kaya, Mustafa Binli, Erkan Ozbay, Hilmi Yanar, and Yuriy Mishchenko. A large electroencephalographic motor imagery dataset for electroencephalographic brain computer interfaces. *Scientific Data*, 5:1–16, 10 2018. doi: 10.1038/sdata.2018.211.

[129] Kanishk Rai, Keshav Thakur, Preethi k Mane, and Narayan Panigrahi. Design of an EEG Acquisition System for Embedded Edge Computing. *Advances in Science, Technology and Engineering Systems Journal*, 5:119–, 07 2020. doi: 10.25046/aj050416.

[130] X. Deng, B. Zhang, K. Liu, J. Wang, P. Yang, and C. Hu. The Classification of Motor Imagery EEG Signals Based on the Time-Frequency-Spatial Feature. *Proceedings of 2021 IEEE 10th Data Driven Control and Learning Systems Conference, DDCLS 2021*, 1(9455464):6–11, 2021. doi: 10.1109/DDCLS52934.2021.9455464.

[131] A.K. Maddirala and K.C. Veluvolu. Eye-blink artifact removal from single channel EEG with k-means and SSA. *Scientific Reports*, 11(1):1–14, 2021. doi: 10.1038/s41598-021-90437-7.

[132] S. Kumar, A. Sharma, and T. Tsunoda. Subject-Specific-Frequency-Band for Motor Imagery EEG Signal Recognition Based on Common Spatial Spectral Pattern. *Lecture Notes in Computer Science (including subseries Lecture Notes in Artificial Intelligence and Lecture Notes in Bioinformatics)*, 11671 LNAI:712–722, 2019. doi: 10.1007/978-3-030-29911-8_55.

[133] E. Yosrita, R.N. Aziza, R.F. Ningrum, and G. Muhammad. Denoising of EEG signal based on word imagination using ICA for artifact and noise removal on unspoken speech. *Indonesian Journal of Electrical Engineering and Computer Science*, 22(1):83–88, 2021. doi: 10.11591/ijeecs.v21.i4.pp83-88.

[134] K. Paulson and O. Alfahad. Identification of multi-channel simulated auditory event-related potentials using a combination of principal component analysis and Kalman filtering. *ACM International Conference Proceeding Series*, 1(1):18–22, 2018. doi: 10.1145/3288200.3288211.

[135] M.M. Wankhade and S.S. Chorage. Eye-Blink artifact Detection and Removal Approaches for BCI using EEG. *2021 6th International Conference on Recent Trends on Electronics, Information, Communication and Technology, RTEICT 2021*, 1(1):718–721, 2021. doi: 10.1109/RTEICT52294.2021.9574024.

[136] H.K. Garg and A.K. Kohli. EEG Spike Detection Technique Using Output Correlation Method: A Kalman Filtering Approach. *Circuits, Systems, and Signal Processing*, 34(8):2643–2665, 2015. doi: 10.1007/s00034-015-9982-y.

[137] T.K. Reddy, V. Arora, L. Behera, Y.-K. Wang, and C.-T. Lin. Multiclass Fuzzy Time-Delay Common Spatio-Spectral Patterns with Fuzzy Information Theoretic Optimization for EEG-Based Regression Problems in Brain-Computer Interface (BCI). *IEEE Transactions on Fuzzy Systems*, 27 (10):1943–1951, 2019. doi: 10.1109/TFUZZ.2019.2892921.

[138] A.S. Eltrass and N.H. Ghanem. A new automated multi-stage system of non-local means and multi-kernel adaptive filtering techniques for EEG noise and artifacts suppression. *Journal of Neural Engineering*, 18(3):036023, 2021. doi: 10.1088/1741-2552/abe397.

[139] C.-L. Teng, Y.-Y. Zhang, W. Wang, Y.-Y. Luo, G. Wang, and J. Xu. A Novel Method Based on Combination of Independent Component Analysis and Ensemble Empirical Mode Decomposition for Removing Electrooculogram Artifacts From Multichannel Electroencephalogram Signals. *Frontiers in Neuroscience*, 15(729403):1–13, 2021. doi: 10.3389/fnins.2021.729403.

[140] H. Zhang, C. Wei, M. Zhao, Q. Liu, and H. Wu. A novel convolutional neural network model to remove muscle artifacts from eeg. *ICASSP, IEEE International Conference on Acoustics, Speech and Signal Processing - Proceedings*, 2021-June:1265–1269, 2021. doi: 10.1109/ICASSP39728.2021.9414228.

[141] S.M.M. Najeeb, H.T.S.A. rikabi, and S.M. Ali. Finding the discriminative frequencies of motor electroencephalography signal using genetic algorithm. *Telkomnika (Telecommunication Computing Electronics and Control)*, 19(1):285–292, 2021. doi: 10.12928/TELKOMNIKA.v19i1.17884.

[142] F.A. Rosli, A. Saidatul, A.A. Abdullah, and R.F. Navea. The Wavelet packet decomposition features applied in EEG based authentication system. *Journal of Physics: Conference Series*, 1997(1):012035, 2021. doi: 10.1088/1742-6596/1997/1/012035.

[143] J. Wang, G. Xu, L. Wang, and H. Zhang. Feature extraction of brain-computer interface based on improved multivariate adaptive autoregressive models. *Proceedings - 2010 3rd International Conference on Biomedical Engineering and Informatics, BMEI 2010*, 2:895–898, 2010. doi: 10.1109/BMEI.2010.5639885.

[144] S.N. Farihah, K.Y. Lee, W. Mansor, N.B. Mohamad, Z. Mahmoodin, and S.A. Saidi. EEG average FFT index for dyslexic children with writing disorder. *ISSBES 2015 - IEEE Student Symposium in Biomedical Engineering and Sciences: By the Student for the Student*, 1:118–121, 2016. doi: 10.1109/ISSBES.2015.7435880.

[145] J.-X. Mi, R.-F. Li, and G. Chen. Exploring Multi-scale Temporal and Spectral CSP Feature for Multi-class Motion Imagination Task Classification. *Lecture Notes in Computer Science (including subseries Lecture Notes in Artificial Intelligence and Lecture Notes in Bioinformatics)*, 12838 LNAI: 174–184, 2021. doi: 10.1007/978-3-030-84532-2_16.

[146] K. Alhasan, S. Aliyu, L. Chen, and F. Chen. ICA-based EEG feature analysis and classification of learning styles. *Proceedings - IEEE 17th International Conference on Dependable, Autonomic and Secure Computing, IEEE 17th International Conference on Pervasive Intelligence and Computing*, 1 (16206704):271–276, 2019. doi: 10.1109/DASC/PiCom/CBDCom/CyberSciTech.2019.00057.

[147] S. Bavkar, B. Iyer, and S. Deosarkar. Optimal EEG channels selection for alcoholism screening using EMD domain statistical features and harmony search algorithm. *Biocybernetics and Biomedical Engineering*, 41(1):83–96, 2021. doi: 10.1016/j.bbe.2020.11.001.

[148] J. Raymaekers, P.J. Rousseeuw, and M. Hubert. Class Maps for Visualizing Classification Results. *Technometrics*, 1050(1):1–15, 2021. doi: 10.1080/00401706.2021.1927849.

[149] E.L. Allwein, R.E. Schapire, and Y. Singer. Reducing multiclass to binary: A unifying approach for margin classifiers. *Journal of Machine Learning Research*, 1(2):113–141, 2001.

[150] N.A. Alzahab, H. Alimam, M.S.D.S. Alnahhas, A. Alarja, and Z. Marmar. Determining the optimal feature for two classes Motor-Imagery Brain-Computer Interface (L/R-MI-BCI) systems in different binary classifiers. *International Journal of Mechanical and Mechatronics Engineering*, 19(1): 132–150, 2019.

[151] J.A. Fdez-Sánchez, J.D. Pascual-Triana, A. Fernández, and F. Herrera. Learning interpretable multi-class models by means of hierarchical decomposition: Threshold Control for Nested Dichotomies. *Neurocomputing*, 463:514–524, 2021. doi: 10.1016/j.neucom.2021.07.097.

[152] L. Ngan Thanh, D. Anh Hoang Lan, N. Dung Xuan, D. Khiet Thi Thu, P. Chau Nu Ngoc, N. Thuong Hoai, and H.T.T. Huong. Classification of Four-Class Motor-Imagery Data for Brain-Computer Interfaces. *IFMBE Proceedings*, 85:763–778, 2022. doi: 10.1007/978-3-030-75506-5_62.

[153] C. Huang. Recognition of psychological emotion by EEG features. *Network Modeling Analysis in Health Informatics and Bioinformatics*, 10(12):1–11, 2021. doi: 10.1007/s13721-020-00283-2.

[154] A. Rakshit, A. Khasnobish, and D.N. Tibarewala. A Naïve Bayesian approach to lower limb classification from EEG signals. *2016 2nd International Conference on Control, Instrumentation, Energy and Communication, CIEC 2016*, 1(16143316):140–144, 2016. doi: 10.1109/CIEC.2016.7513812.

[155] L. Si, Z. Liu, and G. Wang. Depth of Anesthesia Monitoring Method Based on EEG Microstate Analysis and Hidden Markov Model. *2021 IEEE 2nd International Conference on Pattern Recognition and Machine Learning, PRML 2021*, 1(21129983):298–303, 2021. doi: 10.1109/PRML52754.2021.9520709.

[156] J.S. Rani Alex, M.A. Haque, A. Anand, A. Gautam, and N. Venkatesan. A deep learning approach for robotic arm control using brain-Computer interface. *International Journal of Biology and Biomedical Engineering*, 14:128–135, 2020. doi: 10.46300/91011.2020.14.18.

[157] Vernon J Lawhern, Amelia J Solon, Nicholas R Waytowich, Stephen M Gordon, Chou P Hung, and Brent J Lance. EEGNet: a compact convolutional neural network for EEG-based brain–computer interfaces. *Journal of Neural Engineering*, 15(5):056013, jul 2018. doi: 10.1088/1741-2552/aace8c.

[158] R. Widadi, D. Zulherman, and S. Rama Febriyan Ari. Time Domain Features for EEG Signal Classification of Four Class Motor Imagery Using Artificial Neural Network. *Lecture Notes in Electrical Engineering*, 746 LNEE:605–612, 2021. doi: 10.1007/978-981-33-6926-9_53.

[159] Jamolbek Mattiev and Branko KavÅ¡ek. Coverage-based classification using association rule mining. *Applied Sciences*, 10:7013, 10 2020. doi: 10.3390/app10207013.

[160] Hesam Hasanpour, Ramak Ghavamizadeh, and Keivan Navi. Improving rule-based classification using Harmony Search. *PeerJ Computer Science*, 5:e188, 11 2019. doi: 10.7717/peerj-cs.188.

[161] A. Ali, T.A. Soomro, F. Memon, M.Y.A. Khan, P. Kumar, M.U. Keerio, and B.S. Chowdhry. EEG Signals Based Choice Classification for Neuromarketing Applications. *Intelligent Systems Reference Library*, 210:371–394, 2022. doi: 10.1007/978-3-030-76653-5_20.

[162] M. Jordan, Neto Nogueira, G.N., Jr Brito, A., and P. Nohama. Virtual keyboard with the prediction of words for children with cerebral palsy. *Computer Methods and Programs in Biomedicine*, 192 (105402):105402, 2020. doi: 10.1016/j.cmpb.2020.105402.

[163] C.P. Shantala and C.R. Rashmi. Mind Controlled Wireless Robotic Arm Using Brain Computer Interface. *2017 IEEE International Conference on Computational Intelligence and Computing Research, ICCIC 2017*, 1(18262628):1–8, 2018. doi: 10.1109/ICCIC.2017.8524431.

[164] N.N. Shusharina, E.A. Bogdanov, V.A. Petrov, E.V. Silina, and M.V. Patrushev. Multifunctional neurodevice for recognition of electrophysiological signals and data transmission in an exoskeleton construction. *Biology and Medicine*, 8(6):1, 2016. doi: 10.4172/0974-8369.1000331.

[165] H. Kim, K. Song, T. Roh, and H.-J. Yoo. A 95% accurate EEG-connectome processor for a mental health monitoring system. *Journal of Semiconductor Technology and Science*, 16(4):436–442, 2016. doi: 10.5573/JSTS.2016.16.4.436.

[166] World Association. Declaration of helsinki world medical association declaration of helsinki. *Bulletin of the World Health Organization*, 79:373–374, 02 2001. doi: 10.4414/fms.2001.04031.

[167] D.O. Hebb. *The Organization of Behavior: A Neuropsychological Theory*, volume xix, page 378. New York: Wiley, 01 1949.

[168] T. Freeth, D. Higgon, A. Dacanalis, L. MacDonald, M. Georgakopoulou, and A. Wojcik. A Model of the Cosmos in the ancient Greek Antikythera Mechanism. *Scientific Reports*, 11(1):1–15, 2021. doi: 10.1038/s41598-021-84310-w.

[169] T. Freeth. Eclipse prediction on the ancient Greek astronomical calculating machine known as the Antikythera Mechanism. *PLoS ONE*, 9(7):e103275, 2014. doi: 10.1371/journal.pone.0103275.

[170] W.S. McCulloch and W. Pitts. A logical calculus of the ideas immanent in nervous activity. *The Bulletin of Mathematical Biophysics*, 5(4):115–133, 1943. doi: 10.1007/BF02478259.

[171] Rosenblatt and Frank. The Perceptron: A Probabilistic Model for Information Storage and Organization in the Brain. *Psychological Review*, 65(6):386–408, 01 1958.

[172] B. Widrow. Pattern Recognition and Adaptive Control. *IEEE Transactions on Applications and Industry*, 83(74):269–277, 1964. doi: 10.1109/TAI.1964.5407756.

[173] Paul Werbos and Paul John. Beyond regression : new tools for prediction and analysis in the behavioral sciences , 01 1974.

[174] Kurt Hornik, Maxwell Stinchcombe, and Halbert White. Multilayer feedforward networks are universal approximators. *Neural Networks*, 2(5):359–366, 1989. ISSN 0893-6080. doi: 10.1016/0893-6080(89)90020-8.

[175] Seong-Whan Lee. Multilayer cluster neural network for totally unconstrained handwritten numeral recognition. *Neural Networks*, 8(5):783–792, 1995. ISSN 0893-6080. doi: 10.1016/0893-6080(95)00020-Z.

[176] Kunihiko Fukushima. Neocognitron: A hierarchical neural network capable of visual pattern recognition. *Neural Networks*, 1(2):119–130, 1988. ISSN 0893-6080. doi: 10.1016/0893-6080(88)90014-7.

[177] Sepp Hochreiter. *Untersuchungen zu dynamischen neuronalen Netzen*. PhD thesis, Josef Hochreiter Institut f´ur Informatik Technische Universit´at M´unchenen, 04 1991.

[178] David Lowe. Distinctive Image Features from Scale-Invariant Keypoints. *International Journal of Computer Vision*, 60:91–110, 11 2004. doi: 10.1023/B\%3AVISI.0000029664.99615.94.

[179] Julius Hannink, Thomas Kautz, Cristian Pasluosta, Jens Barth, Sam Schülein, Karl Gassmann, Jochen Klucken, and Bjoern Eskofier. Mobile Stride Length Estimation With Deep Convolutional Neural Networks. *IEEE Journal of Biomedical and Health Informatics*, PP:1–1, 03 2017. doi: 10.1109/JBHI.2017.2679486.

[180] Yann Lecun, Leon Bottou, Y. Bengio, and Patrick Haffner. Gradient-Based Learning Applied to Document Recognition. *Proceedings of the IEEE*, 86:2278 – 2324, 12 1998. doi: 10.1109/5.726791.

[181] Kaiming He, Xiangyu Zhang, Shaoqing Ren, and Jian Sun. Deep Residual Learning for Image Recognition. *Conference: 2016 IEEE Conference on Computer Vision and Pattern Recognition (CVPR)*, 1(1):770–778, 06 2016. doi: 10.1109/CVPR.2016.90.

[182] Alexander Waibel, Toshiyuki Hanazawa, G. Hinton, Kiyohiro Shikano, and K.J. Lang. Phoneme recognition using time-delay neural networks. *Acoustics, Speech and Signal Processing, IEEE Transactions on*, 37:328 – 339, 04 1989. doi: 10.1109/29.21701.

[183] Y. Bengio. *A connectionist approach to speech recognition*, volume 7, pages 3–23. Advances in Pattern Recognition Systems Using Neural Network Technologies, 01 1994. ISBN 978-981-279-792-6. doi: 10.1142/9789812797926_0002.

[184] Y. Bengio, R Ducharme, Pascal V. Vincent, and Christian Jauvin. A Neural Probabilistic Language Model. *Journal of Machine Learning Research*, 3:1137–1155, 10 2001.

[185] Juergen Schmidhuber. Deep Learning in Neural Networks: An Overview. *Neural Networks*, 61:85–117, 04 2014. doi: 10.1016/j.neunet.2014.09.003.

[186] Federico Landi, Lorenzo Baraldi, Marcella Cornia, and Rita Cucchiara. Working Memory Connections for LSTM. *Neural Networks*, 144:1–17, 09 2021. doi: 10.1016/j.neunet.2021.08.030.

[187] Bishop and M. Christopher. *Neural Networks for Pattern Recognition*. Oxford University Press, Oxford, 01 1995.

[188] Boris Polyak. Some methods of speeding up the convergence of iteration methods. *Ussr Computational Mathematics and Mathematical Physics*, 4:1–17, 12 1964. doi: 10.1016/0041-5553(64)90137-5.

[189] Jeffrey Dean, G.s Corrado, Rajat Monga, Kai Chen, Matthieu Devin, Quoc Le, Mark Mao, Aurelio Ranzato, Andrew Senior, Paul Tucker, Ke Yang, and Andrew Ng. Large Scale Distributed Deep Networks. *Advances in neural information processing systems*, 25(1):1–9, 10 2012.

[190] John Duchi, Elad Hazan, and Yoram Singer. Adaptive Subgradient Methods for Online Learning and Stochastic Optimization. *Journal of Machine Learning Research*, 12:2121–2159, 07 2011.

[191] Diederik Kingma and Jimmy Ba. Adam: A Method for Stochastic Optimization. *International Conference on Learning Representations*, 1(1):1–15, 12 2014.

[192] Leslie Smith. Cyclical Learning Rates for Training Neural Networks. *2017 IEEE Winter Conference on Applications of ComputerVision (WACV)*, 1(1):464–472, 03 2017. doi: 10.1109/WACV.2017.58.

[193] Xavier Glorot and Y. Bengio. Understanding the difficulty of training deep feedforward neural networks. *Journal of Machine Learning Research - Proceedings Track*, 9(1):249–256, 01 2010.

[194] Alejandro Peña, Juan Arango, and Julián M. Sistema para Rehabilitación del Síndrome del Miembro Fantasma utilizando Interfaz Cerebro-Computador y Realidad Aumentada. *Revista Ibérica de Sistemas y Tecnologías de la Información - RISTI*, 11:93–106, 06 2013. doi: 10.4304/risti.11.93-106.

[195] Jose Salgado, Cristian Barrera, and Barrera Monje. Emotiv EPOC BCI with Python on a Raspberry Pi. *Sistemas y Telemática*, 14:27–38, 03 2016. doi: 10.18046/syt.v14i36.2217.

[196] K. Kato, K. Takahashi, N. Mizuguchi, and J. Ushiba. Online detection of amplitude modulation of motor-related EEG desynchronization using a lock-in amplifier: Comparison with a fast Fourier transform, a continuous wavelet transform, and an autoregressive algorithm. *Journal of Neuroscience Methods*, 293:289–298, 2018. doi: 10.1016/j.jneumeth.2017.10.015.

[197] Baolei Xu, Yunfa Fu, Gang Shi, Xuxian Yin, Zhidong Wang, Hongyi Li, and Changhao Jiang. Enhanced Performance by Time-Frequency-Phase Feature for EEG-based BCI Systems. *The Scientific World Journal*, 2014:420561, 06 2014. doi: 10.1155/2014/420561.

[198] Han-Jeong Hwang, Kiwoon Kwon, and Chang-Hwang Im. Neurofeedback-based motor imagery training for brain-Computer interface (BCI). *Journal of Neuroscience Methods*, 179(1):150 – 156, 2009. ISSN 0165-0270. doi: 10.1016/j.jneumeth.2009.01.015.

[199] M. Lotze, P. Montoya, M. Erb, E. Hũlsmann, H. Flor, U. Klose, N. Birbaumer, and W. Grodd. Activation of cortical and cerebellar motor areas during executed and imagined hand movements: An fMRI study. *Journal of Cognitive Neuroscience*, 11(5):491–501, 1999. doi: 10.1162/089892999563553.

[200] Intel. Intel FPGA SDK for OpenCL Standard Edition. https://www.intel.com/content/dam/www/programmable/us/en/pdfs/literature/hb/opencl-sdk/aocl_c5soc_getting_started.pdf, 2018. [Accessed 7-Feb-2019].

[201] J.D. Guerrero, R. Sepúlveda, O. Montiel, and O. Castillo. Identification of the workspace of a hexapod robot using multiobjective optimization. *Computacion y Sistemas*, 21(2):305–314, 2017. doi: 10.13053/CyS-21-2-2739.

[202] H. Soula, G. Beslon, and O. Mazet. Spontaneous dynamics of asymmetric random recurrent spiking neural networks. *Neural Computation*, 18(1):60–79, 2006. doi: 10.1162/089976606774841567.

[203] Ping Wang, Aimin Jiang, Xiaofeng Liu, Jing Shang, and Li Zhang. LSTM-based EEG Classification in Motor Imagery Tasks. *IEEE Transactions on Neural Systems and Rehabilitation Engineering*, PP: 1–1, 10 2018. doi: 10.1109/TNSRE.2018.2876129.

[204] J.Y.F. Yam and T.W.S. Chow. A weight initialization method for improving training speed in feedforward neural network. *Neurocomputing*, 30(1-4):219–232, 2000. doi: 10.1016/S0925-2312(99)00127-7.

[205] François Chollet. Keras. GitHub. https://github.com/fchollet/keras, 2015.

[206] Bing Xu, Naiyan Wang, Tianqi Chen, and Mu Li. Empirical Evaluation of Rectified Activations in Convolutional Network, 2015.

[207] Bolin Gao and Lacra Pavel. On the Properties of the Softmax Function with Application in Game Theory and Reinforcement Learning. *ArXiv*, 1704.00805(1):1–10, 04 2017.

[208] Saleh Alzahrani and Charles Anderson. A Comparison of Conventional and Tri-Polar EEG Electrodes for Decoding Real and Imaginary Finger Movements from One Hand. *International Journal of Neural Systems*, 31:2150036, 07 2021. doi: 10.1142/S0129065721500362.

[209] Yasuto Tanaka, Norihiko Saga, and Yusuke Hashimoto. Event-related synchronization and desynchronization of EEG in association with electromyography of human limb movement. *The Proceedings of JSME annual Conference on Robotics and Mechatronics (Robomec)*, 2017:1P2–O08, 11 2017. doi: 10.1299/jsmermd.2017.1P2-O08.

[210] M.J. Banissy, L.E. Annett, P. Asiedu-Offei, R. Rosch, and J.M. Gurd. Left, right, hand 'n space. In *Handedness: Theories, Genetics and Psychology*, pages 109–122. Nova Science Publishers, 1 edition, 03 2012. ISBN 978-1614705024.

[211] Yuriy Mishchenko, Murat Kaya, Erkan Ozbay, and Hilmi Yanar. Developing a 3- to 6-state EEG-based brain-computer interface for a robotic manipulator control. *bioRxiv*, 66(4):1–15, 2017. doi: 10.1101/171025.

[212] Paul Von Bünau, Frank C. Meinecke, Simon Scholler, and Klaus-Robert Müller. Finding stationary brain sources in EEG data. In *2010 Annual International Conference of the IEEE Engineering in Medicine and Biology*, volume 1, pages 2810–2813, 2010. doi: 10.1109/IEMBS.2010.5626537.

[213] Maximilian Igl, Gregory Farquhar, Jelena Luketina, Wendelin Boehmer, and Shimon Whiteson. Transient Non-stationarity and Generalisation in Deep Reinforcement Learning. In *International Conference on Learning Representations*, pages 1–16, 2021.

[214] Rob J Hyndman and George Athanasopoulos. *Forecasting: Principles and Practice*. OTexts, 2 edition, 2018.

[215] Norden E. Huang, Zheng Shen, Steven R. Long, Manli C. Wu, Hsing H. Shih, Quanan Zheng, Nai-Chyuan Yen, Chi Chao Tung, and Henry H. Liu. The empirical mode decomposition and the Hilbert spectrum for nonlinear and non-stationary time series analysis. *Proceedings of the Royal Society of London. Series A: Mathematical, Physical and Engineering Sciences*, 454(1971):903–995, 03 1998. doi: 10.1098/rspa.1998.0193.

[216] Yangkang Chen, Guoyin Zhang, Shuwei Gan, and Chenglin Zhang. Enhancing seismic reflections using empirical mode decomposition in the flattened domain. *Journal of Applied Geophysics*, 119: 99–105, 2015. ISSN 09269851. doi: 10.1016/j.jappgeo.2015.05.012.

[217] P. Flandrin, G. Rilling, and P. Goncalves. Empirical mode decomposition as a filter bank. *IEEE Signal Processing Letters*, 11(2):112–114, Feb 2004. ISSN 1558-2361. doi: 10.1109/LSP.2003.821662.

[218] Nicholas Huang, M.-L.C. Wu, S.R. Long, Samuel Shen, W.D. Qu, P. Gloersen, and K.L. Fan. A confidence limit for the empirical mode decomposition and Hilbert spectral analysis. *Proceedings of The Royal Society A: Mathematical, Physical and Engineering Sciences*, 459:2317–2345, 09 2003. doi: 10.1098/rspa.2003.1123.

[219] Yong Zhang, Xiaomin Ji, and Suhua Zhang. An approach to EEG-based emotion recognition using combined feature extraction method. *Neuroscience Letters*, 633(28):152–157, 09 2016. doi: 10.1016/j.neulet.2016.09.037.

[220] Yong Yu, Xiaosheng Si, Changhua Hu, and Jianxun Zhang. A Review of Recurrent Neural Networks: LSTM Cells and Network Architectures. *Neural Computation*, 31(7):1235–1270, jul 2019. ISSN 0899-7667. doi: 10.1162/NECO_A_01199.

[221] Alex Graves and Jürgen Schmidhuber. Framewise phoneme classification with bidirectional LSTM and other neural network architectures. *Neural networks : the official journal of the International Neural Network Society*, 18(5-6):602–610, 07 2005. doi: 10.1016/j.neunet.2005.06.042.

[222] S. Paszkiel and P. Szpulak. Methods of Acquisition, Archiving and Biomedical Data Analysis of Brain Functioning. *Advances in Intelligent Systems and Computing*, 720:158–171, 2018. doi: 10.1007/978-3-319-75025-5_15.

[223] K. Belwafi, F. Ghaffari, R. Djemal, and O. Romain. A Hardware/Software Prototype of EEG-based BCI System for Home Device Control. *Journal of Signal Processing Systems*, 89(2):263–279, 2017. doi: 10.1007/s11265-016-1192-8.

[224] Chin-Teng Lin, Bor-Shyh Lin, Fu-Chang Lin, and Che-Jui Chang. Brain Computer Interface-Based Smart Living Environmental Auto-Adjustment Control System in UPnP Home Networking. *IEEE Systems Journal*, 8:363–370, June 2014. doi: 10.1109/JSYST.2012.2192756.

[225] K. Anam, M. Nuh, and A. Al-Jumaily. Comparison of EEG pattern recognition of motor imagery for finger movement classification. In *International Conference on Electrical Engineering, Computer Science and Informatics (EECSI)*, pages 24–27, 2019. doi: 10.23919/EECSI48112.2019.8977037.

[226] Łukasz Lentka and Janusz Smulko. Analysis of effectiveness and computational complexity of trend removal methods. *Zeszyty Naukowe Wydziału Elektrotechniki i Automatyki Politechniki Gdańskiej*, 51(1):111–114, 2016. ISSN 2353-1290.

[227] Tat'y Mwata-Velu, Jose Ruiz-Pinales, Horacio Rostro-Gonzalez, Mario Alberto Ibarra-Manzano, Jorge Mario Cruz-Duarte, and Juan Gabriel Aviña Cervantes. Motor Imagery Classification Based on a Recurrent-Convolutional Architecture to Control a Hexapod Robot. *Mathematics*, 9(6):606, 2021. ISSN 2227-7390. doi: 10.3390/math9060606. URL https://www.mdpi.com/2227-7390/9/6/606.

[228] Tat'y Mwata-Velu, Juan Gabriel Aviña Cervantes, Jorge Mario Cruz-Duarte, Horacio Rostro-Gonzalez, and Jose Ruiz-Pinales. Imaginary Finger Movements Decoding Using Empirical Mode Decomposition and a Stacked BiLSTM Architecture. *Mathematics*, 9(24):1–14, 2021. ISSN 2227-7390. doi: 10.3390/math9243297. URL https://www.mdpi.com/2227-7390/9/24/3297.